ABSTRACT

Title of Thesis: INVESTIGATION INTO THE INFLUENCE OF BUILD PARAMETERS ON FAILURE OF 3D PRINTED PARTS

Giacomo Fornasini
Master of Science
2016

Thesis Directed By: Professor Linda C. Schmidt
Department of Mechanical Engineering

Additive manufacturing, including fused deposition modeling (FDM), is transforming the built world and engineering education. Deep understanding of parts created through FDM technology has lagged behind its adoption in home, work, and academic environments. Properties of parts created from bulk materials through traditional manufacturing are understood well enough to accurately predict their behavior through analytical models. Unfortunately, Additive Manufacturing (AM) process parameters create anisotropy on a scale that fundamentally affects the part properties.

Understanding AM process parameters (implemented by program algorithms called slicers) is necessary to predict part behavior. Investigating algorithms controlling print parameters (slicers) revealed stark differences between the generation of part layers. In this work, tensile testing experiments, including a full factorial design, determined that three key factors, width, thickness, infill density, and their interactions, significantly affect the tensile properties of 3D printed test samples.

INVESTIGATION INTO THE INFLUENCE OF BUILD PARAMETERS ON FAILURE OF 3D PRINTED PARTS

by

Giacomo Fornasini

Thesis submitted to the Faculty of the Graduate School of the
University of Maryland, College Park, in partial fulfillment
of the requirements for the degree of
Master of Science
2016

Advisory Committee:
Professor Linda C. Schmidt, Chair
Assistant Professor Mark D. Fuge
Assistant Professor Ryan D. Sochol

Dedication

Dedicated to my grandfather, Angelo "Nonno Lino" Fornasini, whose inventive spirit, excitement for building, and passion for perfection was passed on to me, guiding me through my educational and now professional career.

Acknowledgements

First, I would like to thank my parents and family, whose unwavering support and love were a constant throughout all the chapters in my life. They have helped me in ways I cannot begin to express.

I would also like to thank Mr. Majid Aroom, who taught me the practical side of engineering and design that only comes through first-hand experience with machines. David also helped.

I would like to thank the Mechanical Engineering Department for the opportunity afforded me as student lab manager. A special thanks goes out to the faculty who helped me in gathering and understanding data. Dr. Robert Bonenberger for the gratuitous donation of his time and expertise in materials testing. Dr. Bhanu Sood, for his help in obtaining the microscopy images used to understand key aspects of parts. Dr. Mark Fuge and Dr. Ryan Sochol, for their helpful feedback, which allowed me refine this work.

Last, but not least, I want to thank my advisor, Dr. Linda Schmidt. This work would not have been possible without her. Her infectious enthusiasm for this research pushed me to delve deeper into the work and to take pride in it. She has guided me through her areas of expertise, and ventured with me to areas neither of us fully understood. Over the past two and a half years, I have come to see her not only as an incredible advisor and a trusted mentor, but as a true friend.

Table of Contents

List of Tables

List of Figures

List of Terms

Additive Manufacturing (AM) – A manufacturing technology where a part is made by adding material rather than removing it from a stock piece.

Fused Deposition Modeling (FDM) – An AM process where a plastic filament is melted and deposited.

Maker Movement – A community of people who design, create, and build their own objects through a variety of techniques, including 3D printing.

Makerspace – A lab open to the public with many tools that can be used to develop projects and create parts.

Nozzle – A metal funnel that heats up to melt the plastic filament. The nozzle diameter determines the road diameter.

Feed Motor – A motor that pulls the filament from the spool and pushes it through the nozzle.

Extruder – The assembly of a 3D printer consisting of the heated nozzle and feed motor that follows the path set by the slicer.

Build Plate – The area of the FDM machine where the first layer of a part is deposited.

Slicer – A program that generates the path the extruder must follow to create a part.

Sterolithography (STL) – A file type that converts a surface into a series of triangles so that a computer model can be easily processed by a computer.

Deposition Road (Road) – The path that the extruder follows when printing the part

Raster Angle – The angle at which the roads are oriented from the X axis.

Infill – The internal structure of a part that is not seen in a completed part.

Shell – Roads which follow the perimeter and comprise the exterior surfaces of the part giving a smooth finish to the vertical walls.

Air Gap – The distance between roads.

Chapter 1: Introduction

Since its advent in the 1980s, additive manufacturing (AM), often called 3D printing, technology has undergone unprecedented expansion into new materials and applications. AM capabilities have exceeded the original scope of prototyping, becoming a method for creating end-use parts. This is due to the continual advances being made in AM research and technology. Proven potential in a number of fields has fueled continual development into expanding the useable materials and the scales at which 3D printing can be used.

1.1 Overview of Additive Manufacturing

AM was first adopted by consumers and organizations that were interested in creating quick prototypes that did not require high dimensional quality. The Maker Movement embraced the 3D printing technology for many different personal applications, including art, tech projects like telescopes, toys, personal versions of functional objects like a goose-neck lamp, and many more (1).

Improvements in useable materials and print quality allowed high-technology industries to create parts that would otherwise be impossible with traditional machining. Shea designed specialized lattice structures for customized helmet designs (2). GE is using 3D printed fuel injectors to minimize the number of welds and increase safety and reliability (3). Educators are starting to see the advantages that 3D printing can bring into the classroom. This rising importance of AM technology in industrial

and educational settings drives the need to understand all relevant design for AM (DfAM) requirements for current and future part designers.

Significant national support is motivating research into AM processes. The Defense Advanced Research Projects Agency (DARPA) created the Open Manufacturing program to help increase the speed and quality of manufactured parts (4). The National Science Foundation (NSF) has programs for funding research on additive manufacturing processes, materials, and behavior in many of its divisions. This includes research experiences for teachers (RET) for K-12 teachers and community college faculty. NSF also funds workshops dedicated to the advancement in understanding of 3D printing technology and its applications (5).

Attune to the national emphasis on additive manufacturing, many universities have created spaces where students can go learn about and use AM technology for both academic and personal projects (5). Many universities, including the University of Maryland, are creating and expanding their fab labs to include more advanced equipment, such as metal AM machines. The University of Maryland has created Terrapin Works, a collection of services, through which students can submit parts to be 3D printed. Students choose the material and color for their prints. This allows anyone to use the system and create a part without knowledge of the process parameters. While this service makes 3D printing accessible to the entire community, it does not reveal the complexity of the process. More advanced services within departments (e.g., Mechanical Engineering) require students to articulate the end use of the part and justify the selection of 3D printing to make it. This exchange with 3D printing advisors

helps the students understand the process and develop technological competence in 3D printing (6).

Fused deposition modeling (FDM) printers are the most common AM machines in use. FDM uses a heated nozzle to deposit a fused polymer filament into layers that make up the part. The geometries of these layers depend on parameters set by either the user or the machine's processing program. Due to the relatively cheap cost of material and varying capacity of FDM printers, FDM systems are commercially available for home, office, and educational use.

The education of future engineers is also being transformed by AM research and wide-spread availability of FDM printers. FDM printing has been a tool for both students and instructors. It has helped with engineering students' design projects, as well as in teaching valuable technical skills to students. Project prototypes, which would take days to build and test, now take only hours. Faster design process iterations permit a more complete set of options to be explored and tested to solve problems.

Unlike traditional material removal processes, 3D printing is a process-driven technology. The future of 3D printing does not depend so much on the printing technology, but on the development of the materials that are compatible with it (7). Growth of FDM technology increases the need to understand structural and behavioral properties of deposited materials rather than eliminating the need for this knowledge. With such a rapid advancement of the new technology, deep understanding of FDM technology has lagged behind its adoption. The simplicity of creating any part and having a physical model can lead to the false assumption that a part created with AM

has the same properties as one created through traditional machining or molding. The knowledge to understand exactly how these processes differ is not common or complete. Likewise, the tradeoffs that must be addressed when designing and creating a part are not fully understood. Proper research and experimental testing are needed to improve understanding of FDM processes to support this growing technology.

1.2 Research Question

The almost unlimited potential of the FDM technology provides many paths for meaningful research. This work focuses primarily on the use of 3D printers using polymers by university engineering students for research and classwork.

Research Question: Which 3D printer build parameters and their interactions significantly impact the tensile behavior of the final part?

The results found in the answers to this question will have impact on understanding the capabilities of a class of 3D printers and highlight facts about printing processes. These results will provide information for engineering student users and other users of 3D printers.

1.3 How Fused Deposition Modeling Works

Creating a physical part with a FDM machine requires three main steps. The first is that the model must be designed. Next, the path the nozzle must follow in order to create the part must be generated. In the final step, the machine builds the part.

In order to begin the process of creating a part through FDM, a 3D model of the part must be created. Once that model is created, it is converted into a stereolithography (.STL) file. This file type takes the surface of the model, and creates a series of nodes through mathematical integration. Connecting these nodes creates a surface which is like the created part.

After the .STL file is created, it must be processed by a different program to generate the build file for the FDM machine. These programs are called slicers. Slicers take the surface model, and split it up into a series of 2-dimensional layers. When these layers are stacked, they create the original .STL model. Within each layer, the slicer program creates the path that the nozzle must follow in order to lay down the strand of melted material correctly to create the part. This pattern within the layer makes up the road geometry of the layer. This entire process of converting .STL files into road geometries is called slicing.

Creating .STL files is relatively standardized across CAD programs, but there is much greater variation between slicers. Some printers use only proprietary slicers that are provided by the manufacturer. On the other hand, open-source printers are capable of accepting build files from a variety of slicers that are independently available. Each slicer provides users with different degrees of process parameter control (e.g., variables controlling road geometry). Parameters governing the most basic control of the print, such as layer height, print quality, infill density, or orientation. Others give full control over all the parameters such as infill pattern, support location, shell thickness, printing speed, and many more.

Once the print file is generated, it is sent to the printer. Most FDM printers are designed to print materials with melting points between 160°C and 250°C. The most common are the plastics acrylonitrile butadiene styrene (ABS) with a printing temperature of around 230°C, and polylactic acid (PLA), with a printing temperature of around 205°C.

1. The build plate must often be leveled. Depending on the printer, this can be done automatically or manually.
2. The nozzle begins to heats up. Printing begins once a nozzle reaches the melting temperature of the material.
3. A motor pushes the filament through the heated nozzle, melting it. By continuing to push the solid filament through, the melted filament is pushed out of the nozzle tip, onto the build plate.
4. The assembly of feeding motor and nozzle make up the extruder head, which is mounted on a series of Cartesian linear motors. These motors move the head in the X and Y directions, while the build plate moves up and down in the Z direction. Combining these movements allows the extruder head to follow the path generated by the slicer until the part is completed.
5. Some printers will have a heated bed or heated chamber to help the melted material adhere to the build plate. This is especially important with high melting temperature materials, such as ABS, which tend to detach from the build plate during printing.

A diagram showing the printing process is seen in Figure 1 and Figure 2 is a photo of a build area of a 3D printing machine.

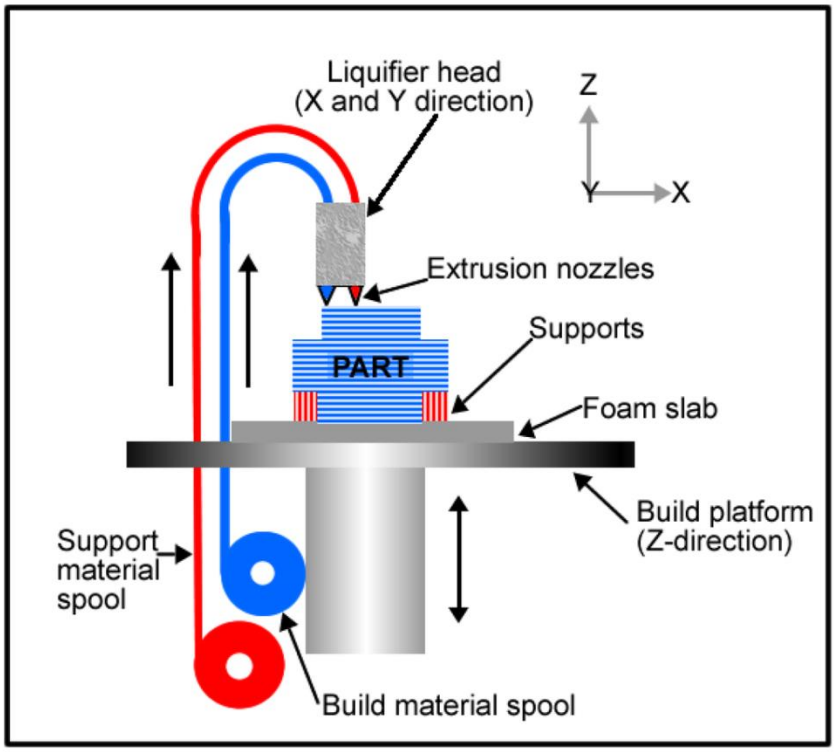

Figure 1: Diagram of how FDM printing works with a dual extrusion system (8)

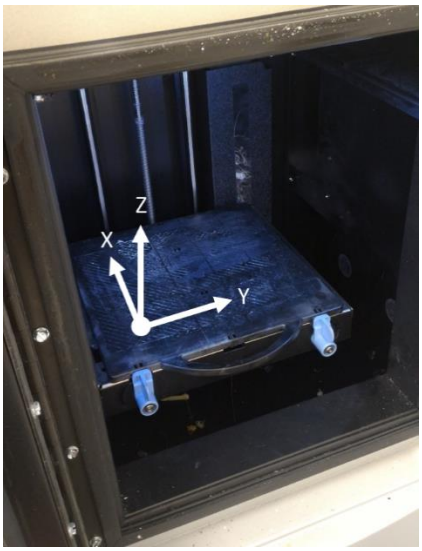

Figure 2: Build chamber of Dimension 1200es printer showing build axes

1.4 Organization of Thesis

This thesis follows the path of exploration and expanding understanding of how build parameters affect the final properties of 3D printed parts. A literature review of research done by other scientists has been compiled (Chapter 2). Next, the preliminary experimental observations that served as the motivation for the expansion of this research are explored (Chapter 3). Informed by the literature (and gaps within it) the first systematic tests and analyses on the stress and strain behavior of 3D printed parts were developed (Chapter 4). These pilot tests suggested a framework for the DOE factorial experiment and analysis in Chapter 5 which clarified observations on how some key parameters affect 3D printed part properties.

Chapter 2: Literature Review

The following is a compilation of research relevant to the exploration of 3D printing and the need for a better understanding of how the process drives the properties. The research is representative of the vast body of knowledge on the subject, and draws useful conclusions on the current state and future of 3D printing. Due to the scope of this thesis and the research question, the majority of the selected research deals with FDM printers.

The expansion of 3D printing into education, highlighting some of its advantages and disadvantages is explored. Studies on the effects of parameters on parts are examined. Research into solving some of the issues with 3D printed parts is discussed. The current state of development of design rules is summarized.

2.1 Effects of FDM Build Parameters on Part Properties

Many parameters can be adjusted and studied with a versatile slicing software. Qureshi (17) tested 13 independent process parameters and ranked them according to the magnitude of their effects on the tensile strength as measured according to the ASTM D638 standard. His results ranked the most important parameters as the thickness of the part, the number of shells, and the raster angle.

Several authors have shown that the strongest orientation for tensile specimens is when the roads are parallel to the applied force direction. For example, Es-Said (18) performed tensile tests following the ASTM D638 standard on parts with various alternating and non-alternating layer orientations. Findings were the number of layers

oriented parallel to the applied force is directly related to the tensile strength of the part. However, if there are no roads oriented parallel to the force, parts made with alternating layers were stronger than those made with non-alternating layers at the same angle.

Expanding on part orientation research, Dawoud et al. (19) investigated the effects of layer orientation when each layer raster orientation is offset by 90° from the previous one. They divided findings into those with a positive air gap and those with a negative air gap. Using the DIN EN ISO 527-2 standard for tensile testing, the parts with rasters oriented at 45/-45° and a positive air gap showed a significantly higher strength than those with other orientations. However, with a negative air gap, the parts with 0/90° oriented rasters had a slightly higher ultimate strength than those with other orientations. It was demonstrated that the denser a part is, the less effect the layer orientations have on part properties.

Yang et al. (20) found similar effects of the air gap. Yang printed parts following ASTM E8/E8M with layers oriented parallel and perpendicular to the force. All layers had the same orientation. The parts with rasters oriented along the direction of the force were stronger than the ones with rasters oriented perpendicular to the force. However, there was a smaller difference between the parts with the negative air gap than the ones with a positive one.

Rankouhi (21) studied layer thickness and found that the thickness of each individual layer also had a significant effect on the tensile properties of parts created with ASTM D638 dimensions. He tested different layer orientations at different layer thicknesses,

and found that parts printed with a layer thickness of .2 mm performed better than those with thicker layers.

In addition to tensile properties, the build parameters have been used to study other mechanical properties. Mohamed et al. (22) studied the dynamic viscoelastic properties of 3D printed parts in order to develop some failure models based on cyclic stresses, forces, or vibrations. The ASTM D5418 standard defined part dimensions. The thinner layer heights of .127 mm resulted in the formation of more pores between layers, which led to cracking. The positive Air gap was shown to have varying effects based on the desired properties. A smaller gap created stronger parts, but a wider gap allowed for more reflow, and raised the thermal conductivity, lowering the stress accumulation, which could otherwise lead to cracks.

Teitelbaum switched from studying mechanical properties of parts to processing properties. He studied effects of layer orientation on part build time and material use. Teitelbaum created a library of parts, ranging from simple to complex, and used the Stratasys CatalystEX software to slice the parts. He used the same parameters for every part, and only changed the orientation of the part on the build plate during the slicing. The results showed that orienting the parts at 45° resulted in statistically less material use and faster build time (23). This was due to the slicer's default raster orientation, which was set at 45° from the XY coordinate system. Orienting the part parallel to the raster direction allowed for longer lines to be made along the whole length rather than shorter lines at an angle within the part.

Thanks to work by these and other researchers, the effects of individual parameters is starting to become clearer. However, the interaction effects between parameters can also play a significant role in determining the part properties. Lanzotti et al. began an exploration into these interaction effects. Through a 3^3 factorial analysis, they determined the main and interaction effects of layer thickness, deposition speed, and flow percentage on the resolution of prints. They compared the dimensions of a printed part with those in the computer model. This allowed insights into both the effect on quality of the prints, as well as on the repeatability of the process. While the effects of these particular interactions were determined to be statistically insignificant, the existence of interactions between parameters was shown to exist (24).

2.2 Strengthening 3D Printed Parts through Material Additives

Many researchers examine ways to strengthen selected part properties. Of particular interest is the research aimed at reducing the anisotropy of the parts. If the anisotropy could be lowered enough, certain parameters such as build orientation could be ignored, making it easier to develop design guidelines.

Torrado (25) has had success with modifying the material itself. ABS was mixed with other materials (metals and other plastics). Parts were printed according to ASTM D638 in different orientations to compare the magnitude of the differences between the two orientations. A lower difference means a lower anisotropy. The different combinations were tested demonstrating that it is possible to lower the anisotropy of 3D printed parts.

Shaffer (26) attempted to reduce the anisotropy by using a different composite material, and treating finished parts with ionizing radiation. Parts following ASTM D638 were

printed in different orientations. He then used radiation at different temperatures to see if there was an optimal point at which to treat parts. At 60°C, he was able to raise the ultimate stress of horizontally printed parts to 35.9 MPa from 23.5 MPa. Comparing this to the 55 MPa of the vertically printed parts shows a significant decrease in anisotropy.

Another researcher, Perez (27), looked at the fracture behavior of modified ABS parts. Parts were designed according to the ASTM D638 standard and printed with both pure ABS and the modified ABS. While pure ABS showed a ductile fracture, the modified ABS showed brittle fracture. There was much less elongation before the break in the modified ABS, which is to be expected when dealing with brittle fracture.

Wu (28) decided to try a new material altogether, studying the properties of polyether-ether-ketone (PEEK), a different thermoplastic. He did a similar study to that of Rankouhi (21), where Wu tested different orientations and layer thicknesses. He used the GB/T 16421-1996 standard for preparing the parts. PEEK showed a slight increase in tensile properties. However, Wu found that parts made with layers alternating between 0° and 90° showed a higher tensile strength than those with the 45/-45° orientation. This is contrary to the findings of other studies, which tested ABS.

Weng (29) combined nanocomposites with ABS so as to improve the material properties of the part. Parts were printed out of the different materials using ASTM D790-03. Weng succeeded in increasing the strength in tension by 43%, but he did not test different orientations to see the effects on the total anisotropy of the mixed material. However, Weng's research approached another issue with 3D printed parts - warping.

Material is extruded at high temperatures, but then cooled to room temperature. These temperature fluctuations can cause layers to expand and contract during heating and cooling, which could warp the part. Weng showed that his modified ABS had a much lower coefficient of thermal expansion than pure ABS. This means that as the part goes through heating and cooling, it will deform less, and so give much more precise parts.

Belter (30) took a different approach, and decided to use resin to fill pores in the printed parts. His tests consisted of changing the infill, creating a hollow shell, and modifying the internals of the part. The resin had similar properties as the plastic, but gave the entire part more isotropic properties. Belter then did a flexural test following the ASTM D790 standard. The resin proved to be stronger than even 100% dense ABS.

2.3 Developing Design Rules for Additive Manufacturing

After seeing what profound effects the build parameters can have on part properties, the need to develop design for additive manufacturing (DfAM) rules is evident. Design for manufacturing rules for traditional machining have been commonplace for a few decades. However, the growth of 3D printing has been so fast, that standards and design guidelines have not had time to catch up. Without guidelines, everyone must rely on their own knowledge of the process. Gao et al. states that this lack of design rules leads to a waste of resources attempting to reach desired features through trial and error (31).

Much of the most recent research on DfAM has been performed for more advanced additive technologies, such as metal printing, which uses lasers to melt metallic powder. Vayre et al. (32) developed some basic guidelines for part designing to increase strength and optimize fabrication of a part when using selective laser sintering.

Their research showed that the laser would create inconsistencies at sharp corners where the laser would need to decelerate and then accelerate again. This led to a longer dwell time over those corner regions, melting them more than the straight areas. Therefore, one of the rules suggested was to make rounded corners, which would allow the laser to continue at the same speed throughout the layer's build. This is similar to the commonly accepted design rule developed for injection molding, where sharp corners can have similar problems when the liquid polymer is pushed into the cavity. Vayre et al. go on to develop a set of rules for designing parts by AM by the following steps: analysis of the specification, developing the basic shape, setting parameters, and parametric optimization. Each step takes the general design rules for developing a part and modifies it specifically for laser sintering AM.

Some recommended design rules were specific to certain applications. For example, Zein et al. (33) studied the effects of printing parameters on the porosity and channel sizes of tissue scaffolding. SEM images of sample cross-sections perpendicular to the road patterns showed clear differences in structure depending on the orientation of each layer. Zein et al. observed correlations between layer orientations and properties of the tissue. Pores created between layers were larger in the scaffolds with layers alternating between 0° and 90°° than in ones with layers alternating between 0°, 60°, and 120°. The channels between filaments in each layer were found to have the opposite correlation. The 0° and 90° alternating scaffolds were also found to have a higher stiffness than the 0°, 60°, and 120° scaffolds, but similar yield strength. From these findings, Zein et al. were able to develop some guidelines for tissue engineering based on the required strength and porosity requirements.

Shea, a design specialist in truss structures, and her colleagues combine the design of 3D printed lattices with optimization (2). They researched multi-material lattice structures in order to understand the anisotropic properties of the structures. Their goal is to use this research in order to develop a method for making helmets formed to the shape of the user's head.

The Direct Manufacturing Research Center (DMRC) at the University of Paderborn, Germany began a three year project in 2010 to develop a comprehensive set of design rules for basic components and features common to many parts. DMRC researchers studied these rules for different AM technologies, including laser sintering and FDM. Their premise was that, as is true of injection molded parts, most complex parts can be broken down to a series of more basic shapes and transitions. These shapes and transitions would be the target of the design rules. The final project consisted of about 60 different shapes and transition elements, each with specific rules for designing them to be as efficient as possible. A follow-up project has begun that intends to test and expand these rules further to include a broader set of machines and process parameters (32).

2.4 Additive Manufacturing in Education

The broad use of 3D printing in education is due in part to the maker movement. Through the development of makerspaces and exhibitions such as the world-wide Maker Faires, an informal education with 3D printing was begun (9). These spaces allow people of all ages to develop their ideas and turn them into physical parts. In the

process, these people learn the technical skills of using 3D printers and other 3D software.

The attraction of the maker movement reached a wide breadth of society. People from all different backgrounds, ages, and disciplines have become part of the movement. Drawing from the experiences and skills of such a broad group of people has transformed the way that people look at projects. Anderson calls it "The new industrial revolution" (10). This "revolution" has led to a democratization of the skills and tools available to create, expanding the informal education that anyone can tap into to learn through making.

The maker movement has a focus on the sharing of invention and creativity, something that can be used by students in academic settings as well. Make Media, one of the driving forces behind the maker movement has developed the Maker Ed program, which helps make the tools for hands-on learning accessible to everyone. They run workshops with young students focused on interaction with others to develop a project (11).

The ability to create physical parts directly from computer models can change the way manufacturing and designing is approached. It gives a physical form to work done in a virtual space, allowing the bridge between the digital and physical world. This has been used to revitalize the vital studio work that has been in decline in higher education (12). This rekindling of interest in designing models and creating parts has led to a new wave of engineers learning through building and hands-on experiences.

This increase in interest has led to a growth in makerspaces and fab labs in many universities. These spaces are either closed spaces where staff run the prints, or open areas where students can run the machines themselves. The University of Texas has taken the makerspace idea one step further, and developed a 3D printing vending machine. The machine consists of two Makerbot printers outfitted with specialized parts such as an automated part removal system. Its automation and ease of use has had great success with both engineering and non-engineering students (13).

Fab Labs provide opportunities to improve design process learning. Smith et al. studied how a design process can help in the development and understanding of ideas. They found that when starting with a loose, general idea for a problem solution, the design process would come to a stop quickly. However, structuring the design process to look at more concrete solutions and iteratively improve upon them, the student was able to be more engaged and solve the problem (14). 3D printing can be beneficial to this kind of learning, because it can give a physical representation of a solution. With something physical, it becomes easier to see flaws in the current solution and develop a better one (6).

While the advantages are many, the relative ease with which a computer model can be turned into a physical part can have downsides when used in the classroom. Blikstein describes the "Keychain Syndrome," where the visual outcome is the only factor considered when using the technology. He says that the rewards from making a part in this way are too great for the little work required to make it (6). No calculations or engineering understanding is required. Nonetheless, the part is made, and it is visually

appealing. Blikstein uses the keychain example as a case of technical literacy. Technical literacy is what allows someone to use a machine and follow the instructions, while technical competence comes from knowledge of the process at a deep level (6). With the speed of development of 3D printing, technological literacy has been mistaken for technical competence due to the ease of use to make a visually appealing part.

While the "Keychain Syndrome" can be detrimental to learning in some cases, it can also be fruitful in others. For example, Buehlet et al. studied the use of 3D printing for education of students with intellectual disabilities. The ease of making a 3D printed part yielded a boost in confidence in these students. This confidence allowed them to expand and use their technical skills beyond what they were capable of before the class (15).

Chapter 3: Demonstration of Slicer Differences

The motivation for this research was born out of the author's position as Student Lab Manager at the mechanical engineering machine shop at the University of Maryland. In this capacity, he managed 3D printing builds for students in the design courses. First-hand experience of helping students design, manufacture, and test prototypes for classes, demonstrated an evident lack of knowledge of 3D printing. Often, the user's end goal was usually a visual prototype, not a functional one. Little knowledge about what parameters could be controlled or how they affected the part was shown. Students viewed 3D printing as the replacement to traditional machining, regardless of part size or complexity.

Looking at parts made by different machines showed slight differences, even on the surface. These observations inspired a deeper look into how the same part is made on different printers. The driver for the work in this chapter is the question: "Are there significant differences in the road geometries generated by slicer algorithms for the Dimension 1200es, CubeX Trio, and Makerbot Replicator 2X 3D printers?"

Content used in this section was presented at the 2015 International Conference on Engineering Design in a paper titled, "A Call for FDM Design Rules to Include Road Deposition" (16).

3.1 Methodology

The printers and software used for this comparative analysis are a Dimension 1200es printer using CatalystEX software, a CubeX Trio printer using Cubify software, and a

Makerbot Replicator 2x using Makerbot Desktop software. These 3D printer models were selected for exploration based on their availability for home, office, and educational use. Their properties are summarized in Table 1.

In order to compare the road geometries of different printers, it was necessary to create 3D computer part models and process the .STL files through the slicer software for each printer. The road geometries that make up the layers in a part depend on algorithms written into the slicer software. Road deposition codes for these printers are not modifiable by the user, but are internal to the system.

Table 1: Properties of printers used for slicer comparison

3D Printer	Slicer Software	Maximum Build Volume (mm)	Materials	Nozzles
Dimension 1200es	CatalystEX	254 x 254 x 305	ABS	2
CubeX Trio	Cubify	230 x 265 x 240	ABS, PLA	3
Makerbot Replicator 2x	Makerbot Desktop	246 x 152 x 155	ABS, PLA	2

There are three main road geometries that make up a part: the shells, the infill, and the surface layers. A 3D model of a rectangular block was used to study these geometries. The block was 100 x 30 x 20 mm in size, with through-holes of various sizes ranging from 1 mm to 20 mm in diameter (Figure 3). The images provided later in this section were obtained by running the slicer software on the test block model with the 100 mm side oriented in the horizontal direction (along the x-axis of the printer).

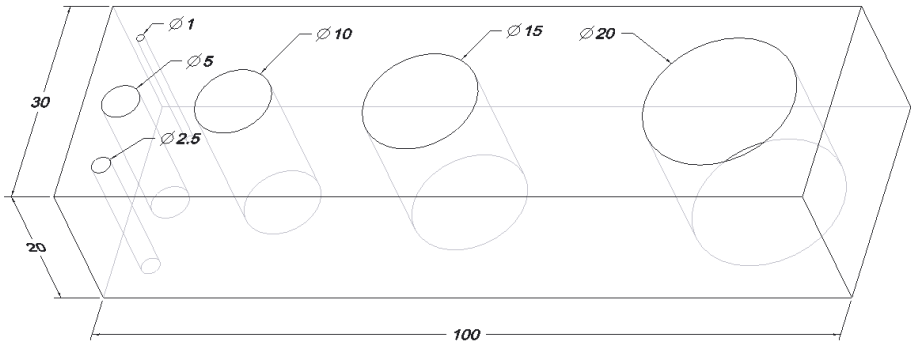

Figure 3: Test block used for slicer comparison. All dimensions in mm

Each slicer has a simulation tool that displays the part's deposition layers at different slice heights. These slices show the roads that make up each individual layer. In order to see the details of the road geometry within the software, it was necessary to zoom in on each layer. This limited the view of the entire part. Observations were made primarily on the area with the three smallest holes in the left of the block shown in Figure 4.

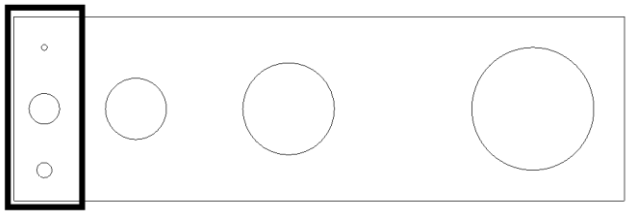

Figure 4: Area used for detailed views of slicer generated roads

3.2 Investigation and Comparison of Slicers

3.2.1 Shells

Shells are the roads that create the vertical walls of the part. These are the surfaces that are created along the z-axis of the build volume (see Figure 2). Shells stack up to form surfaces that will be visible from the outside of the finished part. The perimeters of the

test block consist of the external walls of the block and the walls inside the holes. Road geometry of the shells give a more uniform finish to external surfaces. Slicers accomplish this by generating a single, continuous road, which follows the perimeters of the part, regardless of the part geometry.

There are differences in shell geometry between the slicers.

Dimension's CatalystEX slicer:

- Each layer has two parallel roads comprising the perimeter for each external feature.

CubeX Trio's Cubify slicer:

- There are at least three two parallel roads comprising the perimeter for each external feature.
- Shells are not identical between layers. The four bottom layers have four shells each, while the rest of the part has only three shells per layer (Figure 6).

Makerbot Replicator's Makerbot Desktop slicer:

- The user can set the number of parallel roads comprising the perimeter for each external feature. This is not an option available in the other programs. Figure 7 shows the layer with 2 and 7 shells.
- The number of shells does not vary between layers.

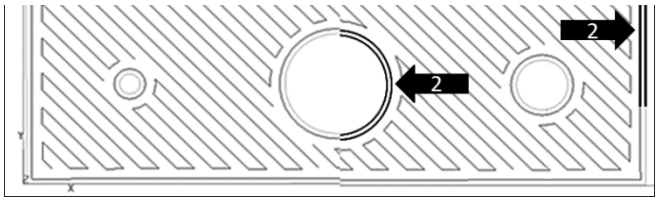

Figure 5: CatalystEX simulation showing 2 shells around the block and holes. The lines represent the centerline the nozzle will follow. Darkened lines highlight the 2 paths that make up the shells on the outer surfaces

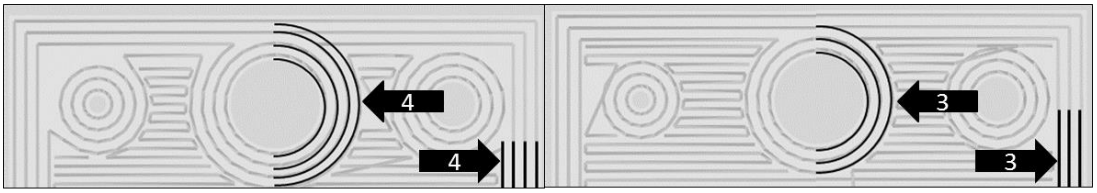

Figure 6: Cubify simulation showing a) 4 shells on the lower layer and b) 3 shells on the upper layer

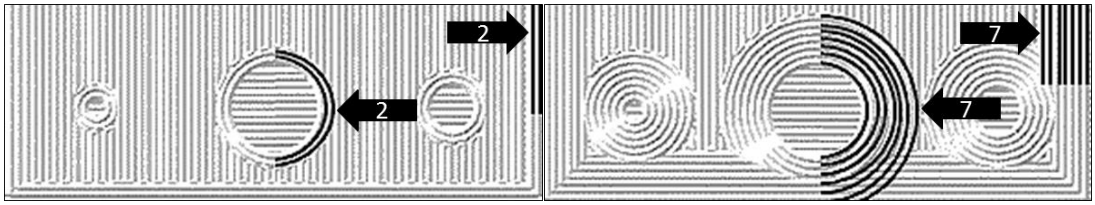

Figure 7: Makerbot Desktop simulation showing a) 2 user-set shells and b) 7 user-set shells

3.2.2 Infill

The infill roads are deposited with a back and forth rastering motion, which fills the spaces between the shells to yield a semi-solid part. Because of this behavior, the orientation of the infill roads is referred to as the raster orientation. The infill geometry is critical to part performance because it dictates the density of the part. A part's density is determined by the distance between infill roads. This distance is called the air gap. The smaller the air gap, the denser the part. A negative air gap indicates overlapping roads and a fully dense part.

Dimension CatalystEX slicer:

- Raster angles alternate between 45° and -45° (relative to the X axis in the X-Y plane of the build plate) on successive layers as seen in Figure 8. For the test block, a high density (though not solid) infill was chosen, resulting in a positive air gap.

CubeX Cubify slicer:

- The raster angle of 45° does not alternate between layers (Figure 9).

Makerbot Replicator Makerbot Desktop slicer:

- Raster angles alternate between 0° and 90° on successive layers.
- The second from the bottom layer shows a grid-like pattern in the simulation (Figure 10). It is impossible to verify the road orientations in this layer without physically printing the part.

3.2.3 Surface Layers

Surface layers give clean finishes to the top and bottom horizontal surfaces, just as shells give clean finishes to vertical walls of printed parts. Surface layers usually have a different road pattern than the infill, though they are still created through the same rastering motion. This smooth finish on the outside surfaces can lead to a false impression that the internal structure is just as dense as the surface.

Dimension CatalystEX slicer:

- Surface layers have an air gap of zero (Figure 8).
- There is one surface layer on the top and one on the bottom of the test block.
- Surface layer raster orientation follows the alternating 45° and -45° raster orientation found in the infill layers.

CubeX Cubify slicer:

- Surface layers have an air gap of zero.
- There are 4 surface layers on the top, and 4 on the bottom of the test block.
- The bottom 4 surface layer raster orientations repeat at 0° (Figure 11); the top four layers alternate between 0° and 90° (Figure 12).

Replicator Makerbot Desktop slicer:

- Surface layers had air gaps identical to those found in infill layers.
- Surface layer raster orientation follows the alternating 0° and 90° raster orientation found in the infill layers.

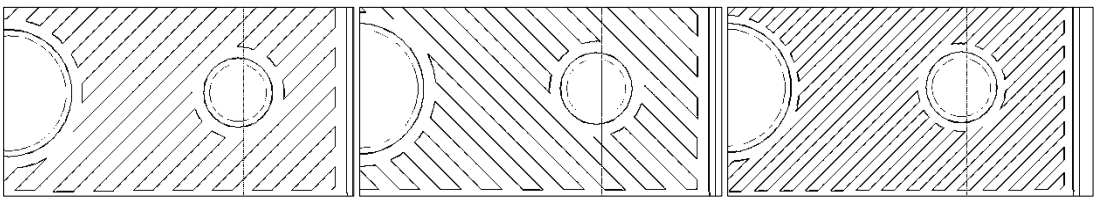

Figure 8: CatalystEX rater angles alternate between 45° and -45°: a) infill layer orientation, b) successive infill layer orientation, c) top layer with smaller air gap between roads

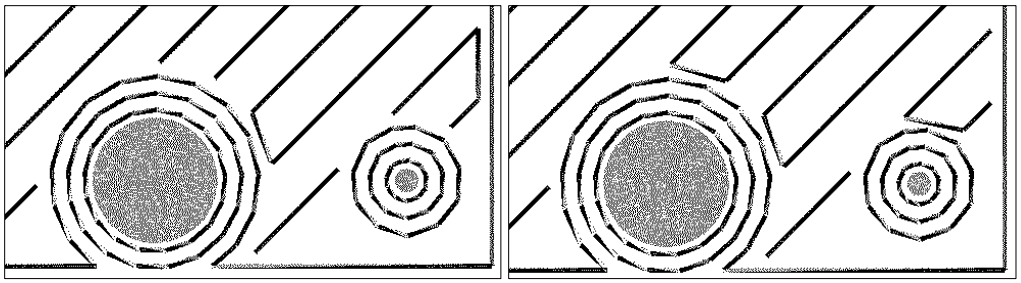

Figure 9: Cubify infill layers at 45° do not alternate raster angles between layers: a) infill layer orientation, b) successive infill layer orientation

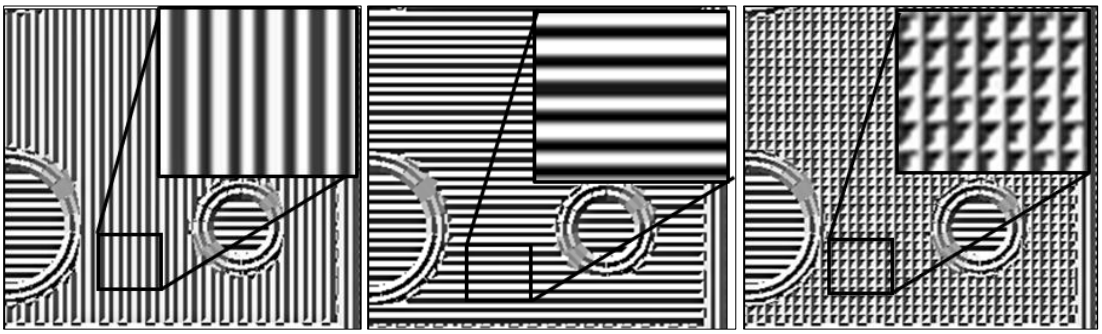

Figure 10: Makerbot Desktop raster angles alternate between 0° and 90°: a) infill layer orientation, b) successive infill layer orientation, c) exception to alternating layers showing grid-like pattern

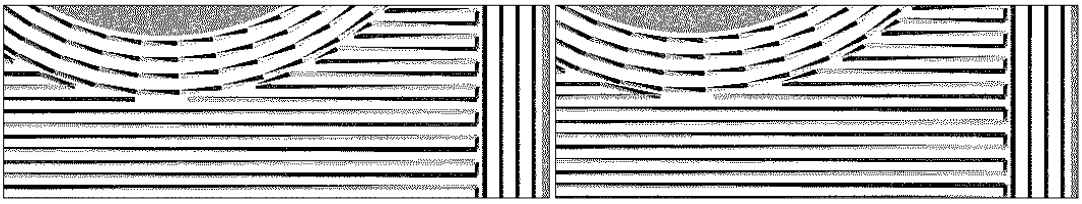

Figure 11: Bottom layers do not alternate deposition angles: a) bottom layer orientation, b) 2nd layer orientation

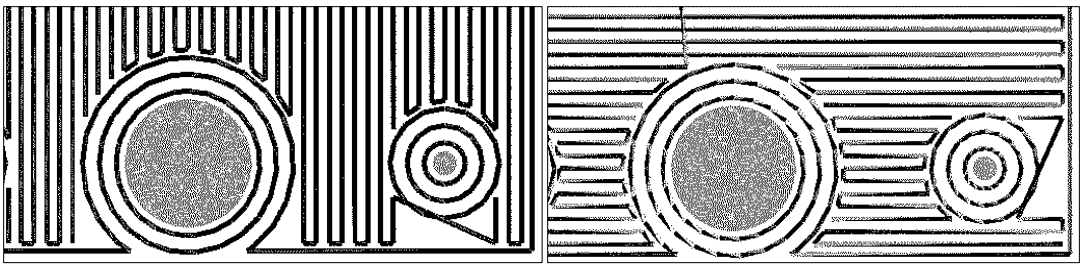

Figure 12: Top layers alternate between 0° and 90°: a) top layer orientation, b) successive layer orientation

3.3 Updates and Unknowns in Slicer Software

Between the times of the experimentation and the analysis, the CatalystEX and Makerbot Desktop slicers were updated. These updates made changes to the algorithms that determined the road geometry. No notification of the update content was made evident upon installation. The changes to the CatalystEX algorithm were only noticed when reexamining the slicer simulation with the original test block. It was found that, while the surface layer geometry remained identical to the previous software version, more high density layers were added below that surface. The previous software version had a single top and bottom surface layer with a zero air gap. The newer version replaced the three infill layers below the surface layers with transition layers that had a different geometry. These transition layers had an air gap slightly larger than the surface layers, but smaller than the infill layers (Figure 13).

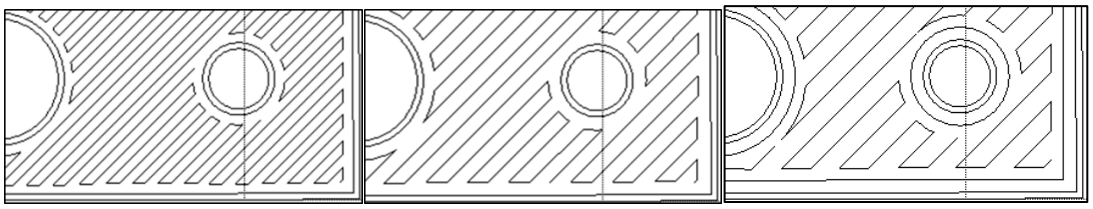

Figure 13: Changes in CatalystEX software showing a surface layer (left), an infill layer (right), and one of the new transition layers (center)

The previously used version of Makerbot Desktop generated almost no layer variation. The updated slicer algorithm varied the road geometry as given in the following list:

- The top 2 surface layer raster orientations are fixed at 45°
- The next 10 surface layer raster orientations alternate at 45/-45°
- The infill layer raster orientations alternate at 0/90°
- 6 surface layer raster orientations alternate at 45/- 45°
- The bottom 4 surface layer raster orientations are fixed at 45°

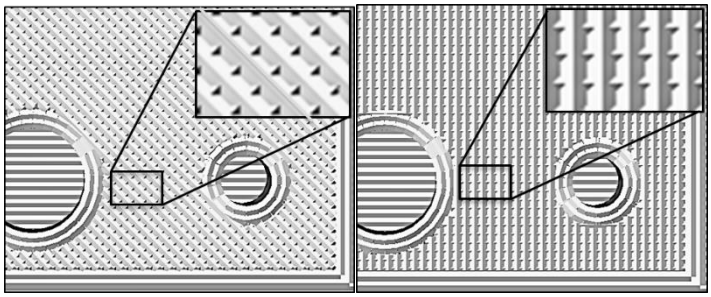

Figure 14: Makerbot Desktop simulation after update showing new geometries of layers

3.4 Physical Evidence and Resulting Behavior

Microscopy was used to provide actual photographic evidence of the road geometries in the test block. Breaking a test block without deforming or melting it was necessary to reveal interior road geometry. Two test blocks were printed on the Dimension, one oriented with alternating 45/-45 raster orientations, and the other with alternating 0/90 raster orientations. Using a similar procedure to that used by Zein et. al. (33) the parts were placed in liquid nitrogen for five minutes until thermal stability was reached. The parts were then broken by impact force from a metal shear. This gave some

directionality to the fracture location. The results of the fractures are seen in Figure 15.

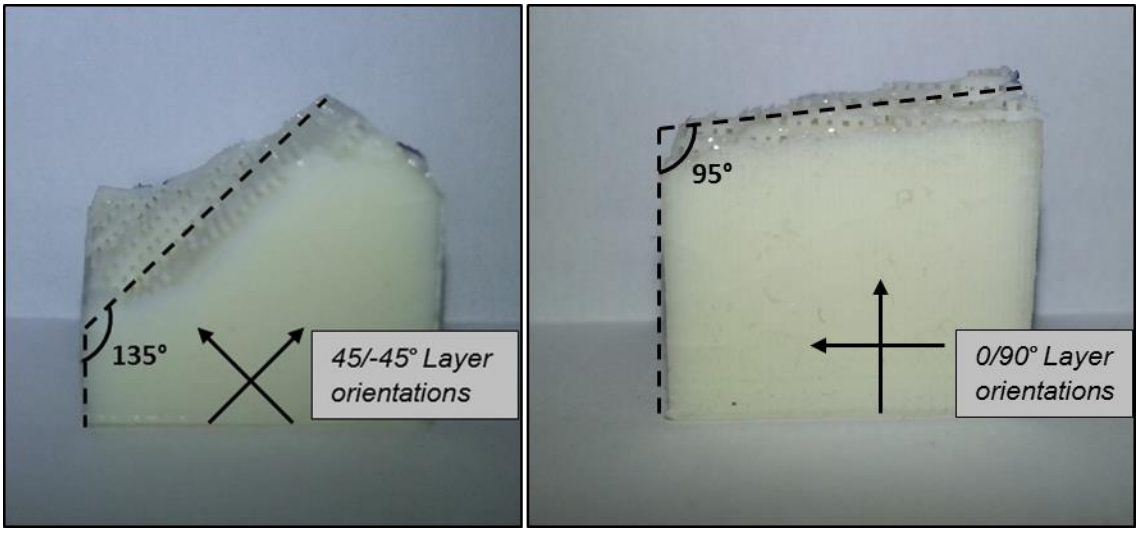

Figure 15: Fracture surfaces for parts with 45/-45 and 0/90 raster orientations (16)

A test block was also broken at the thin point between the outer rectangle perimeter and the largest circle. A closer study of the fracture surfaces showed interesting behavior near the shells of the circle (Figure 16).

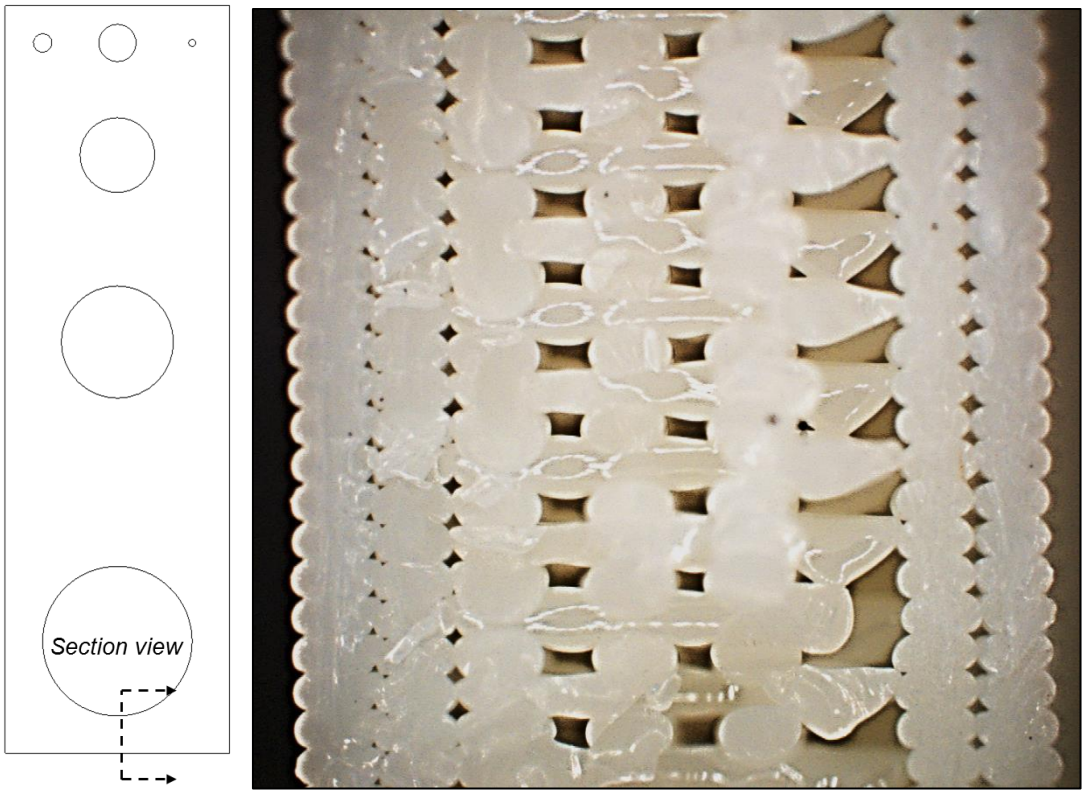

Figure 16: Fracture surface of shown cross-sectional area showing incomplete infill road geometry (16)

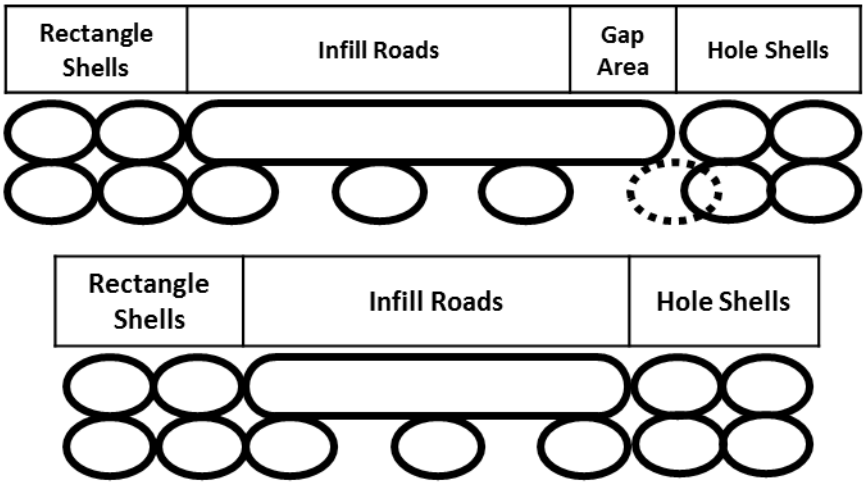

Figure 17: Sketch of actual and ideal part shape based on existing infill road geometry (16)

The infill roads follow a repeating pattern, alternating between a road and an air gap. This was seen in the slicer simulation. However, at this particular point, the distance between the outer rectangle shells and the shells of the circle is not an integer of this pattern. There is not enough space to deposit a road, so the spacing between the last infill road and the circle shells is greater than the air gap (Figure 17). When the next layer is deposited, the roads are stretched across this larger gap. However, the distance is too large to adhere properly, and the road droops into the gap, barely connecting with the shell on the other side.

3.5 Summary of Findings

This investigation revealed stark differences between the road geometry of shells, infill, and surface layers generated by CatalystEX, Cubify, and Makerbot Desktop slicers. The major differences are summarized in Table 2.

Table 2: Summary of major differences between slicer software

Slicer	Shells	Surface Layers	Infill Raster Orientation
CatalystEX	2	1	Every layer alternates
Cubify	3-4	4	Top 4 layers and between 4th and 5th
Makerbot Desktop	User-defined	0	All layers except 2nd from bottom

The same part built on these different printers will look the same from the outside. The differences are only apparent when examining the interior geometry through the simulation.

Updates to the slicer software can occur at any time and add unknown printer instructions that may change road geometry. While the changes are designed to be positive for the user, (e.g., the CatalystEX update created smoother surfaces), they are hidden from the user. There is no easy way of knowing which changes occurred without examining the sliced models and comparing them to previous versions.

Physical parts printed using the CatalystEX algorithm in different orientations showed physical differences in the interior structure of the part and in its fracture behavior. However, the simulation does not show what happens when the part geometry is not fitted to the repeating road geometry pattern (Figure 16). This suggests a design rule that the part dimensions should be related to the road widths in a specific way.

The observations in this chapter demonstrated a difference between the same part printed on the selected printers. Someone with only technological literacy would be able to make a part on each printer, but would perceive them all as identical. In order

to design a part for performance, a student would have to understand how the slicer algorithm generates the roads.

Chapter 4: Pilot Tests

After observing the differences in slicer behavior, the effects of those differences were examined. In order to do this, parts were printed with varying parameters and their tensile properties were tested and compared. The pilot tests were conducted on parts with varying orientation, thickness, and clamping direction of the tensile tester wedge grips.

4.1 Methodology

One of the most basic tests for determining material and part properties is the tensile test. There are currently no tensile testing standards specific to 3D printed parts, but Chapter 2 included the different standards used by researchers. For example, ASTM D638 is a standard for tensile testing of plastics but was used for 3D printed specimens (17) (18) (21). The pilot test specimens were based off the test strips used by Ahn (34) in his research in order to avoid the unwanted stress concentrations present in standard dog-bone shaped test specimens.

4.1.1 Part Design

The modeling of the parts was done using Creo Parametric 3.0. The original dimensions were taken from Ahn's paper (34), following the ASTM D3039 standard. This standard was designed for polymer matrix composite materials. The structure of 3D printed parts is similar to that of composites made of polymer and air gaps. Each part was created with specific dimensions based on the parameters that were to be studied in each particular test. Figure 18 illustrates the dimension terminology used to describe the test

parts. The lengths of the parts were held constant at 4 inches. This was to ensure that there was enough length to clamp the parts in the tensile tester grips while still having a 500 mm (19.685″) length between the grip edges.

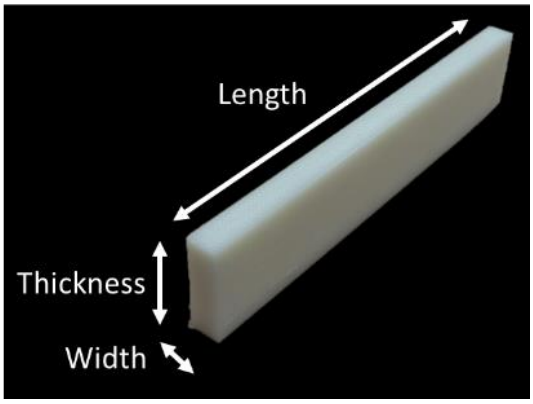

Figure 18: Part dimension terminology

4.1.2 Printer

The printer used to make parts was the Stratasys Dimension 1200es (Dimension). This printer was selected due to its ability to build consistent parts across various locations on the build plate and at different times. The sealed, heated environment is critical to this consistency, because it maintains a uniform temperature of 99°C and constant humidity during the building process, ensuring that parts printed at different times will have similar properties. Minimizing the variation from the printer allowed for a clearer evaluation of the effects caused by the selected parameters.

4.1.3 Slicer

The slicing was done using CatalystEX software, which is the proprietary software required to run prints on the Dimension. This software allows the user relatively little control over the build settings. The density of the part can be selected from “Solid,”

"Sparse – High Density," and "Sparse – Low Density." The part can be oriented automatically or by user input. In order to ensure equal build settings across parts, they were oriented by user input. Regardless of how the part is oriented, subsequent layers will alternate the raster angle by 90°. If the first layer is oriented at 45°, the next layer will be oriented at -45°. In the same way, a layer raster oriented at 90° will be followed by a layer raster oriented at 0°. Once the density and orientation were selected for each part, the software sliced the part and positioned it on the simulated build plate. The program was then sent to the printer.

4.1.4 Tensile Tester

Once the parts were printed, they were tested on a Tinius Olsen H25KT tensile tester (Figure 19) in order to determine the behavior under tensile load. The Tinius Olsen had a 25 kN load cell attached to it.

1. The part dimensions were input in the software. This allowed the program to automatically calculate stress and strain based on elongation and load.
2. The machine was calibrated by manually moving the top grip edge to be 500 mm (19.685″) above the fixed bottom grip edge. The measurement was made using digital calipers. This location of the top grip was set as the zero point and used for all the trials.
3. The part to be tested was then placed between the wedge grips. Wedge grips are common in tensile testing machines, because they tighten as they are pulled upwards. This helps mitigate the risk of the parts slipping out of the grip. The edges of the grips were aligned with the marks on the samples to help center

the sample between the two grips. The wedge grips were then hand-tightened until locked in place.

4. The force readings were zeroed to cancel out any stresses created in the machine during part setting. This ensured an equal starting point across all the trials.
5. The test was run. The top arm of the machine moved upward at a speed of 2 mm/min until the test part fractured. The elongation and force at fracture were recorded in real time through Tinius Olsen software connected to the tester. The test times ranged between 2 and 7 minutes based on the dimensions and other parameters of the parts.
6. The recorded data was then exported as a .CSV file for analysis in Microsoft Excel. An example data set is presented in Appendix A. The data output by the testing software was the input part dimensions, the strain, and the force. Dividing the force by the cross-sectional area yielded the stress. The stress was then plotted against the strain in order to study the behavior of the ultimate tensile strength.

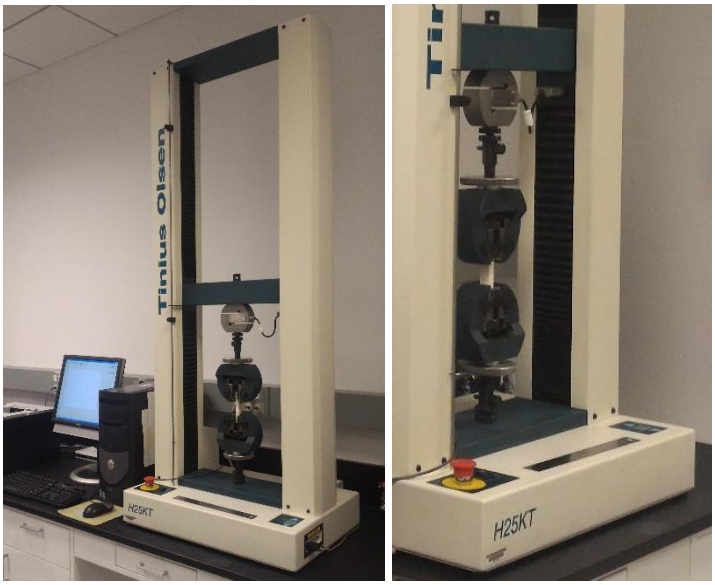

Figure 19: Tinius Olsen H25KT tensile tester setup

4.2 Results and Discussion

In order to begin to understand how build parameters affect 3D printed parts, three different variables were studied: raster orientation, thickness, and clamping force orientation. The density was held constant at the "Sparse – High Density" setting. The parts were all printed with a length of 4 inches, and the distance between wedge grips was always 500 mm (19.685″). In each case, multiple trials were run. The output from each test was a stress vs strain graph.

4.2.1 Effects of Raster Angle Orientation

The first test looked at the effects of raster angle on tensile properties. Looking at the simulations generated by CatalystEX, parts oriented at 45° from the build plate X axis had alternating layers of 0° and 90°. Parts oriented at 90° from the X axis had raster angles alternating between 45° and -45°. These two orientations are the limits of the range of raster angles that can be printed. The first test compared how identical parts

behaved under tension when printed with these two different orientations. Table 3 shows the part parameters used for this test.

Table 3: Parameters of test parts used to determine the effects of raster orientation on part properties

Part Name	Width (in)	Thickness (in)	Raster Angle	UTS 1 (MPa)	UTS 2 (MPa)	UTS 3 (MPa)
OR45°	0.375	0.25	45/-45°	20.52	20.85	20.79
OR90°	0.375	0.25	0/90°	19.80	20.27	20.06

Findings showed that the parts with the 45/-45° raster angle had a higher ultimate tensile strength than those with the 0/90° raster angle. The 45/-45° parts also showed a 6% higher elongation before breaking than the 0/90° parts. However, the Young's moduli were similar for both parts. Figure 20 shows the plots from only one trial at each raster orientation. The plots between trials were similar, so one was selected for illustration purposes.

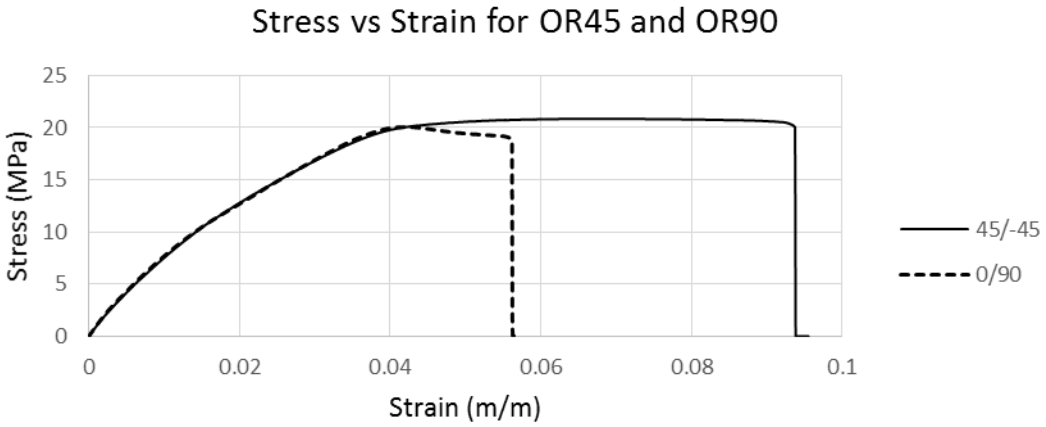

Figure 20: Stress vs strain plot for parts with different raster orientations

The single-factor analysis of variance (ANOVA) results indicate that there is a statistically significant difference at $\alpha = 0.05$ in UTS between the parts with different

raster angle orientations. The full ANOVA analysis for this test is included in Figure 21 to provide clarity.

One-way ANOVA: UTS versus Raster Angle

Method

Null hypothesis	All means are equal
Alternative hypothesis	At least one mean is different
Significance level	α = 0.05

Equal variances were assumed for the analysis.

Factor Information

Factor	Levels	Values
Angle	2	45, 90

Analysis of Variance

Source	DF	Adj SS	Adj MS	F-Value	P-Value
Angle	1	0.6829	0.68295	15.77	0.017
Error	4	0.1732	0.04330		
Total	5	0.8561			

Model Summary

S	R-sq	R-sq(adj)	R-sq(pred)
0.208081	79.77%	74.71%	54.48%

Means

Angle	N	Mean	StDev	95% CI
45	3	20.720	0.177	(20.387, 21.054)
90	3	20.046	0.235	(19.712, 20.379)

Pooled StDev = 0.208081

Figure 21: ANOVA analysis for the effects of raster angle on UTS

These results can be explained by looking at the tensile forces that would be exerted on each layer. In the 45/-45° layers, every layer will be carrying the same load. However, in the layers with alternating 0° and 90° raster angles, the layers with the 90° raster angles will be carrying the vast majority of the load. Because of the gaps between the infill roads, the layers with 0° raster angles will only be carrying load through the shells. This means that only about half of the layers in the part are carrying the majority of the load. Thus, the 0/90° parts fail before the 45/-45° parts. These results are consistent with those found by other researchers (18) (19).

4.2.2 Effects of Varying Thickness

The second test studied the effects of varying thicknesses on 3D printed part tensile properties. The thickness was varied according to Table 4. The raster angle was held constant at 45/-45° because the previous test had shown that this was the strongest

raster orientation. Two trials at each thickness were run. The test procedure was identical to that used for the previous test.

Table 4: Parameters of test parts used to determine the effects of thickness on part properties

Part Name	Width (in)	Thickness (in)	Raster Angle	UTS 1 (MPa)	UTS 2 (MPa)
T15	0.375	0.15	45/-45°	20.81	21.00
T35	0.375	0.35	45/-45°	18.65	18.70
T50	0.375	0.50	45/-45°	17.85	17.80
T65	0.375	0.65	45/-45°	17.54	17.25
T75	0.375	0.75	45/-45°	17.24	17.59
T100	0.375	1.00	45/-45°	16.89	16.96

The results showed that as thickness increased, the modulus and maximum tensile strength decreased (Figure 22). While helpful in understanding properties of 3D printed parts, this behavior can be seen in other materials as well. As a part becomes larger, there is a statistically higher probability that there will be some voids or cracks which will lead to a fracturing under less pressure. This is true for solid materials as well.

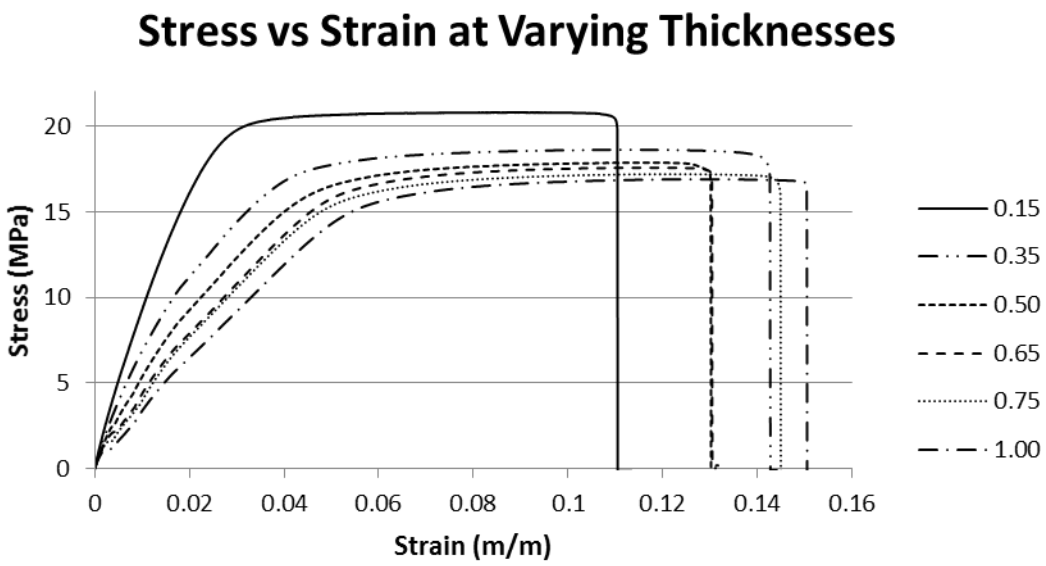

Figure 22: Tensile test results from parts with varying thicknesses

The single-factor analysis of variance (ANOVA) results indicate that there is a statistically significant difference at $\alpha = 0.05$ (p-value = 0.000) in UTS between the parts with different thicknesses. The full ANOVA results can be found in Appendix D.

An interesting behavior was noticed in the region between 1 and 3 MPa in stress. The plot rises steadily for a bit, but then plateaus, as can be seen in Figure 23. After a few tenths of a millimeter, the plot begins to rise again, following the same slope as before,

but shifted slightly. This behavior is visible in all parts with thickness greater or equal to 0.5″, but in none of the thinner parts.

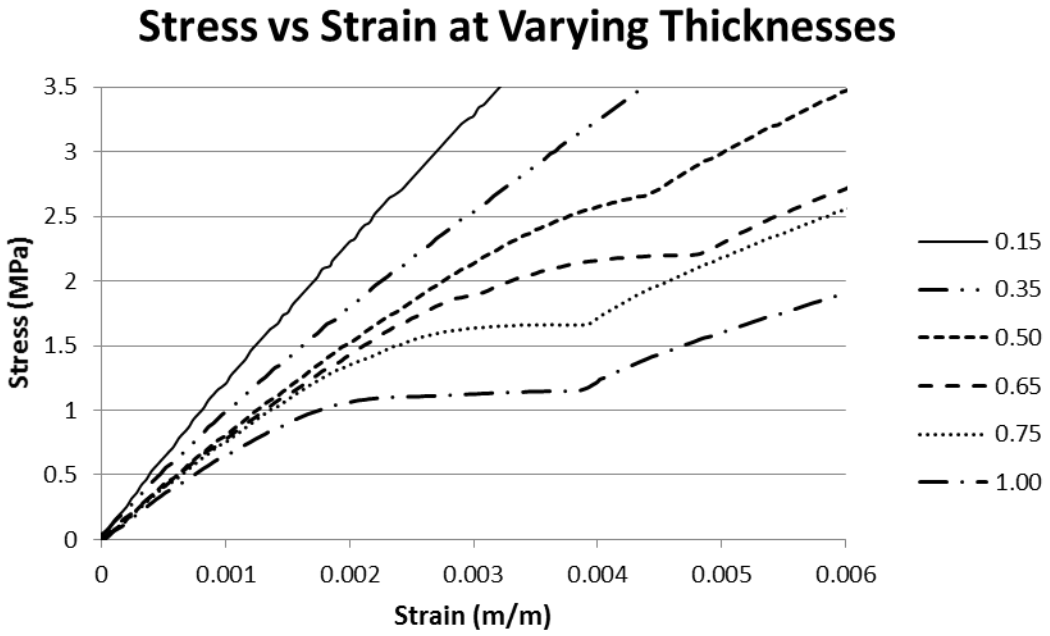

Figure 23: Detail of plot region showing stress plateauing in parts greater than or equal to 0.5 inches

One possible explanation for this behavior is the orientation of the clamping force on the tensile tester. The 0.15″ and 0.35″ thick parts were too thin to be tightened into the grips without rotation. Figure 24 illustrates this issue.

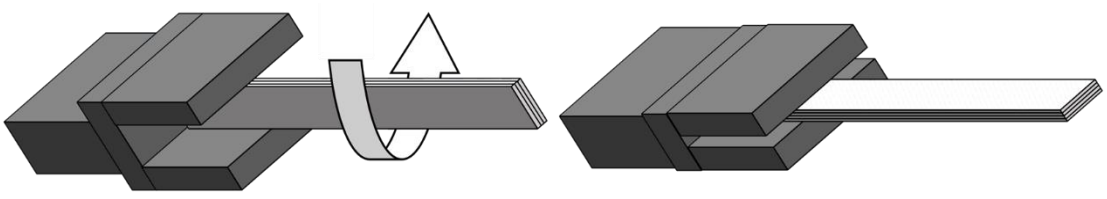

Figure 24: Thin parts clamped in the wedge grips tended to twist as the grips were tightened

4.2.3 Effects of Clamping Orientation

In order to test whether the clamping force orientation caused the plateauing behavior in the stress vs strain plot, another set of parts was printed and tested. These parts had square cross sections with side lengths of 0.25 and 0.5 inches, respectively (Table 5). The same part was tested with the clamping force on the sides of the part and then on the top and bottom of the part (Figure 25). Two trials at each grip orientation were run. The square cross sections eliminated the chance that the aspect ratio with respect to the clamping force played a significant role in the tensile behavior.

Table 5: Parameters of test parts used to determine the effects of clamping force orientation on part properties

Part Name	Width (in)	Thickness (in)	Raster Angle	UTS 1 (MPa)	UTS 2 (MPa)
C25-T	0.25	0.25	45/-45°	22.11	21.97
C25-S	0.25	0.25	45/-45°	22.24	22.32
C50-T	0.50	0.50	45/-45°	18.09	18.15
C50-S	0.50	0.50	45/-45°	18.30	18.46

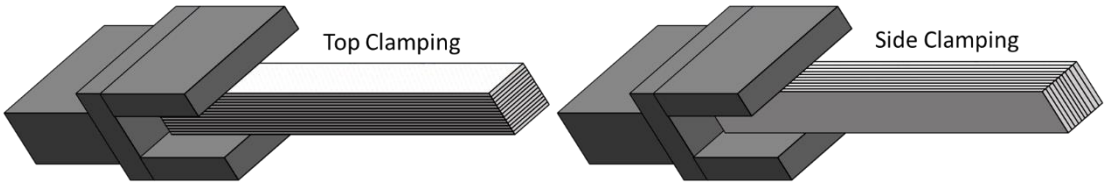

Figure 25: Orientations of parts in the wedge grips with clamping on the sides (left) and on the top and bottom (right)

The results of this test were surprising. Neither of the tests showed the plateauing behavior seen in the thickness test. While there was no plateauing behavior, there was a slight difference between the results from the two clamping force orientations. While small, the results from multiple trials showed the same differences, indicating that even the direction of the clamping force could affect the tensile properties (Figure 26).

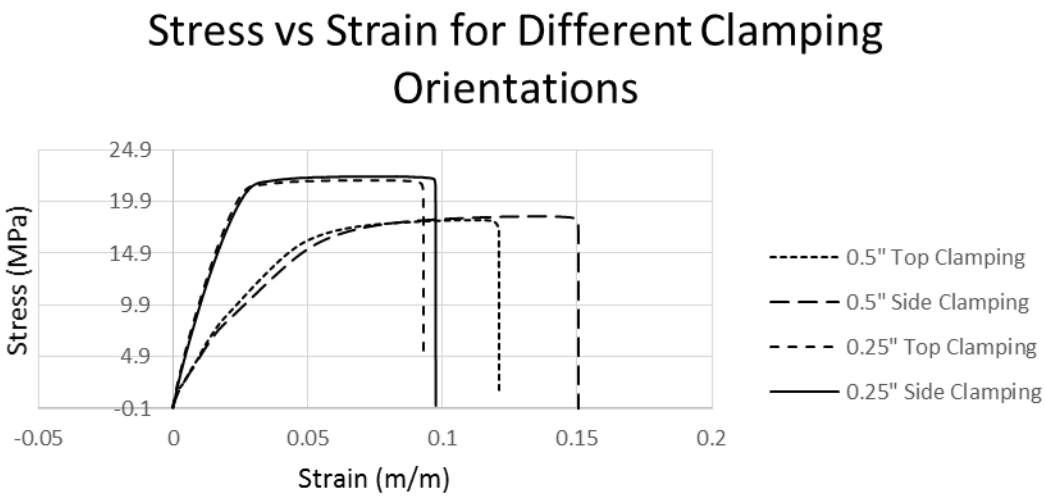

Figure 26: Stress vs strain plot for clamping force orientation test

Observing the test part fracture locations showed that the parts with larger cross-sections failed closer to the edge of the grips than the parts with smaller cross-sections. This could be due to the added stresses from the grips in the larger parts. The smaller parts broke almost exactly in the middle. This is shown in Figure 27 where the black lines show where the edges of the grips were.

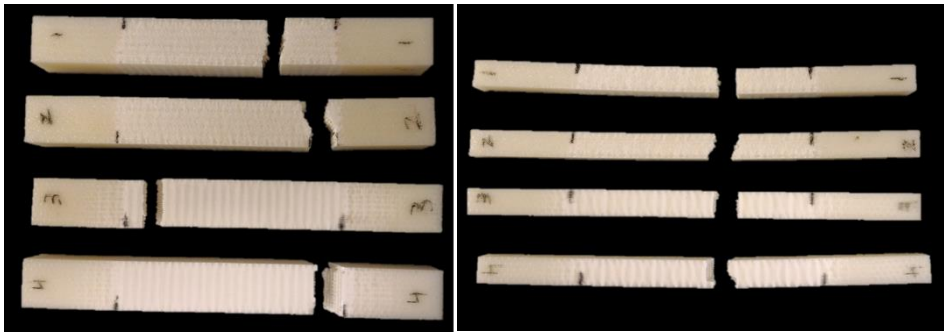

Figure 27: Grip test parts showing fracture planes closer to grip edges in large pieces (left) and more central in smaller pieces (right)

A two-factor ANOVA (cross-sectional area and clamping force orientation) results indicate that there is a statistically significant difference at $\alpha = 0.05$ in UTS between

the parts with different cross-sectional areas (p-value = 0.000) and clamping force orientations (p-value = 0.005). It appears that the relative size of the effects is different.

4.3 Summary of Findings

The results of the pilot tests are as follows:

- Raster orientation test: There is a statistically significant difference in the UTS between parts with rasters oriented at alternating 0/90° and 45/-45°. The 45/-45° raster orientation showed superior strength.
- Thickness test: There is a statistically significant difference in the UTS between parts with different thicknesses. Thicker parts had lower UTS values, likely due to the increased likelihood of crack and void formation.
- Clamping force orientation test: There is a statistically significant difference in the UTS between parts with different cross-sectional areas and clamping force orientations. The larger parts (higher thickness) had a lower UTS value than the smaller parts.

The first two results agree with the literature from Chapter 2, and strengthened the belief that the orientation and thickness play important roles in the determination of 3D printed part tensile strength. The results from the clamping force orientation test indicate the limitations of applying standard test procedures designed for plastics to 3D printed parts. These results motivated a more formal exploration of these and other parameters.

Chapter 5: Factorial Experiment on Key Part Parameters

The significant effects of the parameters of orientation and thickness on UTS have been confirmed. The test parts up to this point have had a constant density. However, the role that the density (determined by the infill roads) played in these results is unknown. From literature and personal practice, it is expected that the infill geometry will play a significant role in the tensile properties of a part. This chapter explores the effects of part width, part thickness, infill density, and their interactions on UTS.

5.1 Methodology

5.1.1 Test Part Dimensions

In order to maintain consistency with the pilot tests, the same rectangular bar shape was used for these tests. A limiting factor was the maximum width of the tensile tester wedge grips. This limited the part thickness to 0.5″.

5.1.2 Design of Experiment

In order to study the effects of parameters and their interactions on tensile properties, it is necessary to use several factors in the study. The factorial design allows the analysis of the effects of multiple single parameters and their interactions at various levels for each factor. Factorial designs are capable of estimating these effects as precisely as a standard test of variance (such as ANOVA), using fewer observations. Three factors were to be chosen, because that was the number necessary to explore the effects of the three types of road geometries common to all 3D printed parts.

Since the exact interaction between parameters is unknown, it was important to have more than two levels for each parameter. Two levels would only be able to show linear effects of the factors. However, having three levels would yield a better understanding of any non-linear relationships between the parameters.

5.1.3 Factor Selection

After deciding on a factorial design, it was necessary to select which parameters would be used as main factors. The effects of the shells on the tensile properties could be studied by modifying the ratio of shells to part infill. This could be accomplished by varying the width of the part. In a similar way, studying the effects of the surface layers could be accomplished by varying the part height. In both these cases, changing the infill density would also alter the relative ratios between shells, surface layers, and infill. The final parameters selected as main factors were the part width, thickness, and infill density.

5.1.4 Factor Level Selection

There were some constraints in choosing the factor levels for this test. The first constraint was with the infill density. In CatalystEX, there are only three possibilities for infill density: Solid, Sparse – High Density, and Sparse – Low Density.

Another constraint was the width of the tensile tester wedge grips. In order to avoid changing the clamping direction for some tests, either the width or the thickness could not be more than 0.625″. In order to explore the plateauing region seen in the thickness tests, the thickness was desired to go beyond the thickness in the previous

experiment, which was more than 0.625″. Because of this, the width would need to be limited to below 0.625″ in order to fit in the grips. Since the dimensions could have any values within the constraints, it was decided to choose values of even increments for the parts. This was done to make trends in the results more apparent. The final factor levels are presented in Table 6. The parts were named according to their dimensions, with the first number representing the width, and the second representing the thickness. For example, part F37.08 is 0.375" wide, and 0.8" thick.

Table 6: Parameter levels used for factorial design

Factor	Level 1	Level 2	Level 3
Width (in)	0.25	0.375	0.50
Thickness (in)	0.4	0.8	1.2
Infill Density	Sparse – Low Infill	Sparse – High Infill	Solid

5.2 Results and Discussion

5.2.1 Visual Results

The fracture behavior is one of these easily observable results. Figure 28 displays some F37.08 parts with varying infill before and after fracture. The fracture surfaces are similar in that they are relatively perpendicular to the applied tensile force. Looking more closely at the sparse - low density parts, the 45° infill roads are clearly visible.

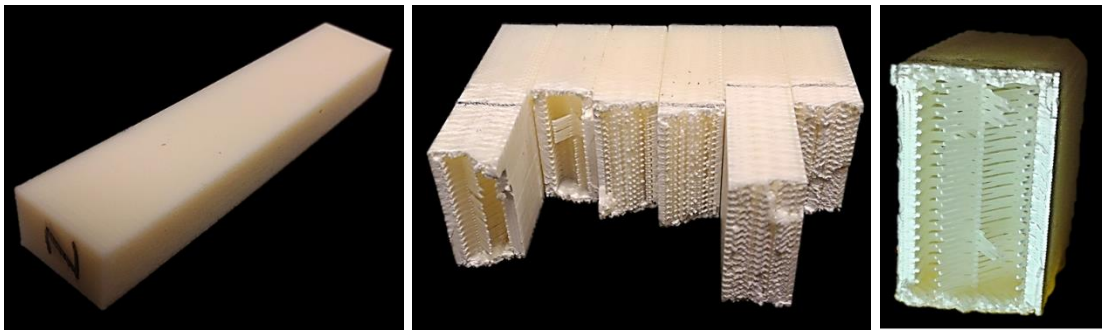

Figure 28: F37.08 test parts before and after testing. Different infills are apparent at the fracture surfaces

The second visual observation is the location of the fracture along the length of the sample. Figure 29 shows the difference between fracture locations for F50.12 and F25.04 parts. The black marks on the samples show the locations of the grip edges. The thicker pieces tended to fracture closer to the grip edge. This behavior was also noticed in the grip test.

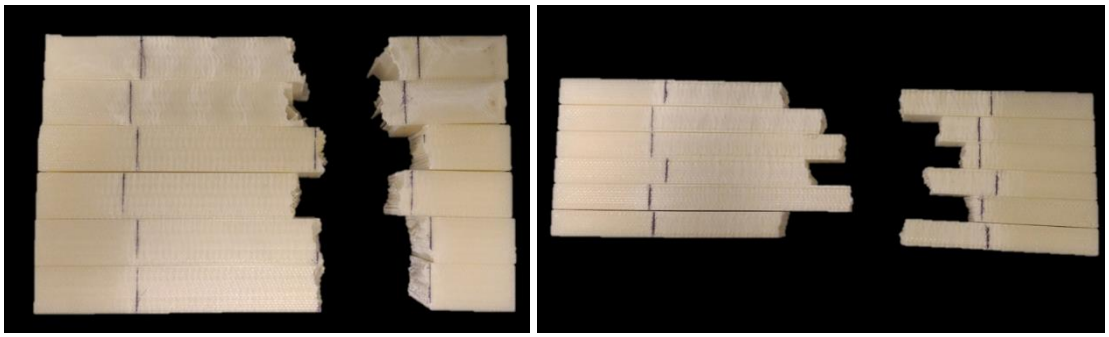

Figure 29: The fracture of larger parts such as F50.12 (left) is much closer to the grip location than smaller parts such as F25.04 (right). The black lines show approximate locations of the grip edge

Fracture along the grip edge is not uncommon in rectangular test strips. The grip introduces additional stresses in a direction perpendicular to the force, adding to the total stress applied on that region. The thicker parts may be more susceptible to this effect, because they have a larger area where the grip is exerting force.

White striations can be observed forming as the parts are being pulled apart (Figure 30). These striations were also observed in the pilot test parts. The color change can be observed in many plastics at points where the part is bent beyond its elastic region. At this point, the color changes to a lighter or white color. This is clearly seen in the LEGO® brick in Figure 31. LEGO® is traditionally made with a type of ABS (like the test parts), and it can be seen that after bending the part in the middle, the black brick turns white.

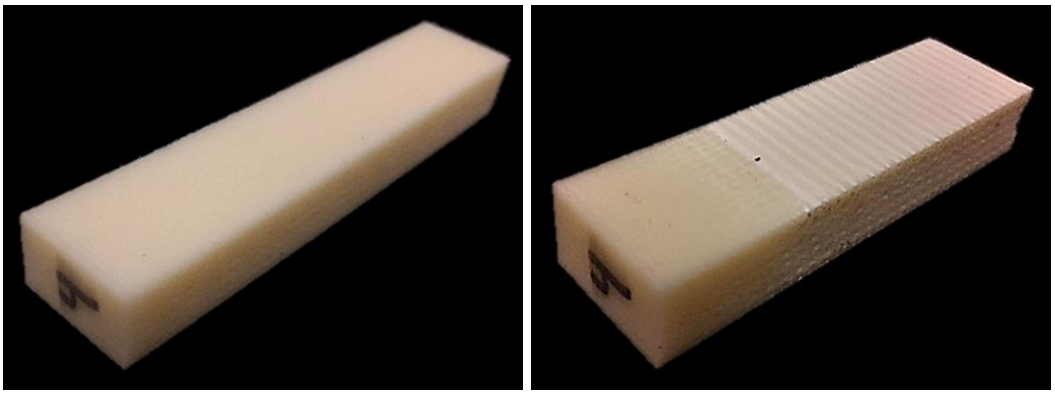

Figure 30: Test part F37.08 before and after testing, showing the development of white striations along the length of the part

Figure 31: LEGO® brick showing color change when bent

Upon closer inspection of the test parts with striations, it can be seen that these stripes line up with the locations where the internal roads connect with the shells (Figure 32). The striation pattern has two main features: the striation height and the striation gap. The striation height is how much white area there is at each striation location. The

striation gap is the distance between striation locations. Figure 33 shows that parts with a sparser infill have a larger striation height and a wider striation gap.

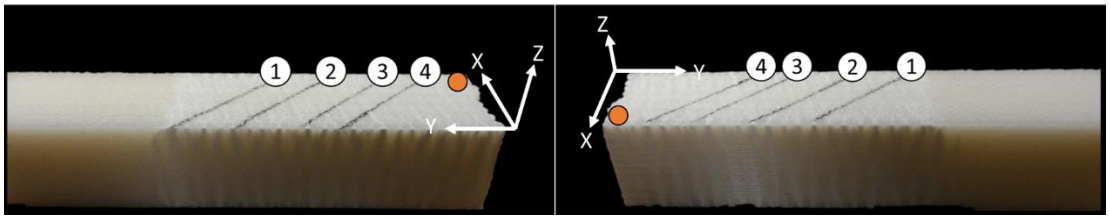

Figure 32: Lines following the 45° raster orientation are drawn on the surface of the part and compared to the locations of the striation. The numbers indicate the same line seen from opposite sides

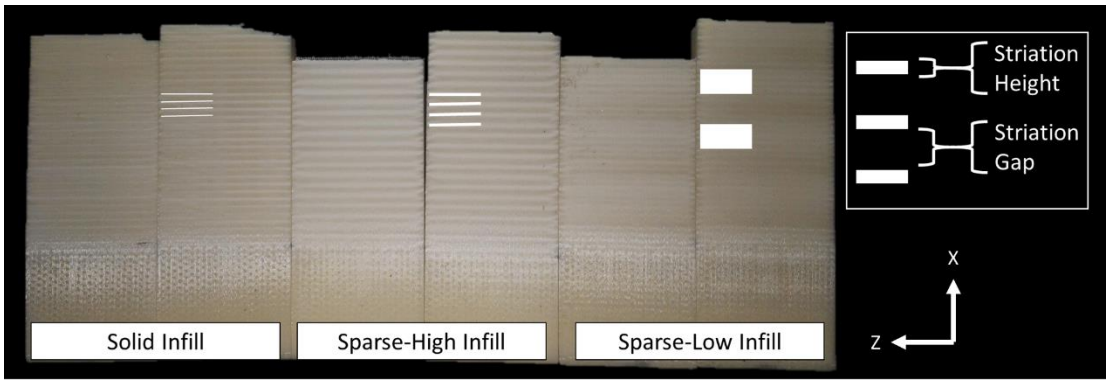

Figure 33: Differences in striation for parts with different density infill. Denser infill shows striations with a smaller striation height and smaller striation gap.

Inferred from this striation appearance is that as the parts are being pulled apart, the internal roads are being pulled inwards and upwards, causing the shells to display a necking behavior. This creates horizontal tension on the shells, which reach the maximum of their elastic deformation and create white lines at the points where they are fused with the infill roads (Figure 34).

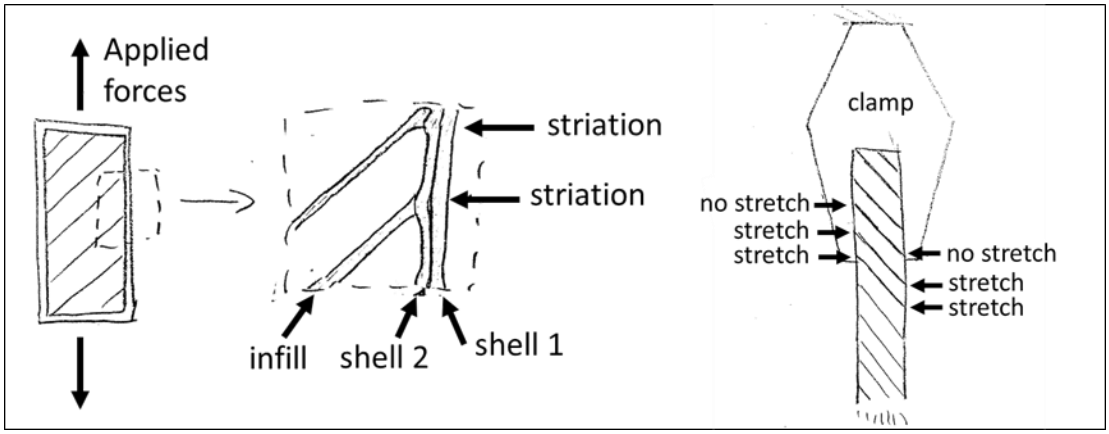

Figure 34: Sketch showing possible reason for development of striations. The infill roads pull the shells beyond their plastic deformation limit, causing the material to turn white

A 45/-45° raster allows the roads to rotate slightly in an attempt to align themselves with the force direction. This rotation pulls on the points where the infill roads meet the shells, causing that point of the shell to be pulled inwards. The parts with alternating 0° and 90° raster orientations do not show this effect as prominently, because there is no rotation of the infill roads. The roads oriented at 90° are already oriented along the force direction, while the roads oriented at 0° mostly experience shear forces from the layers above and below, but little direct force.

In order to test these assumptions, a simplified model of a layer was made and analyzed using FEA analysis in SolidWorks 2014-2015. This model was intended to approximate the behavior of a single layer within the part. In order to give the layer some strength, it was made thicker than a typical layer. It does not show effects of the interactions between layers which occur in a printed part. The results seen in Figure 35 show that points of stress are highest on the side shells when the infill roads are oriented at 45°. With roads oriented at 0°, there are no stress concentration points along the

shell. With the 90° oriented infill roads, stress concentration points developed along the shells, but not nearly as much as in the parts with 45° oriented infill roads.

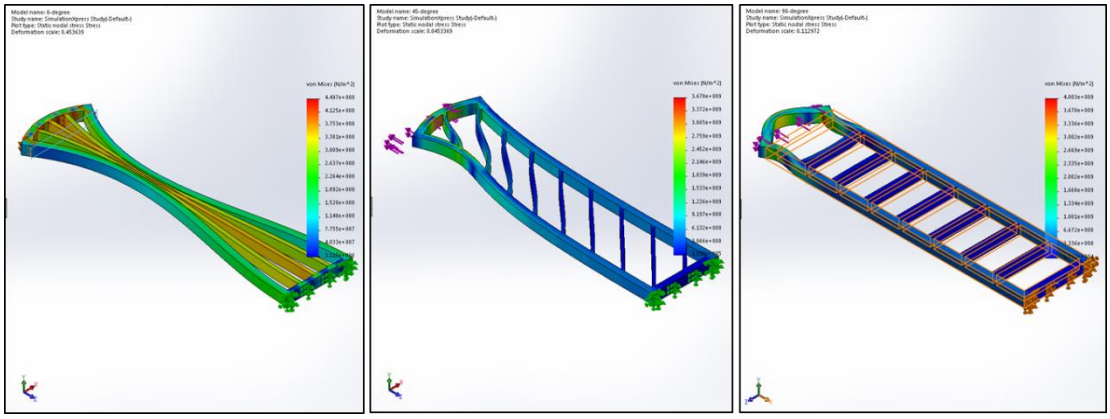

Figure 35: FEA analysis of different infill raster orientations show the stress concentration points along the shells

It can further be observed in Figure 36 that the fracture surfaces occur at the points where these striations are present. This implies that there is a higher stress concentration at the locations where striations occur. Again, this suggests that the infill roads are exerting transverse forces on the interior of the part.

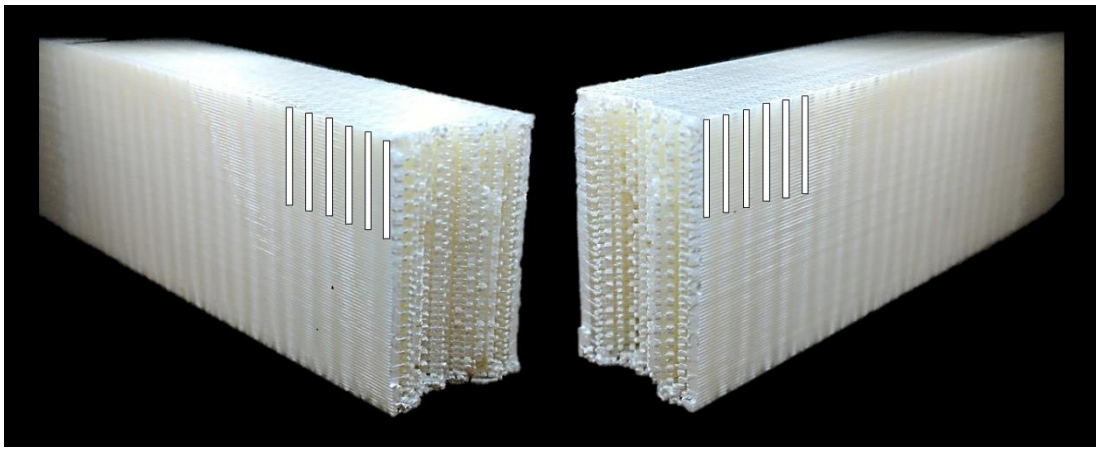

Figure 36: Fractured test part seen from both sides of fracture. White marks highlight the striation locations. The fracture surface lines up with a striation

5.2.2 Numerical Results

Table 7 shows the mean ultimate tensile strengths for each part in the factorial design. The UTS specified by the material data sheet was 33 MPa (35).

After running the tests, the results were plotted. To aid in understanding the differences between the parameters, the plots were organized into a grid. Going from right to left on the grid showed increasing width, while going from bottom to top showed increasing thickness. Each subplot showed the results from the combination of width and thickness corresponding to its plot location. Within each subplot, the results at the different densities were plotted (Figure 37). The full set of plots is given in Appendix B.

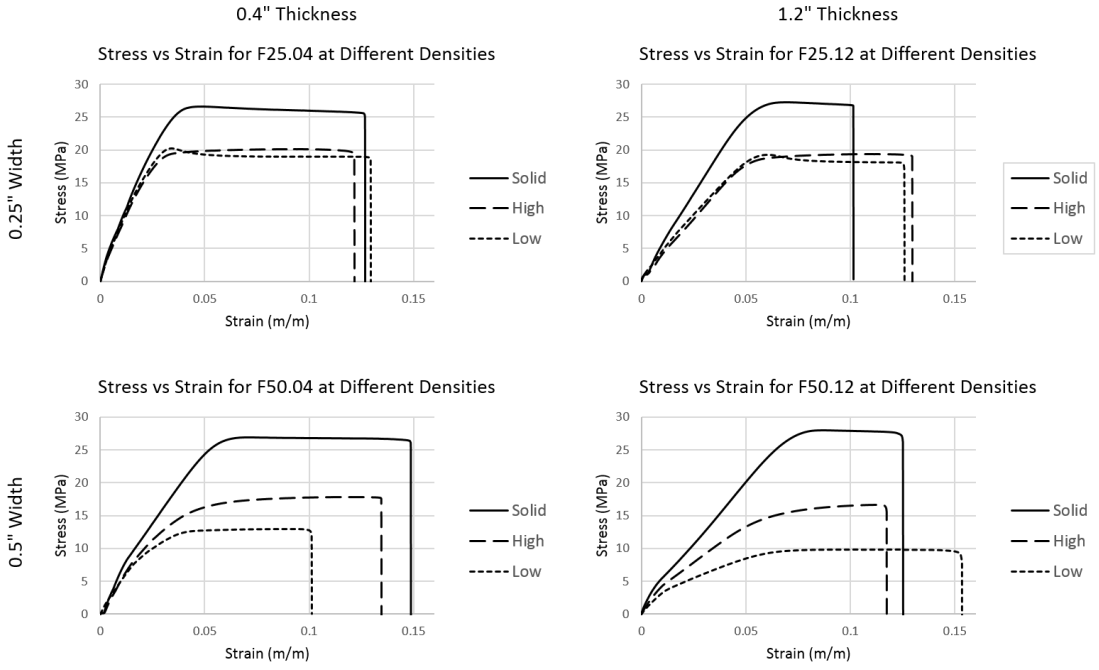

Figure 37: Plots showing factorial test data in grid format with increasing width in the rows, and increasing thickness in the columns. Density is shown within each subplot

The most obvious effect that can be seen is that full density parts have the highest tensile strength. Furthermore, regardless of the width and thickness, the UTS for full density parts is almost constant. This is likely due to the fact that there is a zero or negative air gap between roads in the solid parts. This lack of an air gap causes the individual roads to overlap as they are being deposited, melting onto each other. With the roads melted together, any forces are shared between the joined roads, making the part stronger. When the roads are more strongly bonded together, the load is uniformly distributed. Therefore, the difference in cross sectional area does have an impact on UTS.

Another interesting behavior can be seen across the 0.25″ width row. The difference between the sparse-high and sparse-low density parts is almost indistinguishable. The wider parts show a significant difference between the sparse-high and sparse-low infill. This unchanging behavior across different densities and thicknesses must be explained by some unchanging part characteristic across the different parts. The behavior of the shells could be this unchanging factor. At a constant width, the shells and infill in each layer are constant. Increasing the thickness only increases the number of layers. This data seems to suggest that at small widths the shells are carrying almost the entire load of a sparsely filled part.

As the width increases, there is an increase in the difference between the UTS of the parts with sparse-high and sparse-low density infills. This result is to be expected assuming that the shells are carrying the majority of the load in the 0.25″ wide part. By increasing the width, the ratio between the infill and the shells increases. At some point,

this will lead to the transfer of the load from the shells to the infill. When that happens, having more or less infill will change the UTS of the part.

5.2.3 Statistical Analysis

In order to conduct a more formal analysis of the data, a full factorial design study was created and analyzed in Minitab 17 statistical software. Three independent variables were used: thickness, width, and infill density. UTS was the dependent variable. Running a full factorial analysis with three levels and three factors allowed for the determination of the effects each parameter has on UTS. Table 7 on the following page shows the factors and the UTS output. The interaction effects between parameters were also analyzed.

Table 7: Factorial Trial test parts with UTS means and standard deviation

Part Name	Width (in.)	Thickness (in.)	Infill (%)	UTS 1 (MPa)	UTS 2 (MPa)	Mean UTS (MPa)	Std. Dev.
F25.04-L	0.25	0.4	0.25	20.240	20.254	20.247	0.010
F25.04-H	0.25	0.4	0.75	20.060	19.259	19.659	0.567
F25.04-S	0.25	0.4	1	26.595	26.299	26.447	0.209
F25.08-L	0.25	0.8	0.25	19.414	19.724	19.569	0.219
F25.08-H	0.25	0.8	0.75	18.771	19.654	19.212	0.625
F25.08-S	0.25	0.8	1	27.520	27.063	27.292	0.323
F25.12-L	0.25	1.2	0.25	19.256	19.577	19.416	0.227
F25.12-H	0.25	1.2	0.75	19.375	19.168	19.272	0.146
F25.12-S	0.25	1.2	1	28.551	27.197	27.874	0.957
F37.04-L	0.375	0.4	0.25	14.570	14.518	14.544	0.037
F37.04-H	0.375	0.4	0.75	18.204	18.169	18.187	0.025
F37.04-S	0.375	0.4	1	26.856	26.464	26.660	0.278
F37.08-L	0.375	0.8	0.25	13.464	13.366	13.415	0.069
F37.08-H	0.375	0.8	0.75	17.577	17.474	17.525	0.073
F37.08-S	0.375	0.8	1	27.130	27.838	27.484	0.501
F37.12-L	0.375	1.2	0.25	12.955	12.600	12.777	0.251
F37.12-H	0.375	1.2	0.75	16.971	17.377	17.174	0.287
F37.12-S	0.375	1.2	1	27.001	27.201	27.101	0.141
F50.04-L	0.5	0.4	0.25	12.936	12.652	12.794	0.201
F50.04-H	0.5	0.4	0.75	17.779	18.143	17.961	0.258
F50.04-S	0.5	0.4	1	26.908	27.040	26.974	0.093
F50.08-L	0.5	0.8	0.25	10.637	10.788	10.712	0.107
F50.08-H	0.5	0.8	0.75	16.814	16.969	16.891	0.110
F50.08-S	0.5	0.8	1	27.702	28.055	27.879	0.249
F50.12-L	0.5	1.2	0.25	9.920	9.876	9.898	0.031
F50.12-H	0.5	1.2	0.75	16.665	16.539	16.602	0.090
F50.12-S	0.5	1.2	1	27.993	28.536	28.264	0.384

Before proceeding with the analysis, it was necessary to confirm that the assumptions for a factorial analysis were met. This required plotting the normal probability plot and the versus fits plot. The probability plot shows a normality of standardized residuals due to the generally linear trend of the data points. The general symmetry of the data points in the versus fits plot indicates a homogeneity of variances by. Therefore, the assumptions were satisfied.

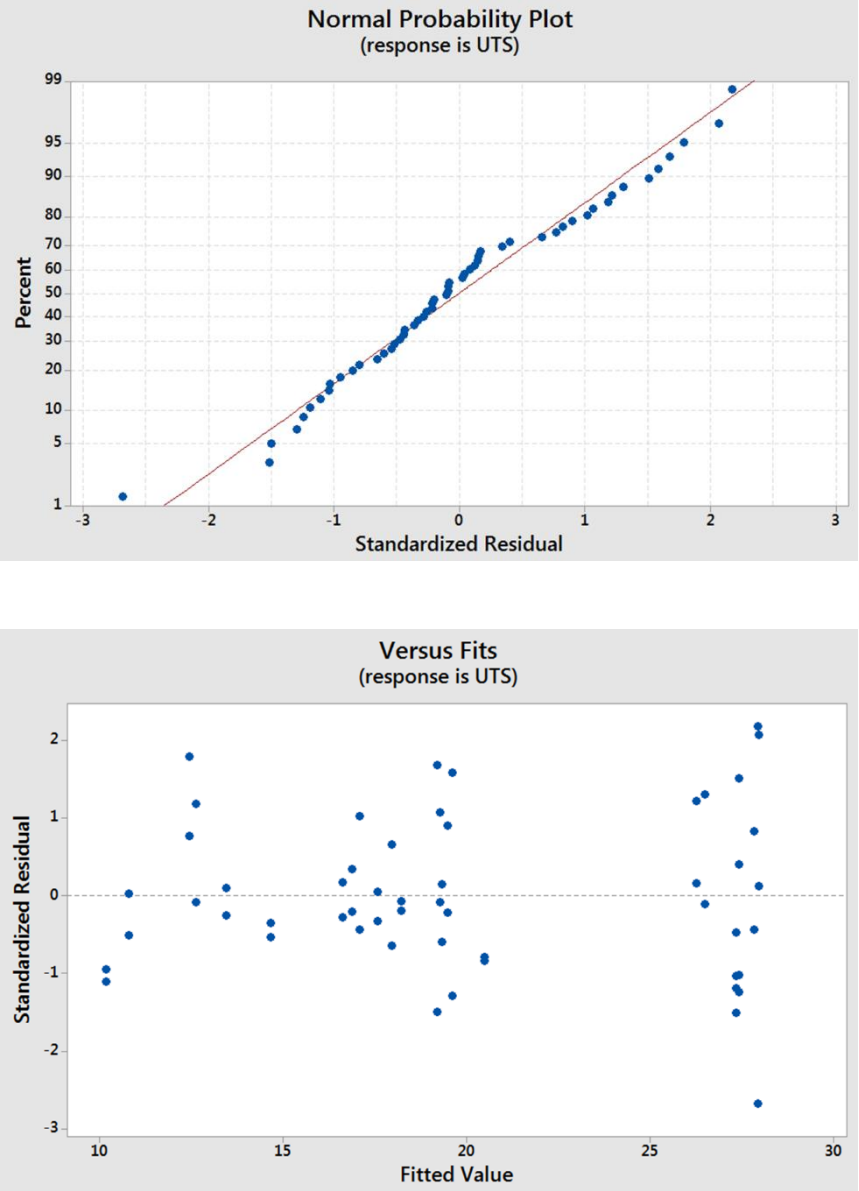

Figure 38: Plots used to test assumptions for factorial ANOVA

After the assumptions were verified, an analysis of variation on the three main factors and their interactions was completed (excluding the three-way interaction) to determine which factors had a statistically significant impact on the UTS. Figure 39 shows the analysis of variance for the full factorial analysis.

Analysis of Variance

Source	DF	Adj SS	Adj MS	F-Value	P-Value
Model	18	1791.70	99.539	832.72	0.000
Linear	6	1639.20	273.200	2285.53	0.000
Width	2	117.86	58.930	493.00	0.000
Thickness	2	3.02	1.508	12.62	0.000
Infill	2	1518.32	759.162	6350.98	0.000
2-Way Interactions	12	152.50	12.708	106.31	0.000
Width*Thickness	4	2.09	0.524	4.38	0.006
Width*Infill	4	136.19	34.048	284.84	0.000
Thickness*Infill	4	14.21	3.552	29.72	0.000
Error	35	4.18	0.120		

Figure 39: ANOVA results for factorial analysis showing main factors and interactions

The ANOVA results showed that all three main factors (width, thickness, and infill density), as well as the interactions between them, were statistically significant. This was an expected result.

The main effects plot is shown in Figure 40. The results agree with the visual analysis made based on looking at the subplots in Figure 37. The width plot suggests a non-linear relationship with the UTS mean. This curve slopes downwards, indicating an inverse relationship between UTS and width. The slope also appears to decrease as the width increases. While it is difficult to say for certain with only three data points, it makes sense that there will be a point where the width will stop having an effect on the UTS. Regardless of the layer shape, there will always be a set number of shells in each layer. As the width increases, the infill density will increase, and the ratio of shells to infill will decrease. The shells will carry less of the load as the infill begins to carry more. Just as the load is carried primarily by shells in the narrow parts, it will be carried primarily by the infill layers in wide parts. This interpretation of the results is consistent with the proposed explanation for striation behavior.

The thickness displays a more linear profile than the other main factors. It also has a shallow slope, indicating that the effect does not have as large an effect on UTS as the other factors. This is reinforced in Figure 37 as well.

The infill density shows the highest slope, indicating the largest effect size, with a marked increase as the density approaches 100%. This makes sense, because the added strength from fully dense parts is due to the overlapping of roads. Once the air gap distance increases to a point where the roads do not overlap, the effect of the density will decrease rapidly.

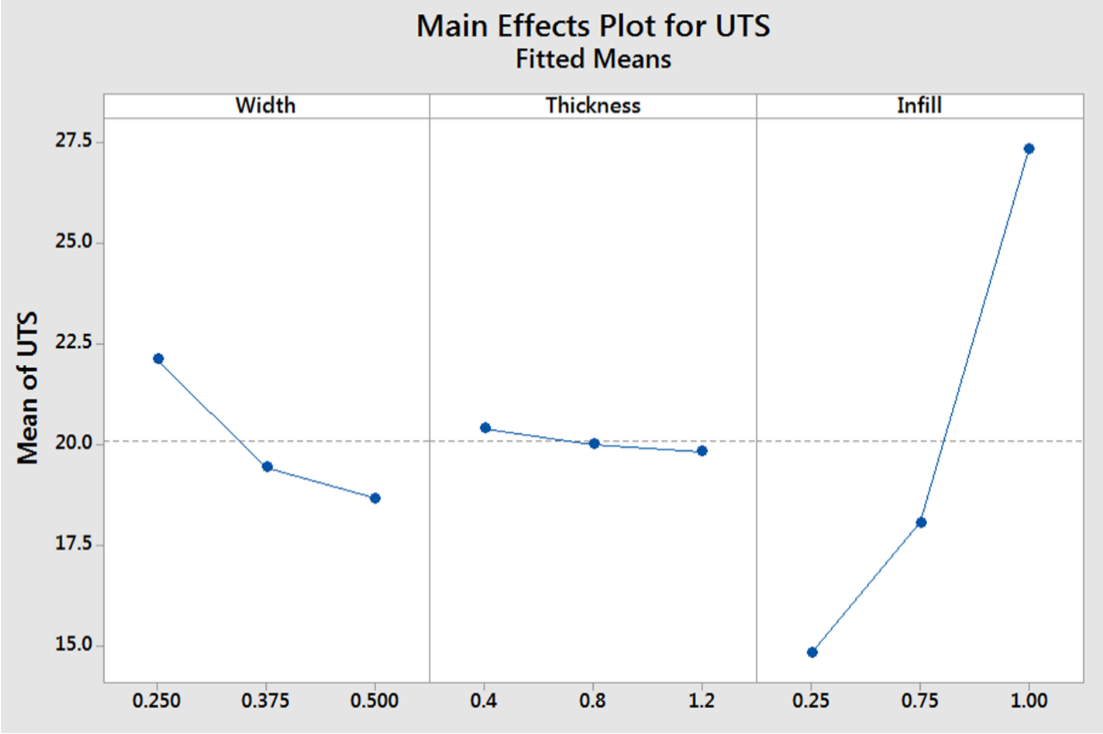

Figure 40: Minitab output showing the fitted means plot for the main effects of UTS

Figure 41 shows the interaction plots. None of the interaction plots show perfectly parallel lines. This implies some level of interaction between all of the variables. The width and infill interaction has the greatest effect size. This makes sense, due to the changing infill to shell ratio.

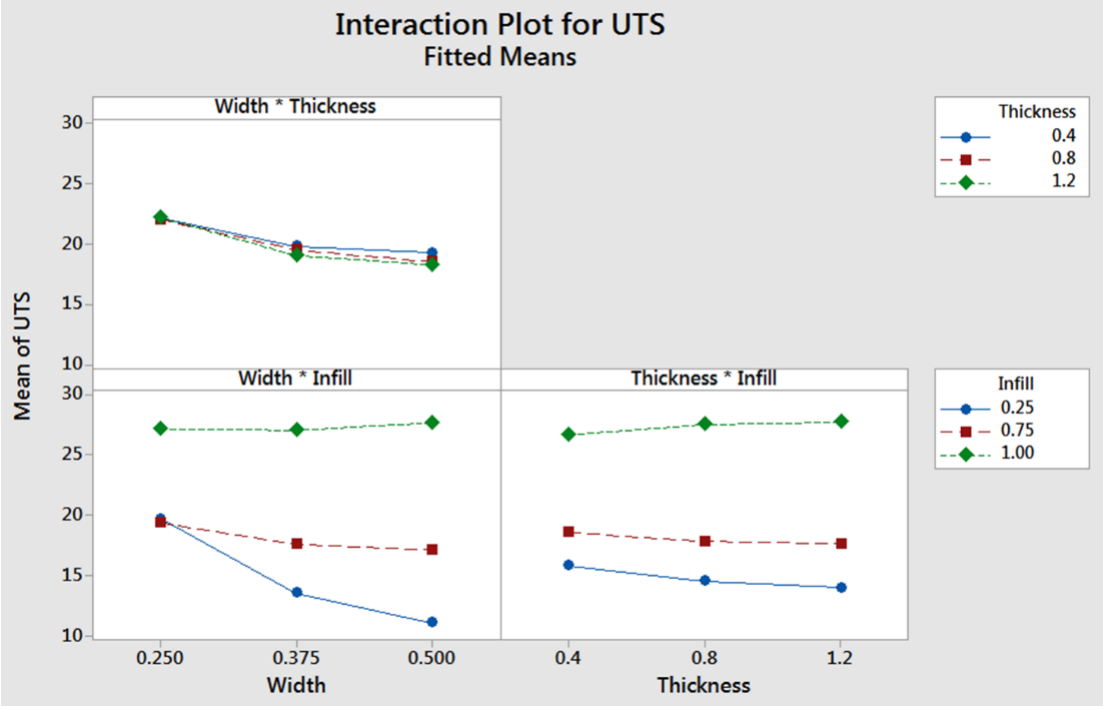

Figure 41: Interaction effects plot

Upon closer inspection of Figure 41, it can be noted that the difference in UTS between the sparse-high and sparse-low density parts is increasing as thickness is increasing. However, it is a smaller change than that seen between the increasing widths.

After analyzing these results, part density was investigated more closely. The part density was determined by dividing the total weight of the part with the total volume. Table 8 shows the part densities for all the parts used in the factorial experiment.

Table 8: Part densities for parts used in factorial experiment

	Density (g/cm^3)								
Part Name	**F50.12**	**F50.08**	**F50.04**	**F37.12**	**F37.08**	**F37.04**	**F25.12**	**F25.08**	**F25.04**
Volume (cm^3)	39.329	26.2193	13.1097	29.4967	19.6645	9.83224	19.6645	13.1097	6.55483
Solid	0.98	0.98	0.98	0.98	0.97	0.98	0.98	0.98	0.98
Sparse - High Infill	0.79	0.80	0.82	0.81	0.81	0.83	0.84	0.85	0.87
Sparse - Low Infill	0.43	0.46	0.52	0.51	0.53	0.57	0.66	0.67	0.70
Material Density	1.04								

An interesting relationship is seen between parts that have the same infill density settings. The parts with a "Solid" infill show a consistent density of 0.98 g/cm^3. However, the part densities of parts with "Sparse" infill vary significantly. The parts with the "Sparse – Low Density" infill range from 0.43 to 0.70 g/cm^3. The material density given by Stratasys states that the material density of the ABS is 1.04 g/cm^3 (35). Therefore, even the "Solid" parts do not have the full density of the material.

The inconsistency in part density at the "Sparse" infill settings showed that part density is not the same as infill density. Part density includes the volume and weight of the shells and surface layers. The actual density of just the part shells and surface layers will be close to the material density, because the spacing between the roads will be very close, with minimal gaps or even overlaps. With changing size, the part density changes, even if the infill density remains constant.

An attempt was made at determining the infill density based on the understanding of the road geometry. The shells and surface layers were modeled as solid blocks due to the zero air gap present between the roads (Figure 42). This is not a perfect estimation, because of the rounded shape of the roads, which create very small gaps at the corners of the roads (Figure 43).

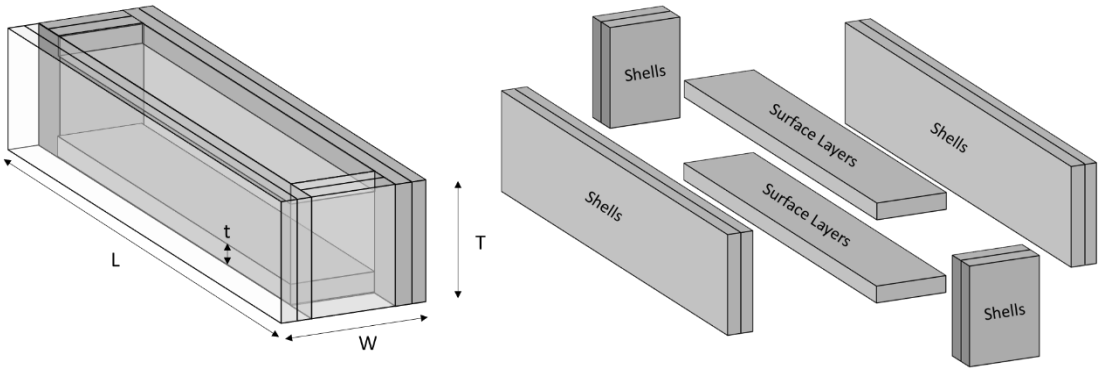

Figure 42: Approximation of shells and surface layers used to determine the infill density.

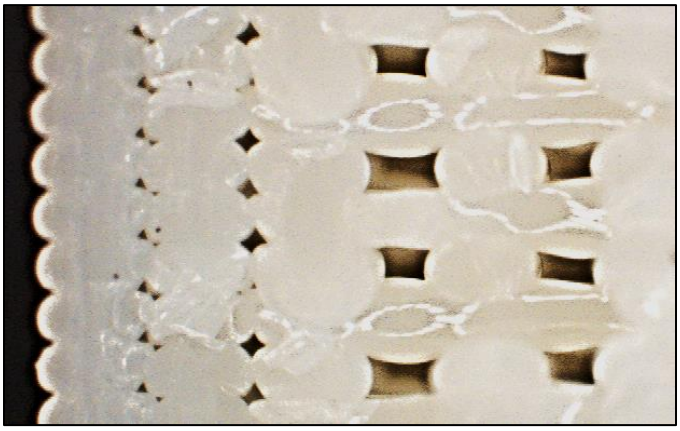

Figure 43: Image taken through microscopy showing miniscule gaps between layers due to the rounded shape of the roads

The volume of each of these rectangular shapes was calculated and summed in order to give an estimate of the total volume occupied by shells and surface layers. The volume was multiplied by the highest density found in the "Solid" parts (0.98 g/cm^3), because that is the maximum achievable density with a zero air gap. This gave the weight of the shells and surface layers, which was then subtracted from the total weight, giving the infill weight. Dividing the infill weight by the infill volume gave the infill density. This density was converted to a percentage, and the results from the analysis were compared in Table 9.

Table 9: Mean and standard deviation between calculated infill percentages for the three infill settings

Infill	Sparse - Low Infill	Sparse - High Infill	Solid
Low	52.9%	62.0%	66.1%
High	62.0%	79.1%	83.1%
Mean	57.8%	71.2%	75.7%
Std. Dev.	2.8%	5.5%	5.4%

These infill percentage calculations show a difference between the infill densities at different settings. However, the large standard deviation points to errors in the assumptions. In reality, the infill density should be identical, or at least negligibly small between parts. The density should not be changing as the part becomes larger, because the spacing between infill roads should be consistent. In addition, the density of the infill of solid parts should be close to the part density, because there should be no difference between layers.

In order to understand how the part density affected the tensile properties, the UTS was plotted against the part density, as seen in Figure 44.

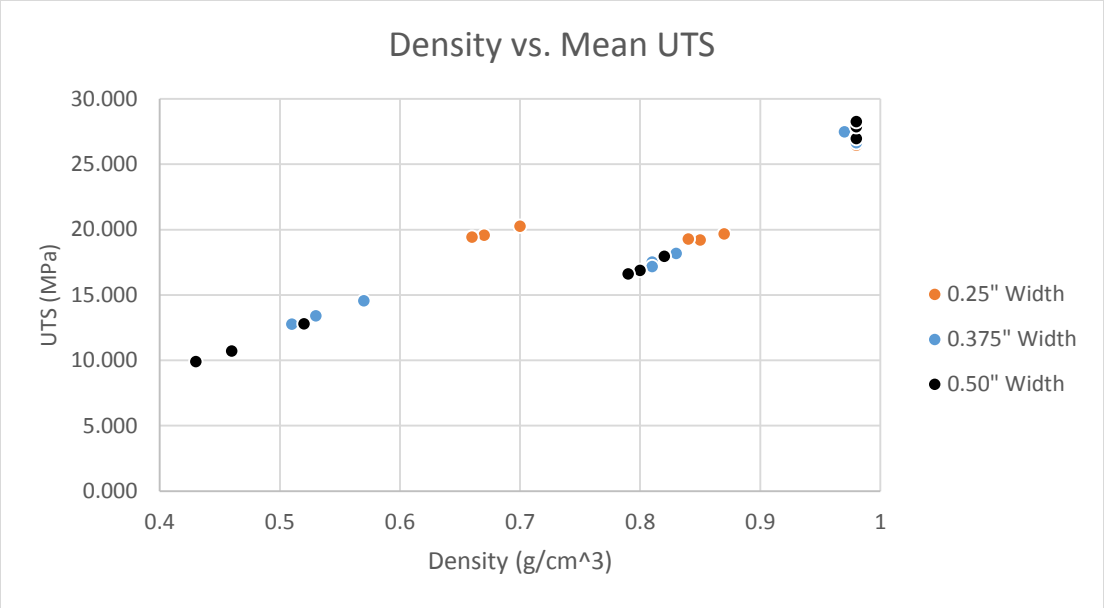

Figure 44: UTS vs Density plot

There is a generally linear trend between the part density and UTS. However, this linear trend breaks down in parts with a 0.25″ width, where the UTS is shown to be the same at densities of about 0.65 g/cm^3 and 0.85 g/cm^3. It is also seen that a part density of 0.98 g/cm^3 corresponds with an almost identical UTS, regardless of part size.

5.3 Analytical Verification

One difficulty in studying the properties of 3D printed parts is the lack of proper finite element analysis (FEA) techniques and programs that allow the simulation of parts under load. This difficulty is due to the anisotropic properties of 3D printed parts. This problem is also seen in other isotropic materials.

A rough, comparative analysis was done using existing FEA methods that are commonly taught to university students. Blocks with the same dimensions as the tested parts were modeled in Creo Parametric 3.0 (Creo). The built-in simulation software

was used with the same constraints and forces found though the factorial experiment. The bottom edges were fixed, while the top edges had a vertical load applied to them, in the same way that the bottom grip was stationary while the top grip pulled upwards in the tensile tester (Figure 45).

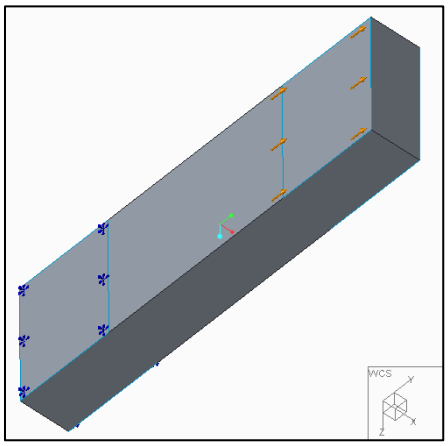

Figure 45: CAD Model showing fixed displacement and applied loads on the edges where grips would be on the tensile tester

Material properties were set as those given by the Stratasys material data sheet (35), with the exception of the density. The density was set as the part density found in Section 5.2. This resulted in a different material model for each part. The applied force for each part was also different. It corresponded with the maximum force applied during the tensile testing of that particular part (see Table 7). The FEA simulation was run, and the displacement of the part was compared with the actual displacement at that force obtained through the factorial experiment. The results can be seen in Table 10.

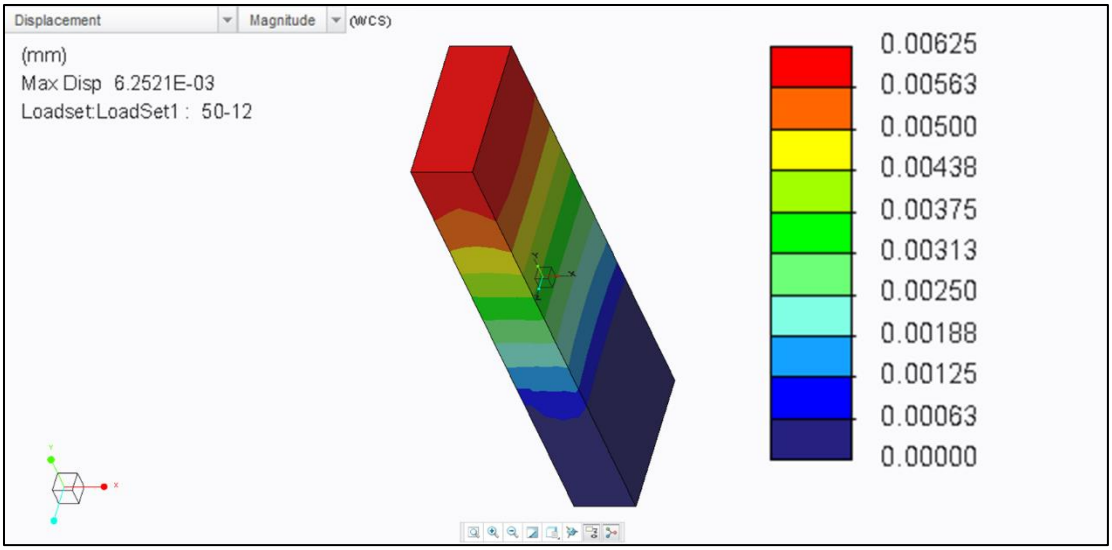

Figure 46: FEA simulation results for F50.12-H

Table 10: Comparison of displacement from FEA simulation and physical testing

	Part	F25.04-S (1)	F25.04-H (2)	F25.04-L (3)	F50.12-S (4)	F50.12-H (5)	F50.12-L (6)
Displacement (mm)	**Measured**	2.369	4.385	1.728	7.200	9.292	7.861
	FEA	0.822	0.611	0.629	0.011	0.006	0.004

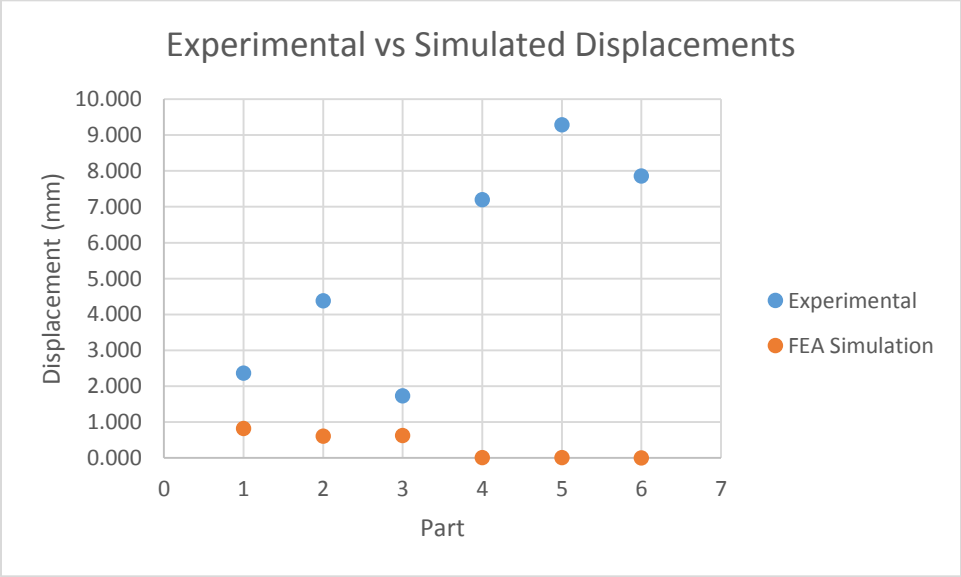

Figure 47: Plot showing the displacement seen experimentally and through FEA simulation

It can be seen that the FEA simulation yielded very different results from the actual displacement seen in the experiments. A different analysis was run, modeling only the

middle section between the grips. The bottom was fixed, and the top had the force applied. The maximum displacement was closer than with the previous simulation, but still very far from the measured value (Figure 48).

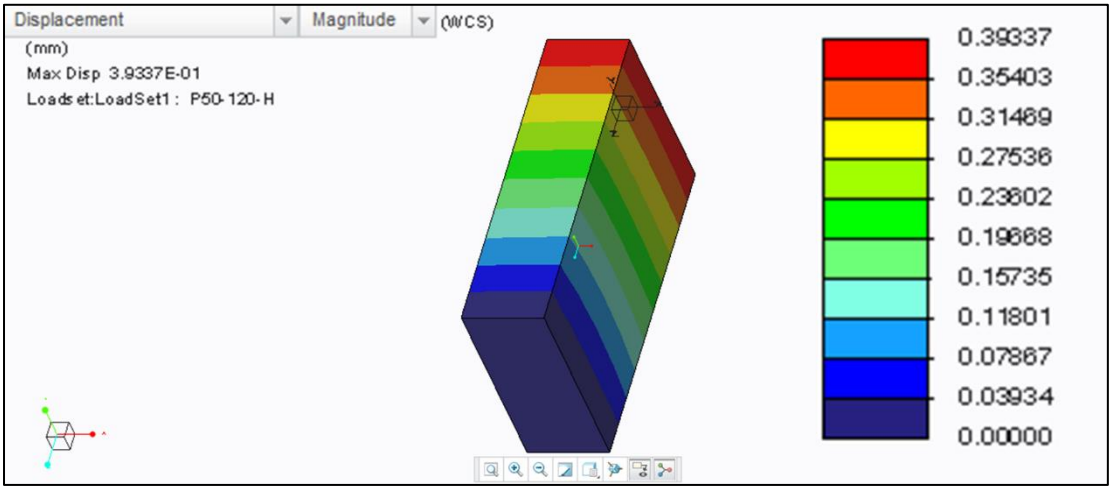

Figure 48: FEA simulation results from modeling only the middle section between grips of F50.12-H

5.4 Summary of Findings

Returning to recent literature, Qureshi's L27 factorial design of 13 factors showed which factors have the greatest effect on part tensile properties. His ranking of the top three factor effects were the component height, the number of shells, and the raster angle. Qureshi's results ranked the infill density as the 11th most important factor that he studied. This thesis shows that infill density was the factor with the greatest effect on UTS (Figure 49).

Rank Number	Factor	Delta
1	Component Scale (thickness)	3.71
2	Number of Shells	2.90
3	Raster Angle	1.26
4	Buildplate Temperature	1.00
5	Speed While Extruding	0.88
6	Layer Thickness	0.87
7	Infill Shell Spacing	0.79
8	Peeling Temperature	0.62
9	Speed While Travelling	0.55
10	Print Location	0.51
11	Infill Density	0.50
12	Infill Pattern	0.44
13	Extruder Temperature	0.03
Total	----------	14.06

Figure 49: Ranking based on the size of the effects of parameters on UTS studied by Qureshi. Highlighted factors are those used in Fornasini factorial experiment.

An explanation of this is that Qureshi's largest component size was significantly smaller than the smallest component size tested here. From the main effects plot and trends seen in the subplots of Figure 37, it can be inferred that the small width of his samples made it so that the shells carried the majority of the load. The results from this factorial design showed that a changes in density of a sparse infill will make very little difference in part properties. In addition, the relative densities used in Qureshi's design were much lower than the ones used in this design.

The results found in this design study and the pilot tests are also consistent. The fracture behavior of larger parts at the grip edges was consistent with those found in the clamping orientation tests. An overall lowering of UTS with an increase in cross-sectional area was seen in the two pilot tests as well as the factorial design results.

The density of the part played a major role in determining the UTS of a part. However, the part density is difficult to calculate from the infill density. The shape of the deposited roads creates small voids between shells and layers, making the volume of

the structure difficult to calculate. This difficulty in modeling the part is seen in the comparison between the FEA analysis and the experimental results. The large difference between the measured and simulated value shows that the solid model based on density estimates is not a good approximation for 3D printed parts.

The results between both previous tests and the literature are consistent. Differences between the results obtained in this factorial design and those obtained in the literature can be explained by the differences in part parameters between the tests, primarily the differences in part dimensions. It is believed that the trends seen in this research, if continued, would align with the results shown in the literature.

Chapter 6: Conclusions and Future Work

Additive manufacturing, including fused deposition modeling (FDM), is transforming the built world and engineering education. Deep understanding of FDM technology has lagged behind its adoption in home, work, and academic environments.

This thesis described three main stages of exploration of the effects of build parameters on tensile failure of 3D printed parts. The first stage focused on the differences between how slicers generated road geometries in part layers (Chapter 3). The second stage consisted of three separate tests studying the effects of varying orientation, thickness, and clamping force orientation on printed parts (Chapter 4). The final stage was conducting a 3^3 full factorial experiment determining the effects on test part UTS from width, thickness, and infill density and their interactions (Chapter 5). The Dimension 1200es printer was used for the printing of all test parts.

6.1 Major Findings

6.1.1 Slicer Differences

Investigation revealed stark differences between the road geometry of shells, infill, and surface layers generated by CatalystEX, Cubify, and Makerbot Desktop slicers. These differences were noted by looking at the layer road simulations generated by the slicers. The same part built on these different printers will look the same from the outside. The differences are only apparent when examining the interior geometry through the simulation.

6.1.2 Research Question: Which 3D printer build parameters and their interactions significantly impact the tensile behavior of the final part?

A series of trials were run in order to obtain preliminary results on the behavior of 3D printed parts under tensile load. The first consisted of varying the orientation of the layers. The second studied the effects of varying part thicknesses. The third tested whether the clamping force had an effect on tensile strength. Performing ANOVA showed the statistical significance of the results. In the final experiment, a 3^3 full factorial design of experiments was developed to test the effects of width, thickness, infill density, and their interactions on UTS. The factorial ANOVA analysis showed that all the main factor and interaction effects were statistically significant at $\alpha = 0.05$. The parts with a higher overall part density are shown to be stronger. This part density is increased by increasing the infill density or reducing the cross-sectional area.

It was shown that the infill density and the part density vary depending on the design of the part. The road geometries responsible for these variations are difficult to model. This makes it difficult to estimate part density prior to printing. The link between part density and UTS makes this estimation important.

Simple FEA simulations also proved to be inadequate for estimating properties based on part density. Neither values nor trends aligned between the simulated and measured values. Better techniques are required in order to simulate 3D printed parts for FEA analysis. The complex interactions between the individual roads in layers must be modeled. In order to create accurate models, there must be a communication between the slicers and the finite element simulation.

Together, the formal experiments answer the research question for the parameters of raster orientation, width, thickness, and infill density. The failure behavior observations discussed in Chapters 4 and 5 linked differences in part UTS to shell and infill road geometries.

6.2 Contributions

Contributions from this thesis are summarized below:

- *The printers used in this study were selected based on their prominent use in academic institutions*. Two of the printers required proprietary software that significantly limited build parameter options.
- *The test sample dimensions used in this study were larger than most standards for plastics tensile testing*. The standards used by others researchers severely limited the size of test samples. The influence of the road geometry of shells and the infill is most significant when the shell to infill ratio is high. The influence is greatly reduced with the ratio. This led to different results than those found by Qureshi. *This work shows that the standards for testing traditionally made plastics are not adequate for testing 3D printed parts*. A new series of standards should be developed that takes into account the intended dimensions of the final part.
- *This study focused on differences between part parameters that determine road geometries.* Other studies covered the effects of the road deposition process. A full factorial design experiment was done to investigate the effects of interactions between these parameters.

6.3 Ramifications

Engineers, especially, must become more aware about how 3D printed parts behave. At the most basic level, a part will look solid, but is not. It has anisotropic properties that would not be expected from a solid part. The part properties cannot be inferred solely by the material properties and the shape of the part. The road orientations play a critical role, a fact of which engineers could easily be unaware.

Understanding how a slicer works is essential to the advancement of 3D printing into end-use parts. While closed slicers make the process of printing parts easier, they hide the variables of the process, and hinder the development of technical competence. So learning outcomes from courses on AM should include these topics. The increase in adoption of open-source printers gives the opportunity to control build processes, but requires an understanding of how process variable affect parts. This is a natural trade-off in the use of FDM manufacturing.

6.4 Future Work

The logical next steps in this research include the following:

- Expanding the range of part property values studied in the factorial experiment. This necessitates the acquisition of new tensile testing equipment.
- Investigating additional factors through CatalystEX, or other slicers (e.g., raster orientations not offset by 90°, different infill patterns, layer height, and road width).

- Performing tensile tests on prototype parts built for ME department student design projects.

The rapid advances of AM technology will continue to generate technical research questions for years to come.

Appendices

Appendix A: Full Data Set for OR45 Trial 1

Strain (m/m)	Force (N)	Strain (m/m)	Force (N)	Strain (m/m)	Force (N)
0	0	0.00134	76.67	0.0028	149.17
0	0	0.00138	79.17	0.00284	151.67
0	0	0.00142	80.83	0.00288	153.33
0.00002	0.8333	0.00146	83.33	0.00292	155
0.00006	2.5	0.0015	85.83	0.00296	156.67
0.00008	4.167	0.00154	87.5	0.003	159.17
0.00012	5	0.00158	90	0.00304	160.83
0.00016	7.5	0.00164	91.67	0.00308	162.5
0.0002	10.833	0.00168	94.17	0.00312	164.17
0.00024	13.333	0.00172	96.67	0.00318	165.83
0.00028	15.833	0.00176	98.33	0.00322	167.5
0.00032	19.167	0.0018	100.83	0.00326	169.17
0.00038	21.67	0.00184	102.5	0.0033	171.67
0.00042	24.17	0.00188	105	0.00334	173.33
0.00046	26.67	0.00192	106.67	0.00338	175
0.0005	29.17	0.00196	109.17	0.00342	176.67
0.00054	31.67	0.002	110.83	0.00346	178.33
0.00058	34.17	0.00204	113.33	0.0035	180
0.00062	36.67	0.00208	115.83	0.00354	181.67
0.00066	39.17	0.00212	117.5	0.00358	183.33
0.0007	41.67	0.00216	119.17	0.00362	185
0.00074	44.17	0.00222	121.67	0.00366	187.5
0.0008	46.67	0.00226	124.17	0.00372	189.17
0.00084	49.17	0.0023	125.83	0.00376	190.83
0.00088	50.83	0.00234	127.5	0.0038	193.33
0.00092	53.33	0.00238	130	0.00384	195
0.00096	55.83	0.00242	131.67	0.00388	196.67
0.001	58.33	0.00246	134.17	0.00392	198.33
0.00104	60	0.0025	135.83	0.00396	200.8
0.00108	62.5	0.00254	138.33	0.004	202.5
0.00112	65	0.00258	140	0.00404	204.2
0.00116	67.5	0.00262	141.67	0.00408	206.7
0.00122	70	0.00266	143.33	0.00414	208.3
0.00126	71.67	0.0027	145.83	0.00416	210
0.0013	74.17	0.00276	147.5	0.0042	211.7

Strain (m/m)	Force (N)	Strain (m/m)	Force (N)	Strain (m/m)	Force (N)
0.00424	214.2	0.00596	288.3	0.00766	357.5
0.0043	215.8	0.006	290	0.0077	359.2
0.00434	217.5	0.00604	291.7	0.00776	360.8
0.00438	219.2	0.00608	293.3	0.0078	362.5
0.00442	220.8	0.00612	295	0.00784	364.2
0.00446	223.3	0.00616	296.7	0.00788	365.8
0.0045	225	0.00622	298.3	0.00792	367.5
0.00454	226.7	0.00626	300	0.00796	369.2
0.00458	228.3	0.0063	301.7	0.008	370.8
0.00462	230.8	0.00634	303.3	0.00804	372.5
0.00466	232.5	0.00638	305	0.00808	374.2
0.00472	234.2	0.00642	307.5	0.00812	375.8
0.00476	235.8	0.00646	309.2	0.00818	377.5
0.0048	237.5	0.0065	310.8	0.00822	379.2
0.00484	240	0.00654	312.5	0.00826	380.8
0.00488	241.7	0.00658	314.2	0.0083	381.7
0.00492	243.3	0.00664	315.8	0.00834	383.3
0.00496	245	0.00668	317.5	0.00838	385
0.005	246.7	0.0067	319.2	0.00842	386.7
0.00504	249.2	0.00674	320.8	0.00846	388.3
0.00508	250	0.0068	322.5	0.0085	390
0.00512	252.5	0.00684	324.2	0.00854	391.7
0.00516	254.2	0.00688	325.8	0.00858	393.3
0.0052	255.8	0.00692	327.5	0.00862	395
0.00526	257.5	0.00696	329.2	0.00866	396.7
0.0053	260	0.007	330.8	0.00872	398.3
0.00534	261.7	0.00704	332.5	0.00876	399.2
0.00538	263.3	0.00708	334.2	0.0088	401.7
0.00542	265	0.00712	335.8	0.00884	402.5
0.00546	266.7	0.00716	337.5	0.00888	404.2
0.0055	268.3	0.00722	339.2	0.00892	405.8
0.00554	270	0.00726	340.8	0.00896	407.5
0.00558	271.7	0.0073	342.5	0.009	409.2
0.00562	274.2	0.00734	344.2	0.00904	410.8
0.00568	275.8	0.00738	345.8	0.00908	412.5
0.00572	277.5	0.00742	347.5	0.00914	414.2
0.00576	279.2	0.00746	349.2	0.00918	415.8
0.0058	280.8	0.0075	350.8	0.00922	416.7
0.00584	282.5	0.00754	352.5	0.00924	419.2
0.00588	284.2	0.00758	354.2	0.0093	420
0.00592	285.8	0.00762	355.8	0.00934	421.7

Strain (m/m)	Force (N)	Strain (m/m)	Force (N)	Strain (m/m)	Force (N)
0.00938	423.3	0.01108	485.8	0.0128	545
0.00942	425	0.01112	487.5	0.01284	546.7
0.00946	426.7	0.01116	489.2	0.01288	547.5
0.0095	428.3	0.01122	490.8	0.01292	549.2
0.00954	430	0.01126	491.7	0.01296	550.8
0.00958	431.7	0.0113	493.3	0.013	551.7
0.00962	432.5	0.01134	495	0.01304	553.3
0.00966	434.2	0.01138	496.7	0.01308	555
0.00972	435.8	0.01142	498.3	0.01312	556.7
0.00976	437.5	0.01146	499.2	0.01318	557.5
0.0098	439.2	0.0115	500.8	0.01322	559.2
0.00984	440.8	0.01154	502.5	0.01326	560
0.00988	442.5	0.01158	503.3	0.0133	561.7
0.00992	443.3	0.01162	505	0.01334	563.3
0.00996	445.8	0.01166	506.7	0.01338	565
0.01	446.7	0.0117	508.3	0.01342	565.8
0.01004	448.3	0.01174	509.2	0.01346	567.5
0.01008	450	0.0118	510.8	0.0135	568.3
0.01012	451.7	0.01184	512.5	0.01354	570
0.01016	452.5	0.01188	513.3	0.01358	571.7
0.0102	454.2	0.01192	515	0.01362	572.5
0.01026	455.8	0.01196	516.7	0.01366	574.2
0.0103	457.5	0.012	518.3	0.0137	575
0.01034	459.2	0.01204	520	0.01376	576.7
0.01038	460.8	0.01208	520.8	0.0138	578.3
0.01042	461.7	0.01212	522.5	0.01384	579.2
0.01046	463.3	0.01216	524.2	0.01388	580.8
0.0105	465	0.01222	525	0.01392	581.7
0.01054	466.7	0.01226	526.7	0.01396	583.3
0.01058	468.3	0.0123	528.3	0.014	584.2
0.01062	470	0.01234	530	0.01404	585.8
0.01068	470.8	0.01238	530.8	0.01408	587.5
0.01072	472.5	0.01242	532.5	0.01412	588.3
0.01076	474.2	0.01246	534.2	0.01418	590
0.0108	475.8	0.0125	535	0.01422	590.8
0.01084	477.5	0.01254	536.7	0.01426	592.5
0.01088	478.3	0.01258	538.3	0.0143	593.3
0.01092	480	0.01262	540	0.01434	595
0.01096	481.7	0.01266	540.8	0.01438	595.8
0.011	483.3	0.0127	542.5	0.01442	596.7
0.01104	485	0.01276	543.3	0.01446	598.3

Strain (m/m)	Force (N)	Strain (m/m)	Force (N)	Strain (m/m)	Force (N)
0.0145	600	0.0162	648.3	0.01792	696.7
0.01454	600.8	0.01626	649.2	0.01796	697.5
0.01458	602.5	0.0163	650.8	0.018	698.3
0.01462	603.3	0.01634	651.7	0.01804	700
0.01468	604.2	0.01638	653.3	0.01808	700.8
0.01472	605.8	0.01642	654.2	0.01812	701.7
0.01476	607.5	0.01646	655	0.01816	703.3
0.0148	608.3	0.0165	656.7	0.01822	704.2
0.01484	610	0.01654	657.5	0.01826	705
0.01488	610.8	0.01658	659.2	0.0183	706.7
0.01492	611.7	0.01662	660	0.01834	707.5
0.01496	613.3	0.01668	661.7	0.01838	709.2
0.015	614.2	0.0167	662.5	0.01842	710
0.01504	615.8	0.01674	663.3	0.01846	710.8
0.01508	616.7	0.0168	665	0.0185	712.5
0.01512	618.3	0.01684	665.8	0.01854	713.3
0.01516	619.2	0.01688	666.7	0.01858	714.2
0.0152	620	0.01692	668.3	0.01864	715.8
0.01526	621.7	0.01696	669.2	0.01868	716.7
0.0153	623.3	0.017	670.8	0.0187	718.3
0.01534	624.2	0.01704	671.7	0.01876	719.2
0.01538	625	0.01708	672.5	0.0188	720
0.01542	626.7	0.01712	674.2	0.01884	721.7
0.01546	627.5	0.01716	675.8	0.01888	722.5
0.0155	629.2	0.01722	676.7	0.01892	724.2
0.01554	630	0.01726	677.5	0.01896	725
0.01558	630.8	0.0173	679.2	0.019	725.8
0.01562	632.5	0.01734	680	0.01904	726.7
0.01568	633.3	0.01738	681.7	0.01908	728.3
0.01572	635	0.01742	682.5	0.01912	729.2
0.01576	635.8	0.01746	683.3	0.01918	730.8
0.0158	636.7	0.0175	685	0.01922	731.7
0.01584	638.3	0.01754	685.8	0.01926	732.5
0.01588	639.2	0.01758	687.5	0.0193	734.2
0.01592	640	0.01764	688.3	0.01934	735
0.01596	641.7	0.01768	689.2	0.01938	735.8
0.016	642.5	0.01772	690.8	0.01942	736.7
0.01604	644.2	0.01776	691.7	0.01946	738.3
0.0161	645	0.0178	692.5	0.0195	739.2
0.01612	645.8	0.01784	694.2	0.01954	740.8
0.01616	647.5	0.01788	695	0.01958	741.7

Strain (m/m)	Force (N)	Strain (m/m)	Force (N)	Strain (m/m)	Force (N)
0.01962	742.5	0.02134	787.5	0.02304	830
0.01966	744.2	0.02138	788.3	0.02308	830.8
0.0197	745	0.02142	790	0.02312	831.7
0.01976	745.8	0.02146	790.8	0.02316	832.5
0.0198	746.7	0.0215	791.7	0.02322	833.3
0.01984	748.3	0.02154	792.5	0.02326	834.2
0.01988	749.2	0.02158	794.2	0.0233	835.8
0.01992	750.8	0.02162	795	0.02334	836.7
0.01996	751.7	0.02168	795.8	0.02338	837.5
0.02	752.5	0.02172	797.5	0.02342	838.3
0.02004	754.2	0.02176	798.3	0.02346	839.2
0.02008	755	0.0218	799.2	0.0235	840.8
0.02012	755.8	0.02184	800	0.02354	841.7
0.02018	757.5	0.02188	800.8	0.02358	842.5
0.02022	758.3	0.02192	802.5	0.02364	843.3
0.02026	759.2	0.02196	803.3	0.02366	844.2
0.0203	760.8	0.022	804.2	0.02372	845.8
0.02034	761.7	0.02204	805	0.02374	846.7
0.02038	762.5	0.02208	806.7	0.0238	847.5
0.02042	764.2	0.02212	807.5	0.02384	848.3
0.02046	765	0.02216	808.3	0.02388	849.2
0.0205	765.8	0.0222	809.2	0.02392	850.8
0.02054	767.5	0.02226	810	0.02396	851.7
0.02058	768.3	0.0223	811.7	0.024	852.5
0.02062	769.2	0.02234	812.5	0.02404	853.3
0.02066	770.8	0.02238	813.3	0.02408	854.2
0.02072	771.7	0.02242	814.2	0.02412	855.8
0.02076	772.5	0.02246	815.8	0.02416	856.7
0.0208	773.3	0.0225	816.7	0.02422	857.5
0.02084	775	0.02254	817.5	0.02426	858.3
0.02088	775.8	0.02258	818.3	0.0243	859.2
0.02092	776.7	0.02262	819.2	0.02434	860.8
0.02096	778.3	0.02268	820.8	0.02438	861.7
0.021	779.2	0.02272	821.7	0.02442	862.5
0.02104	780	0.02276	822.5	0.02446	863.3
0.02108	780.8	0.0228	823.3	0.0245	865
0.02112	782.5	0.02284	824.2	0.02454	865.8
0.02116	783.3	0.02288	825.8	0.02458	866.7
0.0212	784.2	0.02292	826.7	0.02464	867.5
0.02126	785.8	0.02296	827.5	0.02466	869.2
0.0213	786.7	0.023	828.3	0.0247	870

Strain (m/m)	Force (N)	Strain (m/m)	Force (N)	Strain (m/m)	Force (N)
0.02476	870.8	0.02646	911.7	0.02816	952.5
0.0248	871.7	0.0265	912.5	0.0282	953.3
0.02484	872.5	0.02654	914.2	0.02826	954.2
0.02488	874.2	0.02658	915	0.0283	955
0.02492	875	0.02662	915.8	0.02834	955.8
0.02496	875.8	0.02666	916.7	0.02838	956.7
0.025	876.7	0.02672	917.5	0.02842	958.3
0.02504	877.5	0.02676	919.2	0.02846	959.2
0.02508	878.3	0.0268	920	0.0285	960
0.02512	880	0.02684	920.8	0.02854	960.8
0.02516	880.8	0.02688	921.7	0.02858	961.7
0.02522	881.7	0.02692	922.5	0.02862	962.5
0.02526	882.5	0.02696	923.3	0.02868	964.2
0.0253	884.2	0.027	925	0.02872	965
0.02534	885	0.02704	925.8	0.02876	965.8
0.02538	885.8	0.02708	926.7	0.0288	966.7
0.02542	886.7	0.02714	927.5	0.02884	967.5
0.02546	887.5	0.02718	928.3	0.02888	969.2
0.0255	889.2	0.02722	929.2	0.02892	970
0.02554	890	0.02726	930.8	0.02896	970.8
0.02558	890.8	0.0273	931.7	0.029	971.7
0.02562	891.7	0.02734	932.5	0.02904	972.5
0.02568	892.5	0.02738	933.3	0.02908	973.3
0.0257	894.2	0.02742	934.2	0.02912	974.2
0.02576	895	0.02746	935	0.02916	975
0.0258	895.8	0.0275	936.7	0.02922	975.8
0.02584	896.7	0.02754	937.5	0.02926	977.5
0.02588	898.3	0.02758	938.3	0.0293	978.3
0.02592	898.3	0.02762	939.2	0.02934	979.2
0.02596	900	0.02766	940	0.02938	980
0.026	900.8	0.02772	940.8	0.02942	980.8
0.02604	901.7	0.02776	942.5	0.02946	981.7
0.02608	902.5	0.0278	943.3	0.0295	983.3
0.02612	904.2	0.02784	944.2	0.02954	984.2
0.02618	905	0.02788	945	0.02958	985
0.02622	905.8	0.02792	945.8	0.02964	985.8
0.02626	906.7	0.02796	946.7	0.02968	986.7
0.0263	907.5	0.028	948.3	0.02972	987.5
0.02634	909.2	0.02804	949.2	0.02976	989.2
0.02638	910	0.02808	950	0.0298	990
0.02642	910.8	0.02812	950.8	0.02984	990.8

Strain (m/m)	Force (N)	Strain (m/m)	Force (N)	Strain (m/m)	Force (N)
0.02988	991.7	0.03158	1029.2	0.0333	1065
0.02992	992.5	0.03162	1030	0.03334	1065.8
0.02996	993.3	0.03166	1030.8	0.03338	1066.7
0.03	994.2	0.03172	1031.7	0.03342	1067.5
0.03004	995	0.03176	1032.5	0.03346	1068.3
0.03008	996.7	0.0318	1033.3	0.0335	1069.2
0.03012	997.5	0.03184	1035	0.03354	1070
0.03016	998.3	0.03188	1035	0.03358	1071.7
0.03022	999.2	0.03192	1036.7	0.03362	1071.7
0.03026	1000	0.03196	1037.5	0.03368	1072.5
0.0303	1000.8	0.032	1038.3	0.03372	1073.3
0.03034	1001.7	0.03204	1039.2	0.03376	1074.2
0.03038	1003.3	0.03208	1040	0.0338	1075
0.03042	1004.2	0.03214	1040.8	0.03384	1075.8
0.03046	1005	0.03218	1041.7	0.03388	1076.7
0.0305	1005.8	0.0322	1042.5	0.03392	1077.5
0.03054	1006.7	0.03224	1043.3	0.03396	1078.3
0.03058	1007.5	0.0323	1044.2	0.034	1079.2
0.03062	1008.3	0.03234	1045	0.03404	1080
0.03066	1009.2	0.03238	1046.7	0.03408	1080.8
0.0307	1010	0.03242	1046.7	0.03412	1081.7
0.03076	1010.8	0.03246	1048.3	0.03416	1082.5
0.0308	1012.5	0.0325	1049.2	0.03422	1083.3
0.03084	1013.3	0.03254	1050	0.03426	1084.2
0.03088	1014.2	0.03258	1050.8	0.0343	1085
0.03092	1015	0.03262	1051.7	0.03434	1085.8
0.03096	1015.8	0.03266	1052.5	0.03438	1086.7
0.031	1016.7	0.03272	1053.3	0.03442	1087.5
0.03104	1017.5	0.03276	1054.2	0.03446	1088.3
0.03108	1018.3	0.0328	1055	0.0345	1089.2
0.03112	1019.2	0.03284	1055.8	0.03454	1090
0.03118	1020.8	0.03288	1056.7	0.03458	1090.8
0.03122	1021.7	0.03292	1057.5	0.03464	1091.7
0.03126	1021.7	0.03296	1058.3	0.03468	1092.5
0.0313	1022.5	0.033	1059.2	0.0347	1093.3
0.03134	1024.2	0.03304	1060	0.03474	1094.2
0.03138	1025	0.03308	1060.8	0.0348	1095
0.03142	1025.8	0.03312	1061.7	0.03484	1095.8
0.03146	1026.7	0.03316	1062.5	0.03488	1096.7
0.0315	1027.5	0.0332	1063.3	0.03492	1096.7
0.03154	1028.3	0.03326	1064.2	0.03496	1098.3

Strain (m/m)	Force (N)	Strain (m/m)	Force (N)	Strain (m/m)	Force (N)
0.035	1099.2	0.03672	1129.2	0.03842	1155
0.03504	1099.2	0.03676	1130	0.03846	1155.8
0.03508	1100	0.0368	1130.8	0.0385	1156.7
0.03512	1100.8	0.03684	1130.8	0.03854	1156.7
0.03516	1101.7	0.03688	1131.7	0.03858	1157.5
0.03522	1102.5	0.03692	1132.5	0.03862	1158.3
0.03526	1103.3	0.03696	1133.3	0.03868	1158.3
0.0353	1104.2	0.037	1134.2	0.03872	1159.2
0.03534	1105	0.03704	1135	0.03876	1159.2
0.03538	1105.8	0.03708	1135	0.0388	1160
0.03542	1106.7	0.03712	1135.8	0.03884	1160.8
0.03546	1107.5	0.03716	1136.7	0.03888	1160.8
0.0355	1107.5	0.0372	1137.5	0.03892	1161.7
0.03554	1108.3	0.03724	1137.5	0.03896	1162.5
0.03558	1109.2	0.0373	1138.3	0.039	1162.5
0.03562	1110	0.03734	1139.2	0.03904	1163.3
0.03566	1110.8	0.03738	1140	0.03908	1163.3
0.0357	1111.7	0.03742	1140	0.03912	1164.2
0.03576	1112.5	0.03746	1140.8	0.03916	1165
0.0358	1113.3	0.0375	1141.7	0.0392	1165
0.03584	1114.2	0.03754	1142.5	0.03926	1165.8
0.03588	1115	0.03758	1143.3	0.0393	1166.7
0.03592	1115	0.03762	1143.3	0.03934	1166.7
0.03596	1115.8	0.03766	1144.2	0.03938	1167.5
0.036	1116.7	0.03772	1145	0.03942	1167.5
0.03604	1117.5	0.03776	1145.8	0.03946	1168.3
0.03608	1118.3	0.0378	1145.8	0.0395	1168.3
0.03612	1119.2	0.03784	1146.7	0.03954	1169.2
0.03618	1120	0.03788	1147.5	0.03958	1169.2
0.03622	1120.8	0.03792	1148.3	0.03962	1170
0.03626	1120.8	0.03796	1148.3	0.03968	1170.8
0.0363	1121.7	0.038	1149.2	0.03972	1170.8
0.03634	1122.5	0.03804	1150	0.03974	1171.7
0.03638	1123.3	0.03808	1150.8	0.0398	1171.7
0.03642	1124.2	0.03816	1151.7	0.03984	1172.5
0.03646	1125	0.0382	1151.7	0.03988	1172.5
0.0365	1125.8	0.03822	1152.5	0.03992	1173.3
0.03654	1126.7	0.03826	1153.3	0.03996	1173.3
0.03658	1126.7	0.0383	1153.3	0.04	1174.2
0.03662	1127.5	0.03834	1154.2	0.04004	1174.2
0.03666	1128.3	0.03838	1154.2	0.04008	1175

Strain (m/m)	Force (N)	Strain (m/m)	Force (N)	Strain (m/m)	Force (N)
0.04012	1175.8	0.04184	1190	0.04354	1199.2
0.04018	1175.8	0.04188	1190	0.04358	1199.2
0.04022	1175.8	0.04192	1190	0.04362	1200
0.04026	1176.7	0.04196	1190.8	0.04368	1200
0.0403	1176.7	0.042	1190.8	0.04372	1200
0.04034	1177.5	0.04204	1190.8	0.04376	1200
0.04038	1177.5	0.04208	1191.7	0.0438	1200.8
0.04042	1178.3	0.04212	1191.7	0.04384	1200.8
0.04046	1178.3	0.04218	1191.7	0.04388	1200.8
0.0405	1179.2	0.0422	1191.7	0.04392	1200.8
0.04054	1179.2	0.04226	1191.7	0.04396	1200.8
0.04058	1180	0.0423	1192.5	0.044	1201.7
0.04064	1180	0.04234	1192.5	0.04404	1201.7
0.04068	1180.8	0.04238	1192.5	0.04408	1201.7
0.0407	1180.8	0.04242	1193.3	0.04412	1201.7
0.04076	1181.7	0.04246	1193.3	0.04416	1202.5
0.0408	1181.7	0.0425	1193.3	0.0442	1202.5
0.04084	1181.7	0.04254	1194.2	0.04426	1202.5
0.04088	1182.5	0.04258	1194.2	0.0443	1202.5
0.04092	1183.3	0.04262	1194.2	0.04434	1203.3
0.04096	1183.3	0.04266	1194.2	0.04438	1203.3
0.041	1183.3	0.04272	1195	0.04442	1203.3
0.04104	1184.2	0.04276	1195	0.04446	1203.3
0.04108	1184.2	0.0428	1195	0.0445	1203.3
0.04112	1184.2	0.04284	1195.8	0.04454	1204.2
0.04118	1185	0.04288	1195.8	0.04458	1204.2
0.04122	1185	0.04292	1195.8	0.04462	1204.2
0.04126	1185	0.04296	1195.8	0.04468	1204.2
0.0413	1185.8	0.043	1196.7	0.04472	1204.2
0.04134	1185.8	0.04304	1196.7	0.04476	1205
0.04138	1186.7	0.04308	1196.7	0.0448	1205
0.04142	1186.7	0.04314	1197.5	0.04484	1205
0.04146	1186.7	0.04316	1197.5	0.04488	1205
0.0415	1187.5	0.0432	1197.5	0.04492	1205.8
0.04154	1187.5	0.04326	1198.3	0.04496	1205.8
0.04158	1188.3	0.0433	1198.3	0.045	1205.8
0.04162	1188.3	0.04334	1198.3	0.04504	1205.8
0.04166	1188.3	0.04338	1198.3	0.04508	1205.8
0.0417	1189.2	0.04342	1198.3	0.04512	1205.8
0.04176	1189.2	0.04346	1199.2	0.04516	1206.7
0.0418	1189.2	0.0435	1199.2	0.04522	1206.7

Strain (m/m)	Force (N)	Strain (m/m)	Force (N)	Strain (m/m)	Force (N)
0.04526	1206.7	0.04696	1213.3	0.04866	1219.2
0.0453	1206.7	0.047	1213.3	0.04872	1219.2
0.04534	1207.5	0.04704	1214.2	0.04876	1219.2
0.04538	1207.5	0.04708	1213.3	0.0488	1219.2
0.04542	1207.5	0.04712	1214.2	0.04884	1220
0.04546	1207.5	0.04718	1214.2	0.04888	1220
0.0455	1207.5	0.04722	1214.2	0.04892	1220
0.04554	1207.5	0.04726	1214.2	0.04896	1220
0.04558	1208.3	0.0473	1214.2	0.049	1220
0.04564	1208.3	0.04734	1214.2	0.04904	1220
0.04568	1208.3	0.04738	1215	0.04908	1220
0.0457	1208.3	0.04742	1215	0.04914	1220.8
0.04576	1208.3	0.04746	1215	0.04916	1220.8
0.0458	1209.2	0.0475	1215	0.04922	1220.8
0.04584	1209.2	0.04754	1215	0.04926	1220.8
0.04588	1209.2	0.04758	1215	0.0493	1220.8
0.04592	1209.2	0.04762	1215.8	0.04934	1220.8
0.04596	1209.2	0.04766	1215.8	0.04938	1221.7
0.046	1210	0.04772	1215.8	0.04942	1221.7
0.04604	1210	0.04776	1215.8	0.04946	1221.7
0.04608	1210	0.04778	1215.8	0.0495	1221.7
0.04612	1210	0.04782	1215.8	0.04954	1221.7
0.04618	1210	0.04788	1215.8	0.04958	1221.7
0.04622	1210	0.04792	1216.7	0.04962	1221.7
0.04626	1210.8	0.04796	1216.7	0.04966	1221.7
0.0463	1210.8	0.048	1216.7	0.04972	1222.5
0.04634	1210.8	0.04804	1216.7	0.04976	1222.5
0.04638	1210.8	0.04808	1217.5	0.0498	1222.5
0.04642	1211.7	0.04812	1217.5	0.04984	1222.5
0.04646	1211.7	0.04818	1217.5	0.04988	1222.5
0.0465	1211.7	0.0482	1217.5	0.04992	1222.5
0.04654	1211.7	0.04824	1217.5	0.04996	1223.3
0.04658	1211.7	0.0483	1217.5	0.05	1223.3
0.04664	1212.5	0.04834	1218.3	0.05004	1223.3
0.04668	1212.5	0.04838	1218.3	0.05008	1223.3
0.04672	1212.5	0.04842	1218.3	0.05012	1223.3
0.04676	1212.5	0.04846	1218.3	0.05018	1223.3
0.0468	1213.3	0.0485	1218.3	0.0502	1223.3
0.04684	1213.3	0.04854	1218.3	0.05026	1224.2
0.04688	1213.3	0.04858	1219.2	0.0503	1224.2
0.04692	1213.3	0.04862	1219.2	0.05034	1224.2

Strain (m/m)	Force (N)	Strain (m/m)	Force (N)	Strain (m/m)	Force (N)
0.05038	1224.2	0.05208	1228.3	0.0538	1231.7
0.05042	1224.2	0.05212	1228.3	0.05384	1231.7
0.05046	1224.2	0.05216	1228.3	0.05388	1231.7
0.0505	1224.2	0.05222	1228.3	0.05392	1231.7
0.05054	1224.2	0.05226	1228.3	0.05396	1232.5
0.05058	1224.2	0.0523	1229.2	0.054	1232.5
0.05062	1225	0.05234	1229.2	0.05404	1232.5
0.05068	1225	0.05238	1229.2	0.05408	1232.5
0.05072	1225	0.05242	1229.2	0.05414	1232.5
0.05076	1225	0.05246	1229.2	0.05418	1232.5
0.0508	1225	0.0525	1229.2	0.0542	1232.5
0.05084	1225	0.05254	1229.2	0.05424	1232.5
0.05088	1225.8	0.05258	1229.2	0.0543	1232.5
0.05092	1225.8	0.05262	1229.2	0.05434	1232.5
0.05096	1225.8	0.05266	1229.2	0.05438	1232.5
0.051	1225.8	0.0527	1229.2	0.05442	1232.5
0.05104	1225.8	0.05276	1230	0.05446	1232.5
0.05108	1225.8	0.0528	1230	0.0545	1232.5
0.05112	1225.8	0.05284	1230	0.05454	1232.5
0.05116	1225.8	0.05288	1230	0.05458	1232.5
0.05122	1225.8	0.05292	1230	0.05462	1233.3
0.05126	1226.7	0.05296	1230	0.05466	1233.3
0.0513	1226.7	0.053	1230	0.05472	1233.3
0.05134	1226.7	0.05304	1230	0.05476	1233.3
0.05138	1226.7	0.05308	1230	0.0548	1233.3
0.05142	1226.7	0.05312	1230.8	0.05484	1233.3
0.05146	1226.7	0.05316	1230.8	0.05488	1233.3
0.0515	1226.7	0.05322	1230.8	0.05492	1233.3
0.05154	1226.7	0.05326	1230.8	0.05496	1233.3
0.05158	1226.7	0.0533	1230.8	0.055	1233.3
0.05164	1226.7	0.05334	1230.8	0.05504	1234.2
0.05166	1227.5	0.05338	1230.8	0.05508	1234.2
0.05172	1227.5	0.05342	1230.8	0.05514	1234.2
0.05174	1227.5	0.05346	1230.8	0.05518	1234.2
0.0518	1227.5	0.0535	1230.8	0.0552	1234.2
0.05184	1227.5	0.05354	1230.8	0.05526	1234.2
0.05188	1227.5	0.05358	1231.7	0.0553	1234.2
0.05192	1228.3	0.05362	1231.7	0.05534	1234.2
0.05196	1228.3	0.05366	1231.7	0.05538	1234.2
0.052	1228.3	0.05372	1231.7	0.05542	1234.2
0.05204	1228.3	0.05376	1231.7	0.05546	1234.2

Strain (m/m)	Force (N)	Strain (m/m)	Force (N)	Strain (m/m)	Force (N)
0.0555	1234.2	0.05722	1236.7	0.05892	1238.3
0.05554	1235	0.05726	1236.7	0.05896	1238.3
0.05558	1235	0.0573	1236.7	0.059	1238.3
0.05562	1235	0.05734	1236.7	0.05904	1238.3
0.05568	1235	0.05738	1236.7	0.05908	1238.3
0.05572	1235	0.05742	1236.7	0.05912	1238.3
0.05576	1235	0.05746	1236.7	0.05918	1238.3
0.0558	1235	0.0575	1236.7	0.05922	1238.3
0.05584	1235	0.05754	1236.7	0.05924	1238.3
0.05588	1235	0.05758	1236.7	0.0593	1238.3
0.05592	1235	0.05764	1236.7	0.05934	1238.3
0.05596	1235	0.05768	1237.5	0.05938	1238.3
0.056	1235	0.0577	1237.5	0.05942	1238.3
0.05604	1235	0.05776	1237.5	0.05946	1238.3
0.05608	1235	0.0578	1237.5	0.0595	1238.3
0.05612	1235	0.05784	1237.5	0.05954	1239.2
0.05616	1235.8	0.05788	1237.5	0.05958	1238.3
0.0562	1235	0.05792	1237.5	0.05962	1239.2
0.05626	1235	0.05796	1237.5	0.05966	1238.3
0.0563	1235.8	0.058	1237.5	0.05972	1239.2
0.05634	1235.8	0.05804	1237.5	0.05976	1239.2
0.05638	1235.8	0.05808	1237.5	0.0598	1239.2
0.05642	1235.8	0.05812	1237.5	0.05984	1239.2
0.05646	1235.8	0.05818	1237.5	0.05988	1239.2
0.0565	1235.8	0.05822	1237.5	0.05992	1239.2
0.05654	1235.8	0.05826	1237.5	0.05996	1239.2
0.05658	1235.8	0.0583	1237.5	0.06	1239.2
0.05662	1235.8	0.05834	1237.5	0.06004	1239.2
0.05668	1235.8	0.05838	1237.5	0.06008	1239.2
0.05672	1235.8	0.05842	1238.3	0.06012	1239.2
0.05676	1235.8	0.05846	1237.5	0.06016	1239.2
0.0568	1235.8	0.0585	1238.3	0.0602	1239.2
0.05684	1235.8	0.05854	1238.3	0.06026	1239.2
0.05688	1235.8	0.05858	1237.5	0.0603	1239.2
0.05692	1235.8	0.05862	1237.5	0.06034	1239.2
0.05696	1236.7	0.05866	1238.3	0.06038	1239.2
0.057	1236.7	0.0587	1238.3	0.06042	1239.2
0.05704	1235.8	0.05876	1238.3	0.06046	1239.2
0.05708	1236.7	0.0588	1238.3	0.0605	1239.2
0.05712	1236.7	0.05884	1238.3	0.06054	1239.2
0.05718	1236.7	0.05888	1238.3	0.06058	1239.2

Strain (m/m)	Force (N)	Strain (m/m)	Force (N)	Strain (m/m)	Force (N)
0.06062	1239.2	0.06234	1240	0.06404	1240.8
0.06068	1239.2	0.06238	1240	0.06408	1240.8
0.06072	1239.2	0.06242	1240	0.06412	1240.8
0.06076	1239.2	0.06246	1240	0.06418	1240.8
0.0608	1240	0.0625	1240.8	0.06422	1240.8
0.06084	1240	0.06254	1240	0.06426	1240.8
0.06088	1240	0.06258	1240.8	0.0643	1240.8
0.06092	1240	0.06262	1240.8	0.06434	1240.8
0.06096	1240	0.06266	1240.8	0.06438	1240.8
0.061	1240	0.0627	1240.8	0.06442	1240.8
0.06104	1240	0.06276	1240.8	0.06446	1240.8
0.06108	1240	0.0628	1240.8	0.0645	1240.8
0.06112	1240	0.06284	1240.8	0.06454	1240.8
0.06116	1240	0.06288	1240.8	0.06458	1241.7
0.0612	1240	0.06292	1240.8	0.06462	1240.8
0.06126	1240	0.06296	1240.8	0.06466	1240.8
0.0613	1240	0.063	1240.8	0.06472	1241.7
0.06134	1240	0.06304	1240.8	0.06476	1241.7
0.06138	1240	0.06308	1240.8	0.0648	1240.8
0.06142	1240	0.06312	1240.8	0.06484	1241.7
0.06146	1240	0.06318	1240.8	0.06488	1240.8
0.0615	1240	0.06322	1240.8	0.06492	1240.8
0.06154	1240	0.06326	1240.8	0.06496	1240.8
0.06158	1240	0.0633	1240.8	0.065	1241.7
0.06162	1240	0.06334	1240.8	0.06504	1241.7
0.06168	1240	0.06338	1240.8	0.06508	1241.7
0.06172	1240	0.06342	1240.8	0.06512	1241.7
0.06176	1240	0.06346	1240.8	0.06516	1240.8
0.0618	1240	0.0635	1240.8	0.0652	1241.7
0.06184	1240	0.06354	1240.8	0.06526	1241.7
0.06188	1240	0.06358	1240.8	0.0653	1241.7
0.06192	1240	0.06362	1240.8	0.06534	1241.7
0.06196	1240	0.06366	1240.8	0.06538	1241.7
0.062	1240	0.0637	1240.8	0.06542	1241.7
0.06204	1240	0.06376	1240.8	0.06546	1241.7
0.06208	1240	0.0638	1240.8	0.0655	1241.7
0.06212	1240	0.06384	1240.8	0.06554	1241.7
0.06216	1240	0.06388	1240.8	0.06558	1241.7
0.06222	1240	0.06392	1240.8	0.06562	1241.7
0.06226	1240	0.06396	1240.8	0.06568	1241.7
0.0623	1240	0.064	1240.8	0.06572	1241.7

Strain (m/m)	Force (N)	Strain (m/m)	Force (N)	Strain (m/m)	Force (N)
0.06576	1241.7	0.06746	1241.7	0.06918	1241.7
0.0658	1241.7	0.0675	1241.7	0.0692	1241.7
0.06584	1241.7	0.06754	1241.7	0.06924	1241.7
0.06588	1241.7	0.06758	1241.7	0.0693	1241.7
0.06592	1241.7	0.06764	1241.7	0.06934	1241.7
0.06596	1241.7	0.06766	1241.7	0.06938	1241.7
0.066	1241.7	0.0677	1241.7	0.06942	1241.7
0.06604	1241.7	0.06776	1241.7	0.06946	1241.7
0.0661	1241.7	0.0678	1241.7	0.0695	1241.7
0.06612	1241.7	0.06784	1241.7	0.06954	1241.7
0.06616	1241.7	0.06788	1241.7	0.06958	1241.7
0.0662	1241.7	0.06792	1241.7	0.06962	1241.7
0.06626	1241.7	0.06796	1241.7	0.06966	1241.7
0.0663	1241.7	0.068	1241.7	0.06972	1241.7
0.06634	1241.7	0.06804	1241.7	0.06976	1241.7
0.06638	1241.7	0.06808	1241.7	0.0698	1241.7
0.06642	1241.7	0.06812	1241.7	0.06984	1241.7
0.06646	1241.7	0.06818	1241.7	0.06988	1241.7
0.0665	1241.7	0.06822	1241.7	0.06992	1241.7
0.06654	1241.7	0.06826	1241.7	0.06998	1241.7
0.06658	1241.7	0.0683	1241.7	0.07002	1241.7
0.06662	1241.7	0.06834	1241.7	0.07004	1241.7
0.06668	1241.7	0.06838	1241.7	0.07008	1241.7
0.06672	1241.7	0.06842	1241.7	0.07014	1241.7
0.06676	1241.7	0.06846	1241.7	0.07018	1241.7
0.0668	1241.7	0.0685	1241.7	0.0702	1241.7
0.06684	1241.7	0.06854	1241.7	0.07026	1241.7
0.06688	1241.7	0.06858	1241.7	0.0703	1241.7
0.06692	1241.7	0.06862	1241.7	0.07034	1241.7
0.06696	1241.7	0.06866	1241.7	0.07038	1241.7
0.067	1241.7	0.0687	1241.7	0.07042	1241.7
0.06704	1241.7	0.06876	1241.7	0.07046	1241.7
0.06708	1241.7	0.0688	1241.7	0.0705	1241.7
0.06712	1241.7	0.06884	1241.7	0.07054	1241.7
0.06716	1241.7	0.06888	1241.7	0.07058	1241.7
0.06722	1241.7	0.06892	1241.7	0.07062	1241.7
0.06726	1241.7	0.06896	1241.7	0.07068	1241.7
0.0673	1241.7	0.069	1241.7	0.07072	1241.7
0.06734	1241.7	0.06904	1241.7	0.07076	1241.7
0.06738	1241.7	0.06908	1241.7	0.0708	1240.8
0.06742	1241.7	0.06912	1241.7	0.07084	1240.8

Strain (m/m)	Force (N)	Strain (m/m)	Force (N)	Strain (m/m)	Force (N)
0.07088	1241.7	0.07258	1240.8	0.0743	1240.8
0.07092	1241.7	0.07264	1240.8	0.07434	1240.8
0.07096	1241.7	0.07268	1241.7	0.07438	1240.8
0.071	1241.7	0.0727	1241.7	0.07442	1240.8
0.07104	1241.7	0.07276	1241.7	0.07446	1240.8
0.0711	1241.7	0.0728	1240.8	0.0745	1240.8
0.07112	1241.7	0.07284	1240.8	0.07454	1240.8
0.07116	1241.7	0.07288	1240.8	0.07458	1240.8
0.0712	1241.7	0.07292	1240.8	0.07462	1240.8
0.07126	1240.8	0.07296	1240.8	0.07466	1240.8
0.0713	1241.7	0.073	1240.8	0.07472	1240.8
0.07134	1240.8	0.07304	1240.8	0.07476	1240.8
0.07138	1241.7	0.07308	1240.8	0.0748	1240.8
0.07142	1241.7	0.07312	1240.8	0.07484	1240.8
0.07146	1241.7	0.07318	1241.7	0.07488	1240.8
0.0715	1241.7	0.07322	1240.8	0.07492	1240.8
0.07154	1241.7	0.07326	1240.8	0.07496	1240.8
0.07158	1241.7	0.0733	1240.8	0.075	1240.8
0.07162	1241.7	0.07334	1240.8	0.07504	1240.8
0.07168	1240.8	0.07338	1240.8	0.07508	1240.8
0.07172	1241.7	0.07342	1240.8	0.07512	1240.8
0.07176	1241.7	0.07346	1241.7	0.07518	1240.8
0.0718	1241.7	0.0735	1241.7	0.0752	1240.8
0.07184	1241.7	0.07354	1241.7	0.07526	1240.8
0.07188	1241.7	0.07358	1241.7	0.0753	1240.8
0.07192	1241.7	0.07362	1240.8	0.07534	1240.8
0.07196	1241.7	0.07366	1240.8	0.07538	1240.8
0.072	1241.7	0.0737	1240.8	0.07542	1240.8
0.07204	1241.7	0.07376	1240.8	0.07546	1240.8
0.07208	1241.7	0.0738	1240.8	0.0755	1240.8
0.07212	1241.7	0.07384	1240.8	0.07554	1240.8
0.07216	1241.7	0.07388	1240.8	0.07558	1240.8
0.07222	1241.7	0.07392	1240.8	0.07562	1240.8
0.07226	1240.8	0.07396	1240.8	0.07568	1240.8
0.0723	1241.7	0.074	1240.8	0.07572	1240
0.07234	1240.8	0.07404	1240.8	0.07576	1240.8
0.07238	1241.7	0.07408	1240.8	0.0758	1240
0.07242	1241.7	0.07412	1240.8	0.07584	1240
0.07246	1240.8	0.07418	1240.8	0.07588	1240.8
0.0725	1241.7	0.07422	1240.8	0.07592	1240.8
0.07254	1241.7	0.07426	1240.8	0.07596	1240

Strain (m/m)	Force (N)	Strain (m/m)	Force (N)	Strain (m/m)	Force (N)
0.076	1240	0.07772	1239.2	0.07942	1239.2
0.07604	1240.8	0.07776	1239.2	0.07946	1239.2
0.07608	1240	0.0778	1239.2	0.0795	1238.3
0.07612	1240	0.07784	1239.2	0.07954	1239.2
0.07616	1240.8	0.07788	1239.2	0.07958	1239.2
0.0762	1240	0.07792	1239.2	0.07962	1239.2
0.07626	1240	0.07796	1239.2	0.07966	1238.3
0.0763	1240	0.078	1240	0.07972	1238.3
0.07634	1240	0.07804	1240	0.07976	1238.3
0.07638	1240	0.07808	1239.2	0.0798	1238.3
0.07642	1240	0.07812	1239.2	0.07984	1238.3
0.07646	1240	0.07816	1239.2	0.07988	1238.3
0.0765	1240	0.07822	1239.2	0.07992	1238.3
0.07654	1240	0.07826	1239.2	0.07996	1238.3
0.07658	1240	0.0783	1239.2	0.08	1238.3
0.07662	1240	0.07834	1239.2	0.08004	1238.3
0.07668	1240	0.07838	1239.2	0.08008	1238.3
0.07672	1240	0.07842	1239.2	0.08014	1238.3
0.07676	1240	0.07846	1239.2	0.08016	1238.3
0.0768	1240	0.0785	1239.2	0.0802	1238.3
0.07684	1240	0.07854	1239.2	0.08024	1238.3
0.07688	1240	0.07858	1239.2	0.0803	1238.3
0.07692	1240	0.07862	1239.2	0.08034	1238.3
0.07696	1240	0.07866	1239.2	0.08038	1238.3
0.077	1240	0.0787	1239.2	0.08042	1238.3
0.07704	1240	0.07876	1239.2	0.08046	1238.3
0.07708	1240	0.0788	1239.2	0.0805	1238.3
0.07712	1239.2	0.07884	1239.2	0.08054	1238.3
0.07716	1240	0.07888	1239.2	0.08058	1238.3
0.07722	1239.2	0.07892	1239.2	0.08062	1238.3
0.07726	1240	0.07896	1239.2	0.08066	1238.3
0.0773	1240	0.079	1239.2	0.08072	1238.3
0.07734	1240	0.07904	1239.2	0.08076	1237.5
0.07738	1240	0.07908	1239.2	0.0808	1237.5
0.07742	1239.2	0.07914	1239.2	0.08084	1237.5
0.07746	1240	0.07918	1239.2	0.08088	1237.5
0.0775	1240	0.07922	1239.2	0.08092	1237.5
0.07754	1240	0.07926	1239.2	0.08096	1237.5
0.07758	1240	0.0793	1239.2	0.081	1237.5
0.07764	1240	0.07934	1239.2	0.08104	1237.5
0.07768	1239.2	0.07938	1239.2	0.08108	1237.5

Strain (m/m)	Force (N)	Strain (m/m)	Force (N)	Strain (m/m)	Force (N)
0.08112	1237.5	0.08284	1235	0.08454	1230.8
0.08116	1237.5	0.08288	1235.8	0.08458	1230.8
0.0812	1237.5	0.08292	1235	0.08462	1230.8
0.08126	1237.5	0.08296	1235	0.08466	1230.8
0.0813	1237.5	0.083	1235	0.08472	1230
0.08134	1237.5	0.08304	1235	0.08476	1230
0.08138	1237.5	0.08308	1235	0.0848	1230
0.08142	1237.5	0.08312	1235	0.08484	1229.2
0.08146	1237.5	0.08316	1235	0.08488	1229.2
0.0815	1237.5	0.08322	1235	0.08492	1229.2
0.08154	1237.5	0.08326	1235	0.08496	1229.2
0.08158	1237.5	0.0833	1234.2	0.085	1229.2
0.08162	1237.5	0.08334	1234.2	0.08504	1228.3
0.08168	1236.7	0.08338	1234.2	0.08508	1228.3
0.08172	1236.7	0.08342	1234.2	0.08512	1228.3
0.08176	1236.7	0.08346	1234.2	0.08518	1227.5
0.0818	1236.7	0.0835	1234.2	0.0852	1226.7
0.08184	1236.7	0.08354	1234.2	0.08524	1226.7
0.08188	1236.7	0.08358	1234.2	0.0853	1226.7
0.08192	1236.7	0.08362	1233.3	0.08534	1225.8
0.08196	1236.7	0.08366	1233.3	0.08538	1225.8
0.082	1236.7	0.0837	1233.3	0.08542	1225
0.08204	1236.7	0.08376	1233.3	0.08546	1225
0.08208	1236.7	0.0838	1233.3	0.0855	1224.2
0.08212	1236.7	0.08384	1232.5	0.08554	1224.2
0.08216	1236.7	0.08388	1232.5	0.08558	1224.2
0.08222	1236.7	0.08392	1232.5	0.08562	1223.3
0.08226	1236.7	0.08396	1232.5	0.08566	1222.5
0.0823	1236.7	0.084	1232.5	0.08572	1222.5
0.08234	1235.8	0.08404	1232.5	0.08576	1221.7
0.08238	1235.8	0.08408	1232.5	0.0858	1220.8
0.08242	1235.8	0.08412	1232.5	0.08584	1220
0.08246	1235.8	0.08418	1232.5	0.08588	1220
0.0825	1235.8	0.08422	1231.7	0.08592	1219.2
0.08254	1235.8	0.08426	1231.7	0.08596	1218.3
0.08258	1235.8	0.0843	1231.7	0.086	1218.3
0.08264	1235.8	0.08434	1231.7	0.08604	1216.7
0.08268	1235.8	0.08438	1231.7	0.08608	1216.7
0.0827	1235.8	0.08442	1230.8	0.08612	1215.8
0.08276	1235.8	0.08446	1231.7	0.08616	1215
0.0828	1235.8	0.0845	1230.8	0.08622	1214.2

Strain (m/m)	Force (N)
0.08626	1212.5
0.0863	1211.7
0.08634	1210.8
0.08638	1209.2
0.08642	1208.3
0.08646	1206.7
0.0865	1205
0.08654	1203.3
0.08658	1201.7
0.08662	1199.2
0.08668	1195.8
0.08672	1190.8
0.08676	895.8
0.0868	-21.67
0.08684	-21.67
0.08688	-21.67
0.08692	-21.67
0.08696	-21.67
0.087	-21.67
0.08704	-21.67
0.0871	-21.67
0.08714	-21.67
0.08716	-21.67
0.0872	-21.67
0.08726	-21.67
0.0873	-21.67
0.08734	-21.67
0.08738	-21.67
0.08742	-21.67
0.08746	-21.67
0.0875	-21.67
0.08754	-21.67
0.08758	-21.67
0.08764	-21.67
0.08768	-21.67

Appendix B: Full Plots Showing Multiple Trials of Tests

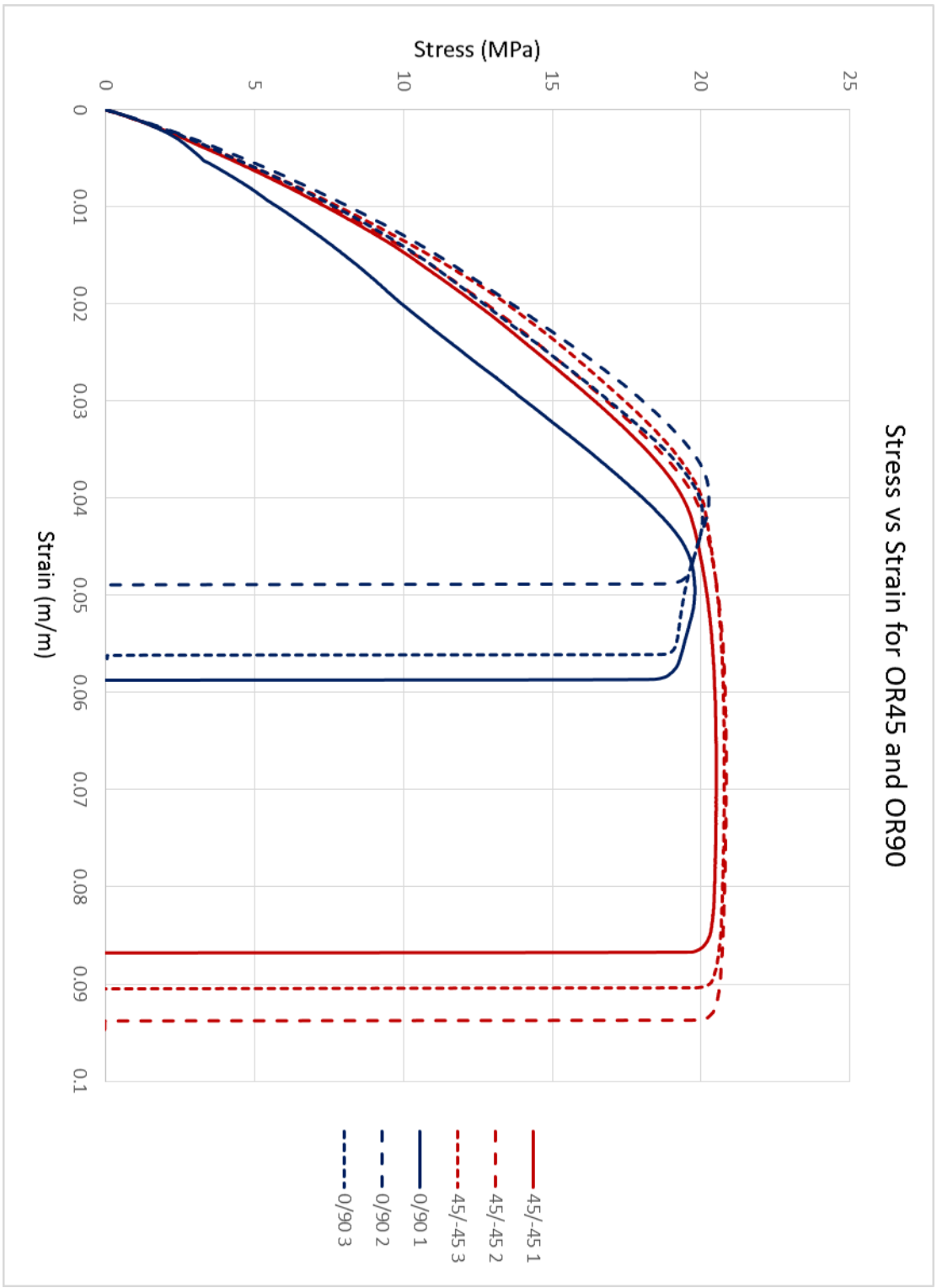
Stress vs Strain for OR45 and OR90
Stress (MPa)
0
5
10
15
20
25
Strain (m/m)
0
0.01
0.02
0.03
0.04
0.05
0.06
0.07
0.08
0.09
0.1
45/-45 1
45/-45 2
45/-45 3
0/90 1
0/90 2
0/90 3

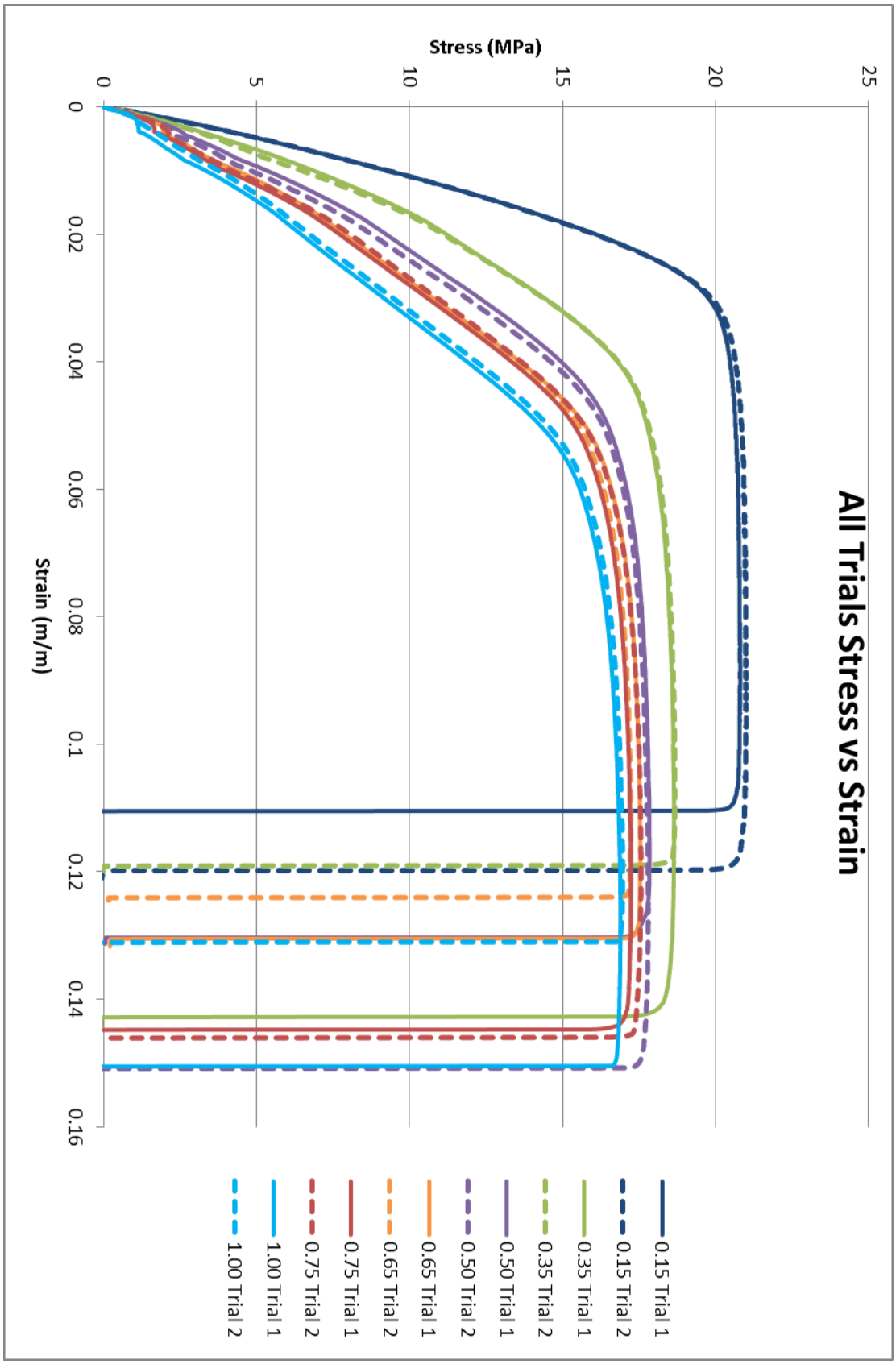
All Trials Stress vs Strain
Stress (MPa)
0
5
10
15
20
25
Strain (m/m)
0
0.02
0.04
0.06
0.08
0.1
0.12
0.14
0.16
0.15 Trial 1
0.15 Trial 2
0.35 Trial 1
0.35 Trial 2
0.50 Trial 1
0.50 Trial 2
0.65 Trial 1
0.65 Trial 2
0.75 Trial 1
0.75 Trial 2
1.00 Trial 1
1.00 Trial 2

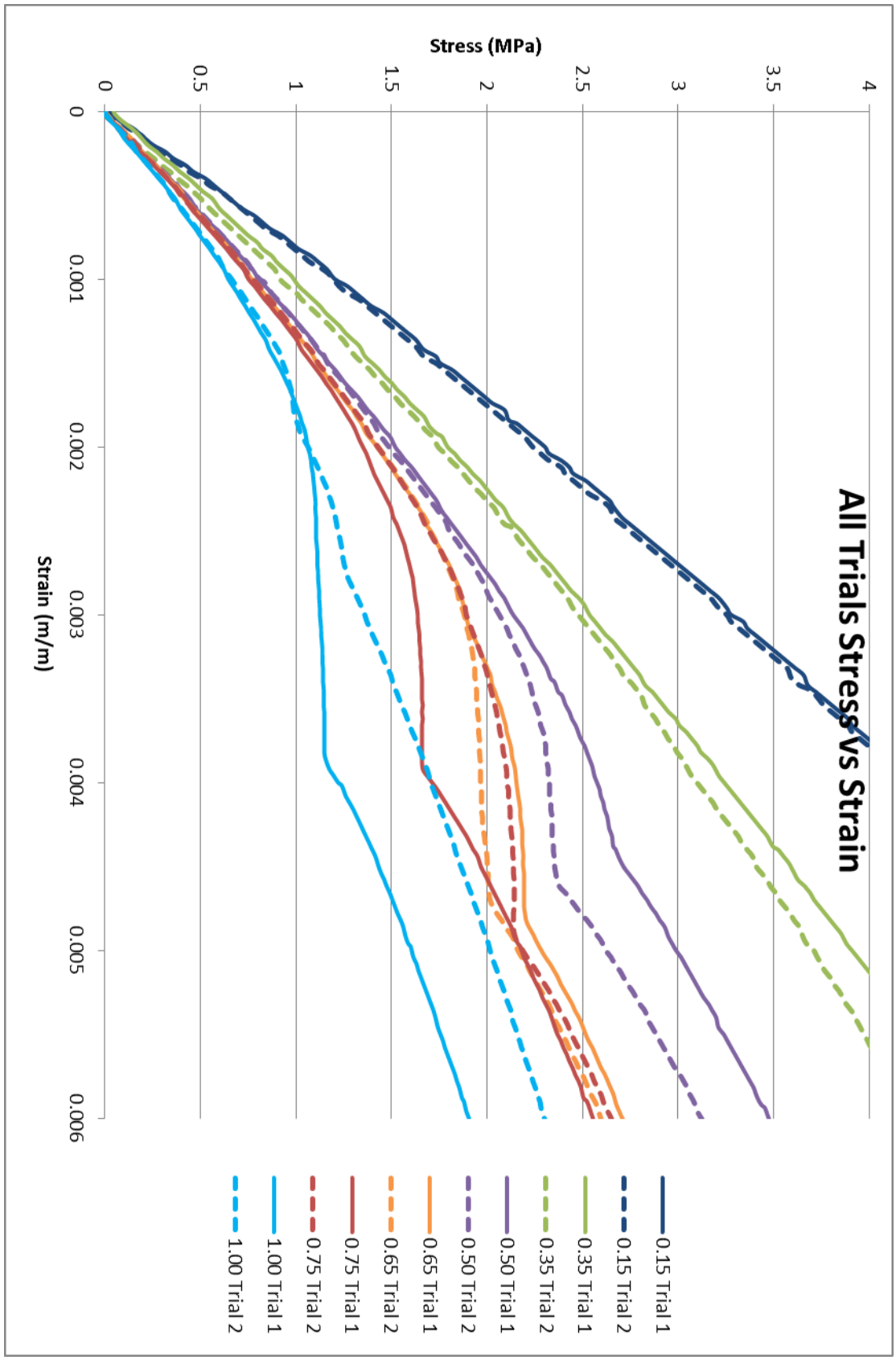
All Trials Stress vs Strain
Stress (MPa)
Strain (m/m)
0
0.5
1
1.5
2
2.5
3
3.5
4
0
0.001
0.002
0.003
0.004
0.005
0.006
0.15 Trial 1
0.15 Trial 2
0.35 Trial 1
0.35 Trial 2
0.50 Trial 1
0.50 Trial 2
0.65 Trial 1
0.65 Trial 2
0.75 Trial 1
0.75 Trial 2
1.00 Trial 1
1.00 Trial 2

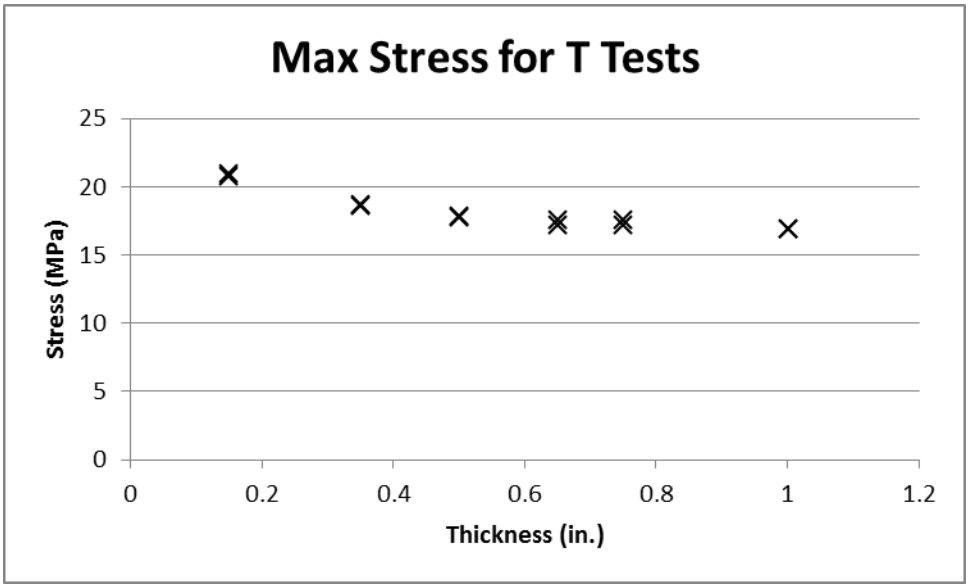
Max Stress for T Tests
Stress (MPa)
25
20
15
10
5
0
0
0.2
0.4
0.6
0.8
1
1.2
Thickness (in.)

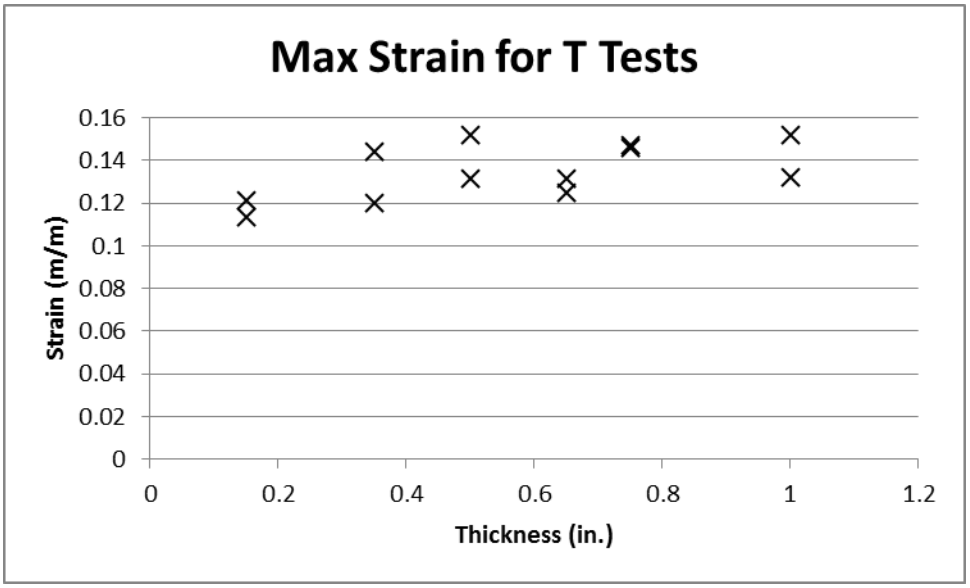
Max Strain for T Tests
Strain (m/m)
0.16
0.14
0.12
0.1
0.08
0.06
0.04
0.02
0
0
0.2
0.4
0.6
0.8
1
1.2
Thickness (in.)

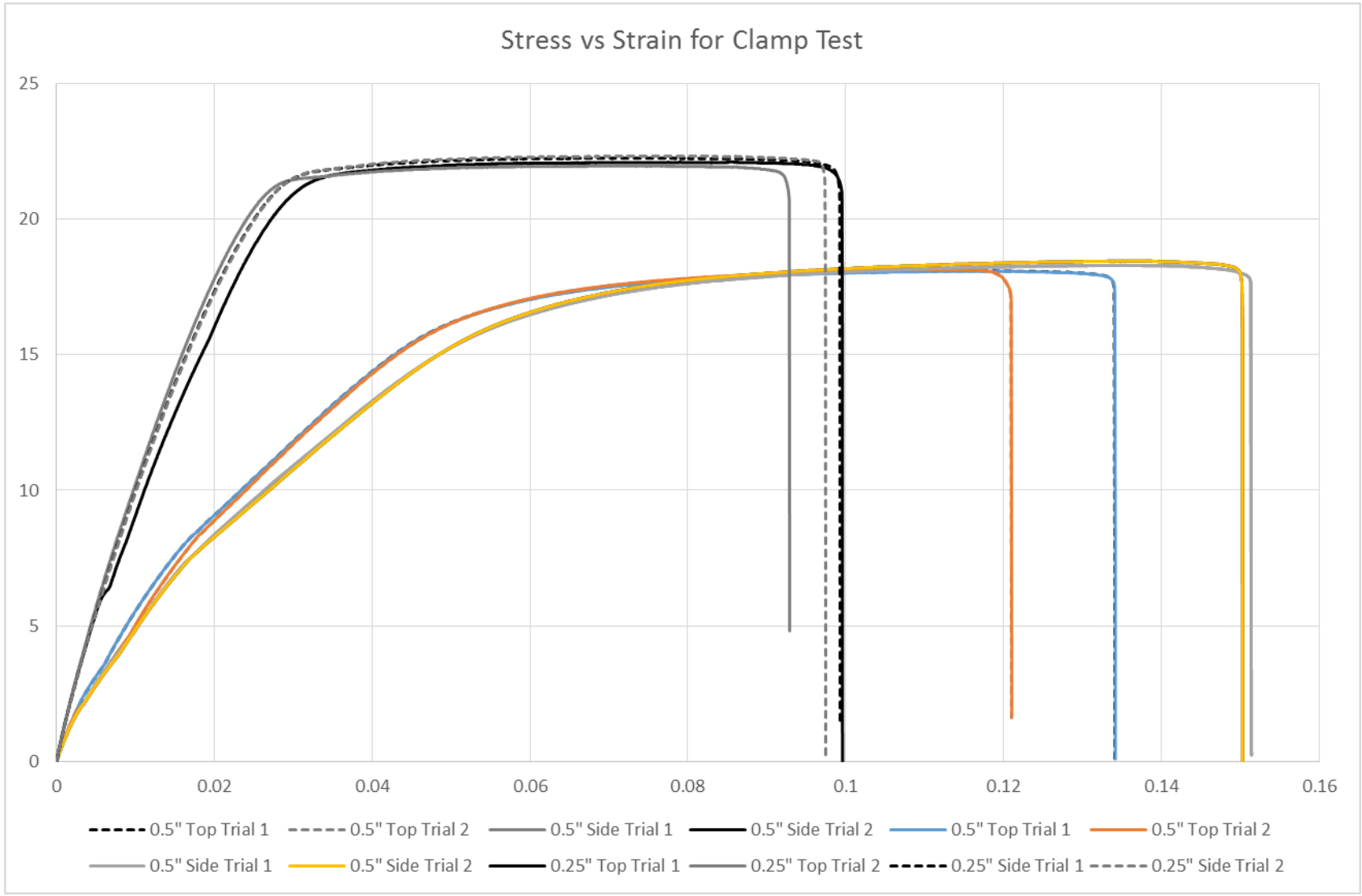
Stress vs Strain for Clamp Test
25
20
15
10
5
0
0
0.02
0.04
0.06
0.08
0.1
0.12
0.14
0.16
0.5" Top Trial 1
0.5" Top Trial 2
0.5" Side Trial 1
0.5" Side Trial 2
0.5" Top Trial 1
0.5" Top Trial 2
0.5" Side Trial 1
0.5" Side Trial 2
0.25" Top Trial 1
0.25" Top Trial 2
0.25" Side Trial 1
0.25" Side Trial 2

	0.4" Thickness	0.8" Thickness	1.2" Thickness
0.25" Width	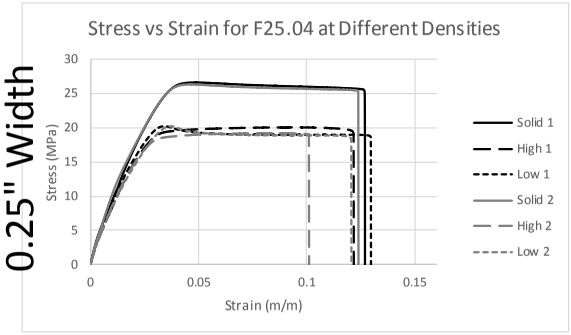	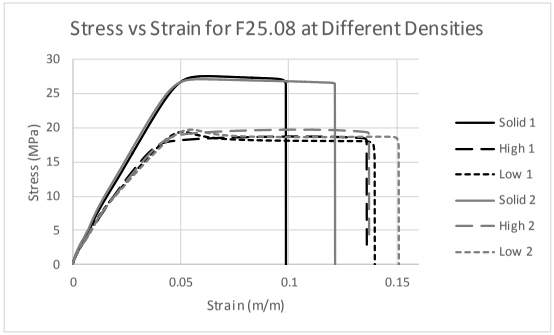	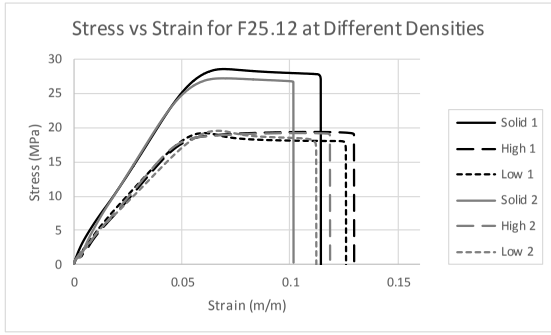
0.375" Width	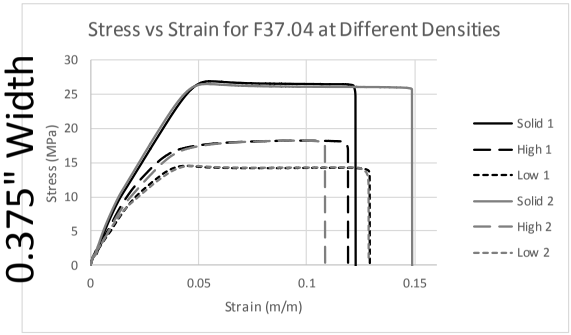	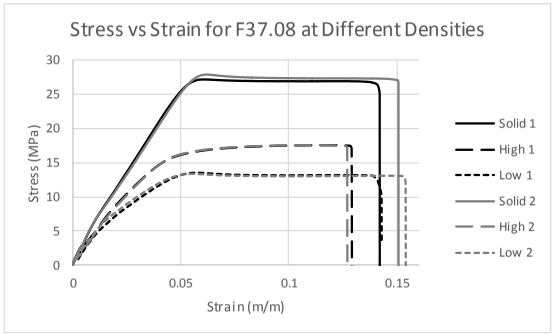	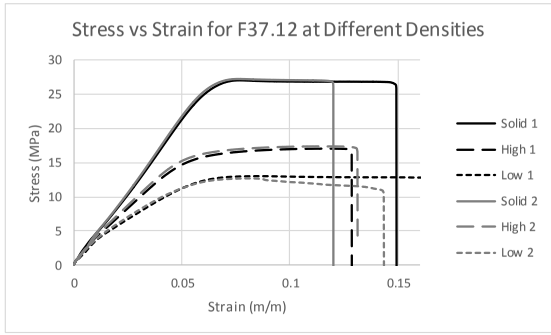
0.5" Width	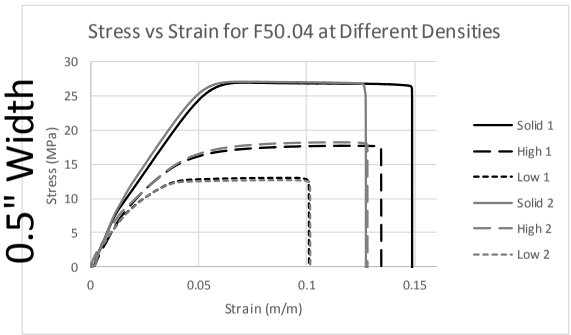	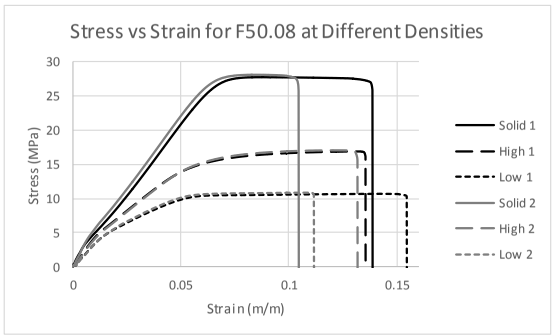	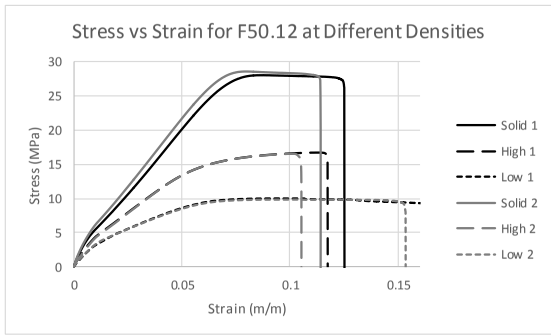

Appendix C: Full Density Data and Calculated Values

Part Name	Density	Infill Volume	Part Volume	Surface Volume	Surface Weight	Total Weight	Infill Weight	Infill Density	Infill %
F25.04-L	0.70	4343.40	6554.826	2211.426	2.167	4.6	2.433	5.60E-04	52.9%
F25.04-H	0.87	4343.40	6554.826	2211.426	2.167	5.7	3.533	8.13E-04	62.0%
F25.04-S	0.98	4343.40	6554.826	2211.426	2.167	6.4	4.233	9.75E-04	66.1%
F25.08-L	0.67	9169.40	13109.651	3940.251	3.861	8.8	4.939	5.39E-04	56.1%
F25.08-H	0.85	9169.40	13109.651	3940.251	3.861	11.1	7.239	7.89E-04	65.2%
F25.08-S	0.98	9169.40	13109.651	3940.251	3.861	12.8	8.939	9.75E-04	69.8%
F25.12-L	0.66	13995.40	19664.477	5669.077	5.556	13.0	7.444	5.32E-04	57.3%
F25.12-H	0.84	13995.40	19664.477	5669.077	5.556	16.6	11.044	7.89E-04	66.5%
F25.12-S	0.98	13995.40	19664.477	5669.077	5.556	19.2	13.644	9.75E-04	71.1%
F37.04-L	0.57	7246.62	9832.238	2585.618	2.534	5.6	3.066	4.23E-04	54.8%
F37.04-H	0.83	7246.62	9832.238	2585.618	2.534	8.2	5.666	7.82E-04	69.1%
F37.04-S	0.98	7246.62	9832.238	2585.618	2.534	9.6	7.066	9.75E-04	73.6%
F37.08-L	0.53	15298.42	19664.477	4366.057	4.279	10.4	6.121	4.00E-04	58.9%
F37.08-H	0.81	15298.42	19664.477	4366.057	4.279	16.0	11.721	7.66E-04	73.3%
F37.08-S	0.97	15298.42	19664.477	4366.057	4.279	19.1	14.821	9.69E-04	77.6%
F37.12-L	0.51	23350.22	29496.715	6146.495	6.024	15.0	8.976	3.84E-04	59.8%
F37.12-H	0.81	23350.22	29496.715	6146.495	6.024	23.8	17.776	7.61E-04	74.7%
F37.12-S	0.98	23350.22	29496.715	6146.495	6.024	28.8	22.776	9.75E-04	79.1%
F50.04-L	0.52	10149.84	13109.651	2959.811	2.901	6.8	3.899	3.84E-04	57.3%
F50.04-H	0.82	10149.84	13109.651	2959.811	2.901	10.8	7.899	7.78E-04	73.1%
F50.04-S	0.98	10149.84	13109.651	2959.811	2.901	12.9	9.999	9.85E-04	77.5%
F50.08-L	0.46	21427.44	26219.302	4791.862	4.696	12.0	7.304	3.41E-04	60.9%
F50.08-H	0.80	21427.44	26219.302	4791.862	4.696	21.0	16.304	7.61E-04	77.6%
F50.08-S	0.98	21427.44	26219.302	4791.862	4.696	25.7	21.004	9.80E-04	81.7%
F50.12-L	0.43	32705.04	39328.954	6623.914	6.491	17.1	10.609	3.24E-04	62.0%
F50.12-H	0.79	32705.04	39328.954	6623.914	6.491	31.1	24.609	7.52E-04	79.1%
F50.12-S	0.98	32705.04	39328.954	6623.914	6.491	38.5	32.009	9.79E-04	83.1%

Appendix D: ANOVA Results

Orientation Tests

One-way ANOVA: UTS versus Raster Angle

Method

Null hypothesis	All means are equal
Alternative hypothesis	At least one mean is different
Significance level	α = 0.05

Equal variances were assumed for the analysis.

Factor Information

Factor	Levels	Values
Angle	2	45, 90

Analysis of Variance

Source	DF	Adj SS	Adj MS	F-Value	P-Value
Angle	1	0.6829	0.68295	15.77	0.017
Error	4	0.1732	0.04330		
Total	5	0.8561			

Model Summary

S	R-sq	R-sq(adj)	R-sq(pred)
0.208081	79.77%	74.71%	54.48%

Means

Angle	N	Mean	StDev	95% CI
45	3	20.720	0.177	(20.387, 21.054)
90	3	20.046	0.235	(19.712, 20.379)

Pooled StDev = 0.208081

Thickness Test

One-way ANOVA: UTS versus Thickness

Method

Null hypothesis	All means are equal
Alternative hypothesis	At least one mean is different
Significance level	α = 0.05

Equal variances were assumed for the analysis.

Factor Information

Factor	Levels	Values
Thickness	6	0.15, 0.35, 0.50, 0.65, 0.75, 1.00

Analysis of Variance

Source	DF	Adj SS	Adj MS	F-Value	P-Value
Thickness	5	21.1579	4.23159	198.29	0.000
Error	6	0.1280	0.02134		
Total	11	21.2860			

Model Summary

S	R-sq	R-sq(adj)	R-sq(pred)
0.146082	99.40%	98.90%	97.59%

Means

Thickness	N	Mean	StDev	95% CI
0.15	2	20.9074	0.1346	(20.6546, 21.1601)
0.35	2	18.6734	0.0335	(18.4207, 18.9262)
0.50	2	17.8216	0.0390	(17.5688, 18.0743)
0.65	2	17.395	0.209	(17.142, 17.648)
0.75	2	17.412	0.247	(17.159, 17.665)
1.00	2	16.9297	0.0505	(16.6770, 17.1825)

Pooled StDev = 0.146082

Clamping Test

Factorial Regression: UTS versus Orientation, Size

Analysis of Variance

Source	DF	Adj SS	Adj MS	F-Value	P-Value
Model	2	30.7317	15.3658	2713.72	0.000
Linear	2	30.7317	15.3658	2713.72	0.000
Orientation	1	0.1258	0.1258	22.22	0.005
Size	1	30.6059	30.6059	5405.23	0.000
Error	5	0.0283	0.0057		
Lack-of-Fit	1	0.0003	0.0003	0.05	0.840
Pure Error	4	0.0280	0.0070		
Total	7	30.7600			

One-way ANOVA: UTS versus Clamp at 0.5”

Method

Null hypothesis	All means are equal
Alternative hypothesis	At least one mean is different
Significance level	α = 0.05

Equal variances were assumed for the analysis.

Factor Information

Factor	Levels	Values
Clamp	2	0, 1

Analysis of Variance

Source	DF	Adj SS	Adj MS	F-Value	P-Value
Clamp	1	0.06943	0.069433	9.97	0.087
Error	2	0.01393	0.006967		
Total	3	0.08337			

Model Summary

S	R-sq	R-sq(adj)	R-sq(pred)
0.0834702	83.29%	74.93%	33.14%

Means

Clamp	N	Mean	StDev	95% CI
0	2	18.1164	0.0438	(17.8625, 18.3704)
1	2	18.3799	0.1096	(18.1260, 18.6339)

Pooled StDev = 0.0834702

One-way ANOVA: UTS versus Clamp at 0.25”

Method

Null hypothesis	All means are equal
Alternative hypothesis	At least one mean is different
Significance level	α = 0.05

Equal variances were assumed for the analysis.

Factor Information

Factor	Levels	Values
Clamp	2	0, 1

Analysis of Variance

Source	DF	Adj SS	Adj MS	F-Value	P-Value
Clamp	1	0.05668	0.056682	8.07	0.105
Error	2	0.01405	0.007027		
Total	3	0.07074			

Model Summary

S	R-sq	R-sq(adj)	R-sq(pred)
0.0838264	80.13%	70.20%	20.53%

Means

Clamp	N	Mean	StDev	95% CI
0	2	22.0410	0.1035	(21.7860, 22.2961)
1	2	22.2791	0.0579	(22.0241, 22.5342)

Pooled StDev = 0.0838264

Bibliography

(1) 2016, "3D Printing & Imaging DIY Projects for Makers | Make: DIY Projects and Ideas for Makers", Make: DIY Projects and Ideas for Makers [Online]. Available: http://makezine.com/category/workshop/3d-printing-workshop/. [Accessed: 25- Jul- 2016].

(2) Stankovic, T., Mueller, J., Egan, P., Shea, K. (2015). A Generalized Optimality Method For Optimization Of Additively Manufactured Multimaterial Lattice Structures. *J. Mech. Des* 137.11: 111405

(3) Kellner, T. (2015). *The FAA Cleared the First 3D Printed Part to Fly in a Commercial Jet Engine from GE - GE Reports*. *GE Reports*. Retrieved 15 July 2016, from http://www.gereports.com/post/116402870270/the-faa-cleared-the-first-3d-printed-part-to-fly/

(4) *About DARPA*. (2016). *Darpa.mil*. Retrieved 18 July 2016, from http://www.darpa.mil/about-us/about-darpa

(5) Williams, C., Simpson, T., & Hripko, M. (2015). Advancing the Additive Manufacturing Workforce: Summary and Recommendations From a NSF Workshop. *Volume 3: 17Th International Conference On Advanced Vehicle Technologies; 12Th International Conference On Design Education; 8Th Frontiers In Biomedical Devices*. http://dx.doi.org/10.1115/detc2015-47274

(6) Blikstein, P. (2013). Digital fabrication and 'making'in education: The democratization of invention. *FabLabs: Of machines, makers and inventors*, 1-21.

(7) *3D Printing Now and Beyond | Stratasys*. (2016). *Stratasys.com*. Retrieved 11 July 2016, from http://www.stratasys.com/resources/white-papers/3d-printing-now-and-beyond

(8) Sidambe, A. (2014). Biocompatibility of Advanced Manufactured Titanium Implants—A Review. *Materials*, *7*(12), 8168-8188. http://dx.doi.org/10.3390/ma7128168

(9) Halverson, E. & Sheridan, K. (2014). The Maker Movement in Education. *Harvard Educational Review*, *84*(4), 495-504. http://dx.doi.org/10.17763/haer.84.4.34j1g68140382063

(10) Jackson, A. (2014). Makers: The New Industrial Revolution. *Journal Of Design History*, *27*(3), 311-312. http://dx.doi.org/10.1093/jdh/ept048

(11) *Making in Education - Maker Media*. (2016). *Maker Media*. Retrieved 11 July 2016, from https://makermedia.com/about-us/making-in-education/

(12) Loy, J. (2014). eLearning and eMaking: 3D Printing Blurring the Digital and the Physical. *Education Sciences*, *4*(1), 108-121. http://dx.doi.org/10.3390/educsci4010108

(13) Bashyam, S., Kuhn, J., & Seepersad, C. (2015). A 3D Printing Vending Machine and its Impact on the Democratization of 3D Printing on a College Campus. Volume 3: 17Th International Conference On Advanced Vehicle Technologies; 12Th International Conference On Design Education; 8Th Frontiers In Biomedical Devices. http://dx.doi.org/10.1115/detc2015-46470

(14) Iversen, O., Smith, R., Blikstein, P., Katterfeldt, E., & Read, J. (2015). Digital fabrication in education: Expanding the research towards design and reflective practices. *International Journal Of Child-Computer Interaction*, *5*, 1-2. http://dx.doi.org/10.1016/j.ijcci.2016.01.001

(15) Buehler, E., Easley, W., McDonald, S., Comrie, N., & Hurst, A. (2015, October). Inclusion and Education: 3D Printing for Integrated Classrooms. In *Proceedings of the 17th International ACM SIGACCESS Conference on Computers & Accessibility* (pp. 281-290). ACM.

(16) Fornasini, G. and L. C. Schmidt, "A Call for FDM Design Rules to Include Road Deposition," 20th International Conference on Engineering Design (ICED15), Milan, Italy, July 27-30, 2015

(17) Qureshi, A.J., Mahmood, S., Wong, W.L.E. & Talamona, D., 2015. Design for Scalability and Strength Optimisation for components created through FDM process. In Proceedings of the 20th International Conference on Engineering Design (ICED15). Milan, Italy, 27-30.07.2015.

(18) Es-Said, O., Foyos, J., Noorani, R., Mendelson, M., Marloth, R., & Pregger, B. (2000). Effect of Layer Orientation on Mechanical Properties of Rapid Prototyped Samples. *Materials And Manufacturing Processes*, *15*(1), 107-122. http://dx.doi.org/10.1080/10426910008912976

(19) Dawoud, M., Taha, I., & Ebeid, S. J. (2016). Mechanical behaviour of ABS: An experimental study using FDM and injection moulding techniques.*Journal of Manufacturing Processes*, *21*, 39-45.

(20) Yang, J. H., Zhao, Z. J., & Park, S. H. (2015, October). Evaluation of directional mechanical properties of 3D printed polymer parts. In *Control, Automation and Systems (ICCAS), 2015 15th International Conference on*(pp. 1952-1954). IEEE.

(21) Rankouhi, B., Javadpour, S., Delfanian, F., & Letcher, T. (2016). Failure Analysis and Mechanical Characterization of 3D Printed ABS With Respect to Layer Thickness and Orientation. *J Fail. Anal. And Preven.*, *16*(3), 467-481. http://dx.doi.org/10.1007/s11668-016-0113-2

(22) Mohamed, O., Masood, S., & Bhowmik, J. (2015). Experimental Investigations of Process Parameters Influence on Rheological Behavior and Dynamic Mechanical Properties of FDM Manufactured Parts. *Materials And Manufacturing Processes*. http://dx.doi.org/10.1080/10426914.2015.1127955

(23) Teitelbaum, G., (2009) Proposed design and build guidelines for use in fused deposition modelling to reduce build time and material volume, College Park, Maryland, University of Maryland

(24) Lanzotti, A., Martorelli, M., & Staiano, G. (2014). Understanding Process Parameter Effects of RepRap Open-Source Three-Dimensional Printers Through a Design of Experiments Approach. *Journal Of Manufacturing Science And Engineering*, *137*(1), 011017. http://dx.doi.org/10.1115/1.4029045

(25) Torrado, A., Shemelya, C., English, J., Lin, Y., Wicker, R., & Roberson, D. (2015). Characterizing the effect of additives to ABS on the mechanical property anisotropy of specimens fabricated by material extrusion 3D printing. Additive Manufacturing, 6, 16-29.http://dx.doi.org/10.1016/j.addma.2015.02.001

(26) Shaffer, S., Yang, K., Vargas, J., Di Prima, M., & Voit, W. (2014). On reducing anisotropy in 3D printed polymers via ionizing radiation. *Polymer*, *55*(23), 5969-5979. http://dx.doi.org/10.1016/j.polymer.2014.07.054

(27) Torrado Perez, A., Roberson, D., & Wicker, R. (2014). Fracture Surface Analysis of 3D-Printed Tensile Specimens of Novel ABS-Based Materials. *J Fail. Anal. And Preven.*, *14*(3), 343-353. http://dx.doi.org/10.1007/s11668-014-9803-9

(28) Wu, W., Geng, P., Li, G., Zhao, D., Zhang, H., & Zhao, J. (2015). Influence of Layer Thickness and Raster Angle on the Mechanical Properties of 3D-Printed PEEK and a Comparative Mechanical Study between PEEK and ABS. *Materials*, *8*(9), 5834-5846. http://dx.doi.org/10.3390/ma8095271

(29) Weng, Z., Wang, J., Senthil, T., & Wu, L. (2016). Mechanical and thermal properties of ABS/montmorillonite nanocomposites for fused deposition modeling 3D printing. *Materials & Design*, *102*, 276-283. http://dx.doi.org/10.1016/j.matdes.2016.04.045

(30) Belter, J. & Dollar, A. (2015). Strengthening of 3D Printed Fused Deposition Manufactured Parts Using the Fill Compositing Technique. *PLOS ONE*, *10*(4), e0122915. http://dx.doi.org/10.1371/journal.pone.0122915

(31) Gao, W., Zhang, Y., Ramanujan, D., Ramani, K., Chen, Y., & Williams, C. et al. (2015). The status, challenges, and future of additive manufacturing in engineering. *Computer-Aided Design*, *69*, 65-89. http://dx.doi.org/10.1016/j.cad.2015.04.001

(32) Vayre, B., Vignat, F., & Villeneuve, F. (2012). Designing for Additive Manufacturing. *Procedia CIRP*, *3*, 632-637. http://dx.doi.org/10.1016/j.procir.2012.07.108

(33) Zein, I., Hutmacher, D., Tan, K., Teoh, S., (2001), Fused deposition modelling of novel scaffold architectures for tissue engineering applications. Biomaterials, Vol. 23, No. 4, pp. 1169-1185.

(34) Ahn, S., Montero, M., Odell, D., Roundy, S., Write, P., (2002), Anisotropic properties of fused deposition modelling ABS. Rapid Prototyping Journal, Vol. 8, No. 4, pp. 248-257.

(35) "Absplus, Fortus 3D Production Systems FDM Materials | Stratasys". *Stratasys.com*. N.p., 2016. Web. 11 July 2016